This article has been accepted for publication in a future issue of this journal, but has not been fully edited. Content may change prior to final publication. Citation information: DOI 10.1109/COMST.2015.2394911, IEEE Communications Surveys & Tutorials

Performance Improvement and Cost Reduction Techniques For Radio Over Fiber Communications

Varghese Antony Thomas, Mohammed El-Hajjar and Lajos Hanzo
School of ECS, University of Southampton, SO17 1BJ, United Kingdom.
Email: {vat1g10, meh, lh}@ecs.soton.ac.uk, http://www-mobile.ecs.soton.ac.uk

***Abstract*— Advanced cost reduction and performance improvement techniques conceived for Radio Over Fiber (ROF) communications are considered. ROF techniques are expected to form the backbone of the future 5G generation of wireless networks. The achievable link performance and the associated deployement cost constitute the most salient metrics of a ROF architecture. In this paper, we commence by providing a rudimentary overview of the ROF architecture and then elaborate on ROF techniques designed for improving the attainable system performance. We conclude by describing the ROF techniques conceived for reducing the ROF system installation costs.**

I. INTRODUCTION

Due to the proliferation of various high-bandwidth applications, the most benign, low frequency radio spectrum is becoming over-crowded. A natural option is to use higher carrier frequencies, such as for example millimeter-waves (mm-waves) at say 60 GHz, where these high-frequency carriers have a potentially high bandwidth, but are characterized by a low wireless propagation range [1]. Therefore, a large number of Radio Access Points (RAPs) are required for providing seamless coverage. In order to cope with the increasing bandwidth demand per user, network operators often have to split the existing cells into smaller cells. However, increasing the number of base-stations is not always a feasible option due to the higher infrastructure costs involved [2].

One of the major access network solutions for future high-bandwidth wireless communication systems is based on optical fibers for the transmission of radio signals between the Base Station (BS) and RAPs, which is generally referred to as a Radio Over Fiber (ROF) solution [2], [3], [4], [5], [6]. Fig. 1 shows the simplified diagram of a ROF link, where the wireless Radio Frequency (RF) signal is converted into an optical signal in an electrical-to-optical (E-O) converter at the BS [7]. The optical signal is transmitted through the fiber and detected at the RAP, where an optical-to-electrical (O-E) converter recovers the original RF signal, which is amplified and transmitted from the RAP antenna to the Mobile Station (MS), as shown in Fig. 1.

Fig. 2 shows two cellular architectures, namely one with and one without using ROF assistance. Fig. 2(a) represents the existing cellular systems that are based on macrocells, while Fig. 2(b) is a futuristic cellular architecture that relies on a ROF backhaul designed for supporting smaller cells. The architecture seen in Fig. 2(a) has a lower-quality wireless coverage, a lower power efficiency and a limited ability to use small cells, whilst these challenges are overcome in the architecure of Fig. 2(b) at the added cost of laying more fiber, as discussed below.

The financial support of the EPSRC, UK under the auspices of the India-UK Advanced Technology Centre and that of the European Research Council under its Advanced Fellow Grant is gratefully acknowledged.

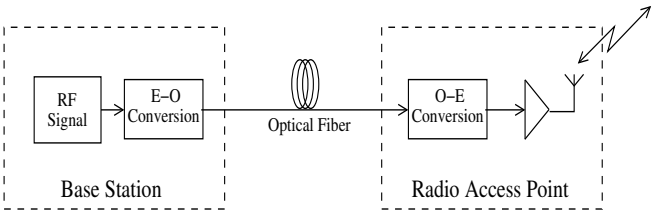

Fig. 1. Simple ROF link. (E-O- Electrical-to-Optical; O-E- Optical-to-Electrical)

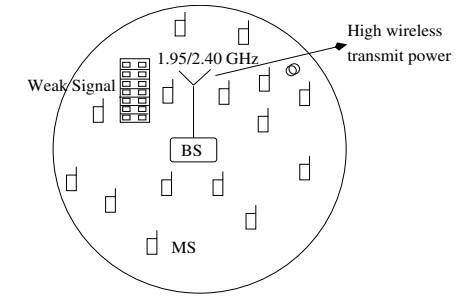

(a) Without using ROF

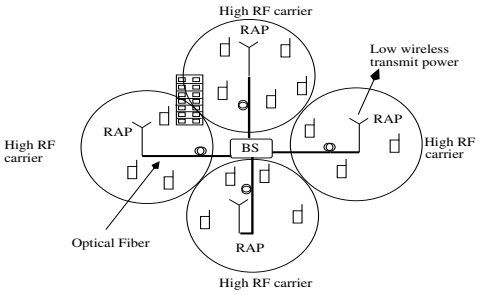

(b) Using ROF

Fig. 2. Cellular Architecture (BS- Base Station; RAP- Radio Access Point; MS- Mobile Station)

As seen from Fig. 1 and Fig. 2, ROF solutions belong to the family of hybrid techniques, since they rely on both optical and wireless communication. The advantage of a ROF system is its ability to amalgamate the benefits of these two diverse communication techniques. Explicitely, the advantages of an ROF system can be summarised as follows [8], [9], [10].

This article has been accepted for publication in a future issue of this journal, but has not been fully edited. Content may change prior to final publication. Citation information: DOI 10.1109/COMST.2015.2394911, IEEE Communications Surveys & Tutorials

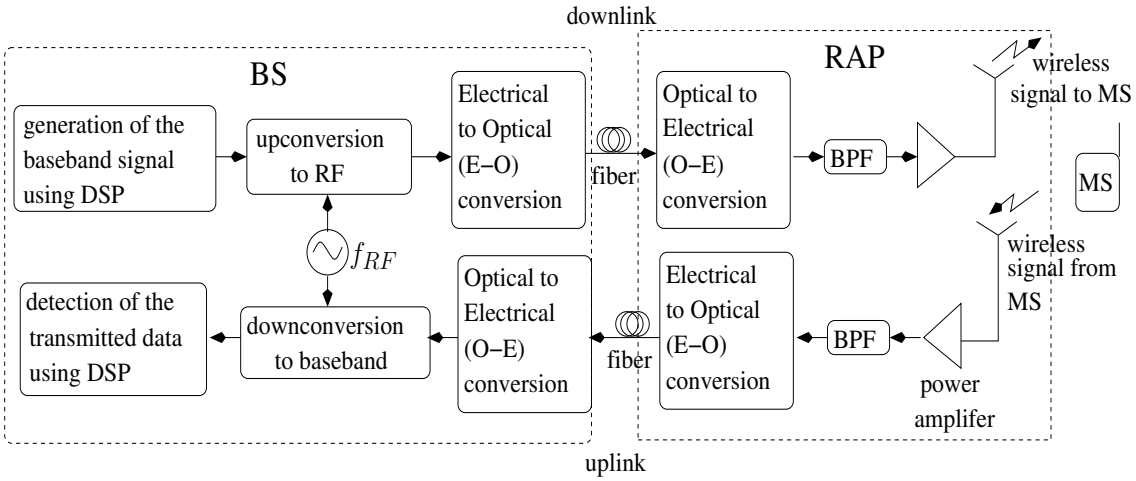

Fig. 3. Block diagram of a ROF link (BS- Base Station; RAP- Radio Access Point; MS- Mobile Station; BPF- Band Pass Filter; DSP- Digital Signal Processing)

1. **Low fiber attenuation**: The low attenuation of glass optical fiber[1] (0.2 dB/Km) effectively facilitates the creation of a geographically distributed large system of antennas that are connected to the central BS, as shown in Fig. 2(b), where the BS is connected to four RAPs via optical fiber. This architecture is referred to as a Distributed Antenna System (DAS) [5], where each BS supports a large geographical coverage area by using optical fibers as long as 30 Km without amplification.

2. **Large fiber bandwidth**: The optical fiber is characterised by large bandwidths and we will discuss the techniques that exploit this large bandwidth in Section IV of this manuscript.

3. **Economically viable small cells**: In a ROF system, each BS serves a number of RAPs as shown in Fig. 2(b), where centralised signal processing takes place at the BS, while the RAPs have a low cost, hence reducing the cost of setting up a cellular system that employs small cells [11]. This is one of the major aims of the architectures and techniques discussed in Sections II and VI of this paper. Moreover, the concentration of most of the signal processing tasks in the BS ensures that upgrades in technology and hardware may be readily carried out in conjunction with efficient dynamic resource allocation techniques [12].

4. **Improved wireless coverage**: As shown in Fig. 2(a), there exists regions that do not receive the wireless signal with sufficient field strength in the existing cellular architecture. The area of these low-signal-strength regions is minimized in a ROF assisted cellular architecture, as shown in Fig. 2(b) [2].

5. **Ability to implement Multiple Input Multiple Output (MIMO) schemes** [13]: The wireless communication schemes that employ multiple transmitters and receivers for supporting a single mobile user are referred to as MIMO schemes [14], [15]. The parallel MIMO links either create multiple streams and hence increase the achievable throughput, or provide a diversity gain by exploiting the fact that each RF link fades independently. The DAS architecture facilitates the design of networks in which each MS of Fig. 2(b) is served by multiple RAPs, as in the Co-ordinated Multipoint (CoMP) architecture discussed in [8]. Thus, efficient MIMO schemes may be constructed with the aid of a ROF network [3].

6. **Power Efficiency**: The deployement of smaller cells, as is seen from Fig. 2(b), provides a stronger line of sight link and ensures a lower wireless path loss [2]. Hence, a lower level of wireless transmit power is needed at the RAPs, which has the added advantage of reduced inter-cell interference [16].

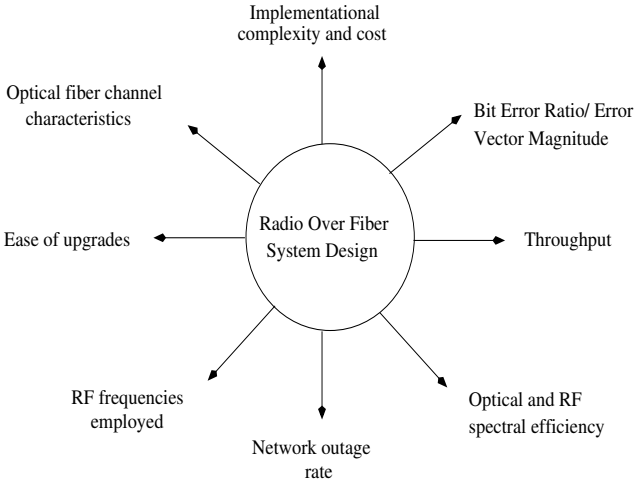

Fig. 4. Stylized representation of the design challenges involved in the design of the ROF network

Fig. 4 illustrates the various design challenges of the ROF network. For example, the deployement of higher RF frequencies results in higher fiber dispersion, which degrades the Bit Error Ratio (BER). The BER may be reduced by using dispersion compensation mechanisms, which however increase the implementational complexity and cost of the system. Alternatively, the BER may be reduced by using lower-order modulation schemes, which would however reduce the overall throughput. On the other hand, the overall throughput may be improved by ensuring better optical spectral efficiency through schemes like Dense Wavelength Division Multiplex-

[1]The terminology of glass optical fibers refers to fibers made from silica.

This article has been accepted for publication in a future issue of this journal, but has not been fully edited. Content may change prior to final publication. Citation information: DOI 10.1109/COMST.2015.2394911, IEEE Communications Surveys & Tutorials

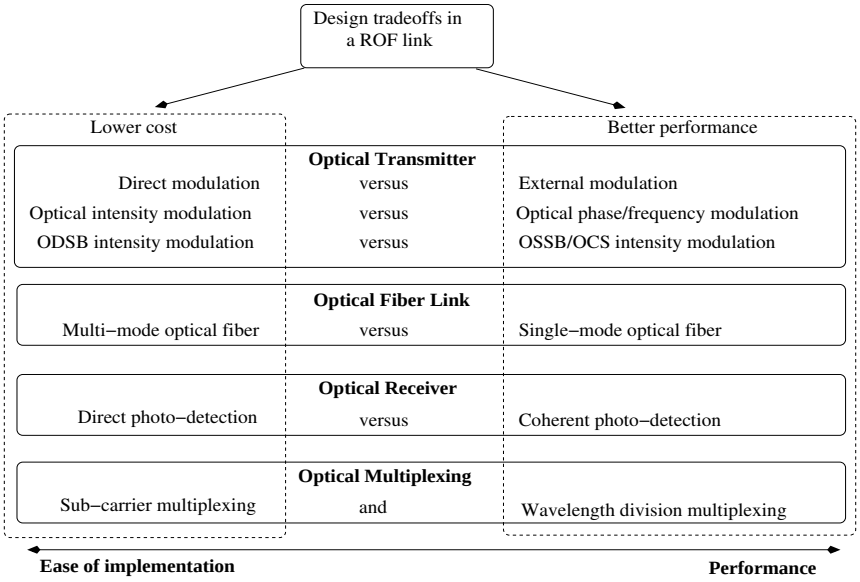

Fig. 5. Design trade-offs in the design of a conventional ROF link(ODSB- Optical Double Side Band; OSSB- Optical Single Side Band; OCS- Optical Carrier Suppressed

ing (DWDM), which however would increase the implementational complexity and cost. The network outage rate or probability featuring in Fig. 4 is defined as the proportion of time for which the network is unable to serve the MSs. A common reason for outage is that the RAP is overloaded by a large number of MSs and hence it is unable to maintain the minimum signal to interference plus noise ratio required for communication with each MS [17]. The outage rate is also increased by shadowing imposed by large obstructing structures, as in Fig. 2(a) [17]. The network outage rate can be reduced by having a larger number of RAPs, which would reduce both shadowing as well as the load (or MSs) per RAP. However, this would increase the system's cost and complexity. Thus, most design questions usually boil down to a cost versus performance tradeoff. This manuscript presents a range of techniques that are either aimed at cost reduction or at performance improvement.

Comparison with other backhaul techniques: Wireless backhauls like the microwave backhaul are competing backhaul techniques. The advantage of the wireless backhaul is that the installation cost does not scale significantly with the distance between the transmitter and receiver. Moreover, a wireless backhaul can be readily installed as well as disassembled and set up elsewhere [18]. However, a wireless backhaul also suffers from several disadvantages. Firstly, it requires wireless spectrum, which could otherwise have been employed for wireless communication with mobile devices. Moreover, in the case of a microwave backhaul, line of sight communication is a necessity [18]. Finally, a wireless backhaul is influenced by the climatic conditions [18]. On the other hand, a fiber-based backhaul does not require wireless spectrum and has much higher usable bandwidth than the wireless backhaul. Additionally, a fiber-based backhaul does not require line of sight communication and it is not influenced by the climatic conditions [18]. However, the installation cost of a fiber-based backhaul is higher than that for a wireless backhaul, especially when the terrain is rough and this cost increases as the distance between the transmitter and receiver increases. Finally, a fiber-based backhaul, unlike the wireless backhaul, cannot be deployed or moved easily [18]. At this point it is worth noting that a copper wire based backhaul has severe bandwith restrictions and is being gradually phased out.

When employing the fiber-based backhaul, the designer has two options, namely the standard digital fiber-based backhaul or the ROF backhaul proposed in this paper. In case of the digital PCM-over-fiber backhaul, each small cell of Fig. 2(b) would need a fullfledged BS for detecting/transmitting the wireless signal as well as for transmitting/detecting the bits to/from the backhaul, which employs protocols like the Ethernet protocol. However, as discussed earlier, a ROF backhaul will ensure that multiple cells are served by a single BS, as shown in Fig. 2(b), thereby reducing the network's installation cost. Moreover, the ROF technique involves the transmission of the analog RF signal to the BS and hence it will reduce the latency, because the signal processing carried out in the RAP is minimized. ROF is a potential backhaul technique for the Long Term Evolution (LTE) advanced [19] [20] standard as well as for future millimeter wave standards [21]. The fewer BSs of a ROF assisted cellular network may be served by a digital fiber optic backhaul or a wireless backhaul. At this point, it is worth mentioning that standards like the Open Base Station Architecture Initiave (OBSAI) ensure compatibility between the different BS modules manufactured by different companies, thereby resulting in cost savings.

This paper firstly discusses the components and modulation schemes of a basic ROF link in Sections II and III, repectively. A range of optical multiplexing techniques are then described in Section IV, followed by a discussion on diverse ROF link performance improvement techniques in Section V. Afterwards, a discussion of cost reduction techniques is

This article has been accepted for publication in a future issue of this journal, but has not been fully edited. Content may change prior to final publication. Citation information: DOI 10.1109/COMST.2015.2394911, IEEE Communications Surveys & Tutorials

presented in Section VI, followed by our design guidelines and conclusions in Sections VIII and IX, respectively. It must be pointed out that throughout this paper, f_i refer to frequencies, while ω_i refer to the corresponding angular frequency, which are related as follows:

$$\omega_i = 2\pi f_i. \quad (1)$$

II. ROF COMMUNICATIONS BASICS

The block diagram of a typical ROF link is shown in Fig. 3 [7]. The downlink (DL) baseband (BB) signal is generated in the BS and upconverted to the carrier frequency in order to generate the RF signal. After the upconversion stage of Fig. 3, E-O conversion is achieved by modulating the optical carrier by the analog RF signal [22] [23] using the techniques discussed in Section II-A. Then, as seen in Fig. 3, the signal propagates through the fiber to the RAP. The various fiber impairments that affect the propagating optical signal are discussed in Section II-B. At the RAP of Fig. 3, O-E conversion is achieved using the techniques that will be discussed in Section II-C, where the electronic signal generated by the O-E conversion is filtered using a Band Pass Filter (BPF), in order to obtain the RF signal. As shown in Fig. 3, this RF signal is then amplified and transmitted wirelessly by the antenna to the MS. During the uplink (UL) transmission, the RF signal received by the RAP from the MS is bandpass filtered and E-O converted in order to generate the optical UL signal, which is then transmitted over the fiber and subsequently O-E converted, followed by signal detection. It is worth mentioning that the wireless system of Fig. 3 is also referred to as a Fi-Wi system, whose basics have been discussed in [9], along with a discussion of FiWi channel estimation and equalization algorithms.

Fig. 5 shows the trade-offs in the design of a conventional ROF link, including the various design options in the optical transmitter, optical fiber link, optical receiver and in optical multiplexing. These design options present the designer with a cost versus performance trade-off. The techniques shown in Fig. 5 are discussed in this Section (Section II) as well as in Sections III and IV.

A. *Modulation Techniques*

As shown in Fig. 3, E-O conversion is performed by optical modulation. Modulation of the optical carrier can be achieved by either directly modulating the optical source or by using a separate optical modulator. These two techniques are typically referred to as direct modulation and external modulation, respectively.

In **direct modulation**, a Laser Diode (LD) is driven by a current I_{drive} in order to generate an optical output [24]. As shown in Fig. 6(a), modulation of the optical output power[1] of a laser can be inexpensively accomplished by varying the drive current level using an electronic RF Transmitter, referred to as RF Tx in Fig. 6(a). This is normally referred to as direct

[1]Optical power can also be measured in terms of optical intensity, which is defined as the optical power per unit area

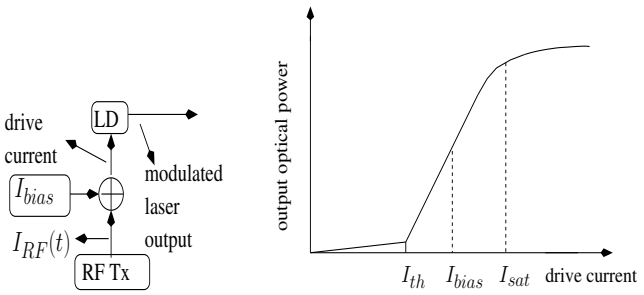

(a) Direct modulation setup (b) Power vs. drive current curve of a laser

Fig. 6. Direct modulation (LD- Laser Diode; RF Tx- RF Transmitter)

modulation of lasers. Fig. 6(b) illustrates the Power vs. Current (P-I) characteristic of a laser, showing in a stylized manner the output optical power level for different values of the drive current. Within the linear region of the P-I characteristic in Fig. 6(b), the output power is related to the drive current as follows: $P(t) = k(I_{drive} - I_{th}) = k(I_{bias} + I_{RF}(t) - I_{th})$, where I_{th} is the threshold current of the laser, I_{bias} is the bias current, $I_{RF}(t)$ is the modulating RF signal, while k is the proportionality constant that depends on the laser source employed.

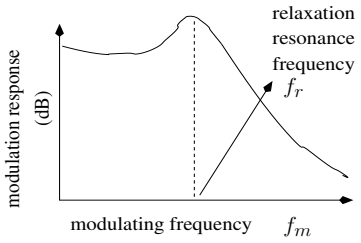

Fig. 7. Direct modulation bandwidth of the laser

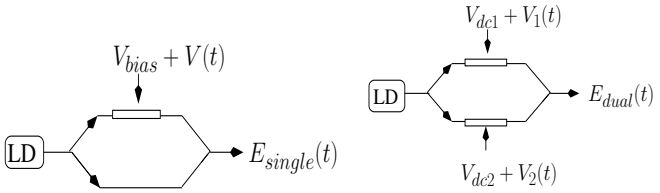

(a) Single Drive MZM (b) Dual Drive MZM

Fig. 8. Single and Dual-drive Mach Zehnder Modulator (MZM) external modulators (LD- Laser Diode)

Fig. 7 plots the modulation response versus the modulation frequency, where the modulation response at f_m Hz is the strength of the modulated signal when a sinusoidal modulating signal having a frequency of f_m Hz is employed. As seen from Fig. 7, the modulation response peaks at $f_m = f_r$, beyond which the modulation response decreases dramatically. Here, f_r is called the relation resonance frequency and it decides the 3-dB modulation bandwidth f_{3dB} of the laser, where $f_{3dB} = \sqrt{3} f_r$ [24]. The designer should ensure that the modulating current has frequencies which are well below f_r.

Furthermore, the optical carrier is a sinusoidal signal, also often referred to as a tone, that has an amplitude, phase and frequency. The Frobenius norm of the tone is referred to as

This article has been accepted for publication in a future issue of this journal, but has not been fully edited. Content may change prior to final publication. Citation information: DOI 10.1109/COMST.2015.2394911, IEEE Communications Surveys & Tutorials

the intensity. Both the intensity [25] and the angle [26] of the optical carrier can be modulated using **external modulators**. External intensity modulation can be implemented using a Mach-Zehnder Modulator (MZM) or an Electro-Absorption Modulator (EAM).

A MZM [27] is one of the popular optical external modulators, where the incoming signal is split into two arms, as shown in Fig. 8. The MZMs, which apply a drive voltage to either one or to both of the arms are referred to as single-drive and dual-drive MZMs, respectively. The output optical field $E_{single}(t)$ of a single-drive MZM that is biased at a voltage of V_{bias} and driven by an electronic signal $V(t)$ can be represented as follows:

$$E_{single}(t) = \frac{1}{2}[e^{j(\frac{\pi V_{bias}}{V_\pi}+\frac{\pi V(t)}{V_\pi})}+1]\sqrt{2P_{in}}e^{j\omega_c t}$$
$$= \cos(\frac{\pi V_{bias}}{2V_\pi}+\frac{\pi V(t)}{2V_\pi})e^{j(\frac{\pi V_{bias}}{2V_\pi}+\frac{\pi V(t)}{2V_\pi})}\sqrt{2P_{in}}e^{j\omega_c t}, \quad (2)$$

where f_c is the optical carrier frequency, V_π is the switching voltage of the MZM and P_{in} is the ouput optical power of the laser feeding the MZM. The switching voltage of a MZM is the voltage that changes the phase of the propagating signal by π radians, when applied to the arm of a MZM. In the case of the dual-drive MZM of Fig. 8, the bias voltage V_{bias} is applied differentially via voltages V_{dc1} and V_{dc2}, while the modulating voltage $V(t)$ is applied differentially via the voltages $V_1(t)$ and $V_2(t)$. Mathematically, this is formulated as follows: $V_{bias} = V_{dc1} - V_{dc2}$ and $V(t) = V_1(t) - V_2(t)$. The output optical field of the dual-drive MZM is given by the following equation:

$$E_{dual}(t)$$
$$= \frac{1}{2}[e^{j(\frac{\pi V_{dc1}}{V_\pi}+\frac{\pi V_1(t)}{V_\pi})}+e^{j(\frac{\pi V_{dc2}}{V_\pi}+\frac{\pi V_2(t)}{V_\pi})}]\sqrt{2P_{in}}e^{j\omega_c t}$$
$$= \cos(\frac{\pi(V_{dc1}-V_{dc2})}{2V_\pi}+\frac{\pi(V_1(t)-V_2(t))}{2V_\pi})$$
$$e^{j[\frac{\pi(V_{dc1}+V_{dc2})}{2V_\pi}+\frac{\pi(V_1(t)+V_2(t))}{2V_\pi}]}\sqrt{2P_{in}}e^{j\omega_c t} \quad (3)$$
$$= \cos(\frac{\pi V_{bias}}{2V_\pi}+\frac{\pi V(t)}{2V_\pi})$$
$$e^{j[\frac{\pi(V_{dc1}+V_{dc2})}{2V_\pi}+\frac{\pi(V_1(t)+V_2(t))}{2V_\pi}]}\sqrt{2P_{in}}e^{j\omega_c t} \quad (4)$$

The output intensity $P_{single}(t) = |E_{single}(t)|^2$ and $P_{dual}(t) = |E_{dual}(t)|^2$ of the single- and dual-drive MZMs, respectively, can be expressed as follows using Equations (2) and (4):

$$P_{dual}(t) = P_{single}(t)$$
$$= P_{in}[1+\cos(\frac{\pi V_{bias}}{V_\pi}+\frac{\pi V(t)}{V_\pi})]. \quad (5)$$

Fig. 9(a) shows the transmittance plot of a MZM, where the output optical power $P(t)$ of the MZM is plotted for various values of the bias voltage V_{bias}. Modulation can be interpreted as a voltage variation around the bias point. It can be seen from Equations (2) and (4) that the output optical field has exponential terms of the form $e^{j\phi(t)}$. Thus, there is residual phase modulation, which is referred to as chirp. This residual phase modulation is potentially converted to intensity modulation during its transmission over the fiber, thereby

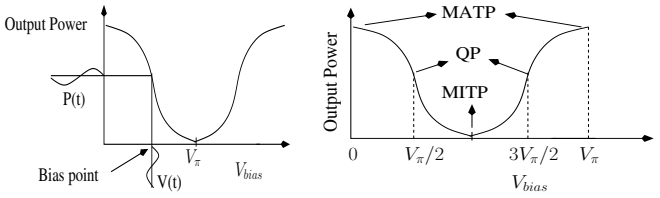

(a) MZM transmittance (b) MZM bias points

Fig. 9. Biasing for Mach-Zehnder Modulator (MZM) (MATP- Maximum Transmission Point; QP- Quadrature Point; MITP- Minimum Transmission Point)

corrupting the signal that was transmitted using intensity modulation. The chirp in a dual-drive scenario is adjustable, where the dual-drive MZM modulation scheme of Fig. 8 would be chirp free if we have: $V_1(t) = -V_2(t) = \frac{V(t)}{2}$. This is referred to as the push-pull mode of operation, because the voltages $V_1(t)$ and $V_2(t)$ are equal in magnitude and opposite in sign.

Fig. 9(b) shows the various MZM biasing techniques that can be employed, which include Quadrature Point (QP) biasing, Minimum Transmission Point (MITP) biasing and Maximum Transmission Point (MITP) biasing. QP biasing corresponds to $V_{bias} = V_\pi/2 + m2V_\pi$ or $V_{bias} = -V_\pi/2 + m2V_\pi$, while MITP biasing corresponds to $V_{bias} = V_\pi + m2V_\pi$, where m is an integer. Furthermore, MATP biasing corresponds to $V_{bias} = 0 + m2V_\pi$. When a sinusoidal modulating signal of $V(t) = V_{LO}\cos(\omega_{LO}t)$ is employed, the mathematical expression for the photo-detected signals in each of these biasing scenarios can be obtained from Equation (5) as follows:

$$I_{QP}(t) \propto P_{QP}(t)$$
$$= P_{in}\left[1 \mp \sin(\frac{\pi V_{LO}\cos(\omega_{LO}t)}{V_\pi})\right] \quad (6)$$
$$= P_{in}\left[\frac{1}{2} \pm \sum_{n=1}^{\infty}(-1)^n J_{2n-1}(\frac{\pi V_{LO}}{V_\pi})\cos((2n-1)\omega_{LO}t)\right]$$
$$I_{MITP}(t) \propto P_{MITP}(t)$$
$$= P_{in}\left[1-\cos(\frac{\pi V_{LO}\cos(\omega_{LO}t)}{V_\pi})\right]$$
$$= P_{in}\left[1 - J_0(\frac{\pi V_{LO}}{V_\pi})\right.$$
$$\left. - 2\sum_{n=1}^{\infty}(-1)^n J_{2n}(\frac{\pi V_{LO}}{V_\pi})\cos(2n\omega_{LO}t)\right] \quad (7)$$

(8)

$$I_{MATP}(t) \propto P_{MATP}(t)$$
$$= P_{in}\left[1+\cos(\frac{\pi V_{LO}\cos(\omega_{LO}t)}{V_\pi})\right]$$
$$= P_{in}\left[1 + J_0(\frac{\pi V_{LO}}{V_\pi})\right.$$
$$\left. + 2\sum_{n=1}^{\infty}(-1)^n J_{2n}(\frac{\pi V_{LO}}{V_\pi})\cos(2n\omega_{LO}t)\right] \quad (9)$$

This article has been accepted for publication in a future issue of this journal, but has not been fully edited. Content may change prior to final publication. Citation information: DOI 10.1109/COMST.2015.2394911, IEEE Communications Surveys & Tutorials

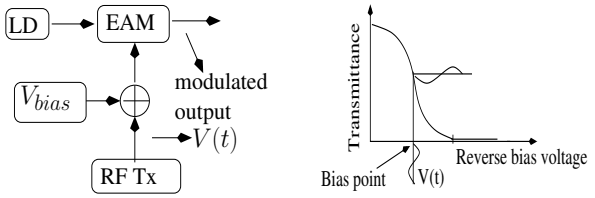

(a) optical modulation using an EAM

(b) EAM Transmittance vs. applied voltage

Fig. 10. External modulation using an Electro-Absorption Modulator (EAM) (LD- Laser diode; RF Tx- RF Transmitter)

On the other hand, as shown in Fig. 10(a), an Electro-Absorption Modulator (EAM) modulates the intensity of the optical signal by using an electric voltage that controls the absorbtion[1] of the modulator, which is referred to as the Franz-Keldysh effect [28]. As the reverse bias voltage V_{bias} of the EAM increases, the amplitude of the output optical field is reduced by a factor of $T(V)$, where $T(V)$ is the amplitude transmittance.

Fig. 10(b) shows the variation of $T(V)$ as a function of the reverse bias voltage applied [29], where $T(V) = 0$ corresponds to complete extinction of the MZM output, while $T(V) = 1$ corresponds to the extinction-free scenario. The output optical field $E(t)$ of the EAM modulator seen in Fig. 10(a), that is biased at a voltage of V_{bias} and driven by an electronic signal $V(t)$ is given by the following expression : $E(t) \propto T(V_{bias} + V(t))$.

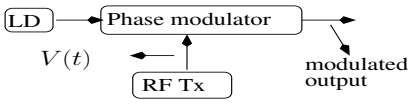

Fig. 11. Optical phase modulator (LD- Laser Diode; RF Tx- RF Transmitter)

Additionally, external optical phase modulation is implemented in ROF links using an optical phase modulator. This is implemented by using the same concept as in the MZMs of Fig. 8 with the difference that a phase modulator, unlike the MZM, has a single arm. If an electronic signal $V(t)$ is used for driving a phase modulator as shown in Fig. 11, then the output optical field may be written as: $E(t) = e^{j\frac{\pi V(t)}{2V_\pi}}\sqrt{2P_{in}}e^{j\omega_c t}$, where f_c is the optical carrier frequency, V_π is the switching voltage of the phase modulator and P_{in} is the operating laser power.

External modulation is more expensive than direct modulation due to the need for additional equipment, while the direct modulation of lasers suffers from several drawbacks, thereby giving rise to the cost versus performance trade-off alluded to in Fig. 5. Firstly, the modulation bandwidth of directly modulated lasers, shown in Fig. 7, restricts the spectrum of usable modulating signals, while the saturation of the P-I characteristics of Fig. 6(b) limits the output power of directly modulated lasers. Additionally, direct modulation of the laser's output intensity is accompanied by undesired frequency modulation. Finally, if a laser is directly modulated using signals having frequencies close to f_r in Fig. 7, then both the non-linear products and noise in the modulated output increased.

Let us now discuss the various aspects of the fiber channel employed in a ROF link.

B. *Fiber Impairments*

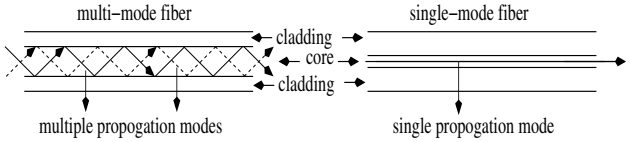

Fig. 12. Multi-mode and single-mode fiber

An optical fiber consists of an inner core through which the light propagates and an outer cladding. Optical fibers may operate either in a single-mode or in multi-mode fashion, depending on whether single or multiple propagation modes exist in the fiber. Fig. 12 shows the propagation modes of the single-mode and multi-mode fiber, where the cross-section of the core in the multi-mode fiber is larger than that of the single-mode fiber [30]. All the architectures considered in this paper employ Single-Mode Fiber (SMF), because it provides a larger optical bandwidth and hence it is capable of supporting longer transmission distances without a repeater [30]. However, we hasten to add that the cost of multi-mode fibers is lower than that of a single-mode fiber, thereby giving rise to the cost versus performance trade-off alluded to in Fig. 5.

Fiber impairments refer to the fiber characteristics that affect the signal transmitted in the fiber. This includes attenuation, dispersion and non-linearities, as discussed below.

Firstly, the signal power decreases as the signal propagates through the optical fiber, which is due to the impurities of the material and owing to Rayleigh scattering [24]. This results in **fiber attenuation**. Mathematically, the net signal power attenuation imposed by the optical fiber can be expressed as follows: $P_{received} = P_{transmitted}\ e^{-\alpha z}$, where $P_{transmitted}$ is the optical power that is coupled into the optical fiber, $P_{received}$ is the optical power after propagation through z km of the fiber and α is the fiber attenuation constant, which has a typical value of 0.2 dB/Km [24].

Secondly, there is **fiber dispersion**, where the refractive index $n(\omega)$ of the fiber depends on the frequency $f = \frac{\omega}{2\pi}$ of the propagating optical wave [24]. Mathematically, we have $v_p(\omega) = c/n(\omega)$, where $v_p(\omega)$ is the phase velocity of the optical wave as it propagates through the fiber. Thus, the propagation velocity depends on the optical frequency, and this phenomenon results in dispersion. The extent of dispersion is quantified by the dispersion parameter D [24]:

$$D = -\frac{2\pi c}{\lambda_c^2}\beta_2 \text{ where } \beta_2 = [\frac{1}{c}(2\frac{dn}{d\omega} + \omega\frac{d^2n}{d\omega^2})]_{\omega=\omega_c}, \quad (10)$$

where f_c and λ_c are the frequency and wavelength of the optical carrier. This fiber disperison is also referred to as Group Velocity Dispersion (GVD) or chromatic dispersion [24].

Thirdly, a dielectric medium (e.g. a fiber) is an electrical insulator that can be polarized by an appropriately applied

[1]The absorption of an optical device refers to the phenomenon of a portion of the propagating optical power being absorbed by the device material.

This article has been accepted for publication in a future issue of this journal, but has not been fully edited. Content may change prior to final publication. Citation information: DOI 10.1109/COMST.2015.2394911, IEEE Communications Surveys & Tutorials

electric field. **Fiber non-linearity** arises from the fact that the polarization is a non-linear function of the electric field $E(t)$ of the light, especially when the optical intensity is high [24]. This results in a non-linear refractive index as a function of the total propagating signal power $P(t)$. This time-varying $P(t)$-dependent refractive index then modulates the phase of the optical signal. Time-varing phase shifts in turn result in an instantaneous optical frequency deviation from the nominal value of f_c, which is referred to as frequency chirping. Phase modulation arising from fiber-nonlinearity includes Self-Phase Modulation and Cross-Phase Modulation [24]. Self-Phase Modulation (SPM) occurs because of the time-varying nature of the propagating signal's own instantaneous power [24], while, Cross-Phase Modulation (XPM) occurs when multiple optical signals are transmitted simultaneously. In XPM, the extent of nonlinear distortion imposed on each channel depends not only on its own optical power, but also on the optical power of the co-propagating signals [24].

On the other hand, the non-linear interaction of multiple optical signals that are propagating in a single optical fiber leads to the generation of optical signals at new frequencies. This phenomenon is typically referred to as Four-Wave Mixing (FWM) [24]. For example, when the signals having optical frequencies of f_1, f_2 and f_3 Hz are propagating in the fiber, FWM results in the generation of an optical signal at $f_{FWM} = f_1 \pm f_2 \pm f_3$ Hz, where the most significant contributions are those at [24]:

$$f_{FWM} = f_i + f_j - f_k, \tag{11}$$

where, we have $i, j, k \in 1, 2, 3$. The above expression includes frequencies of the form

$$f_{FWM,1} = 2f_i - f_j \tag{12}$$

FWM becomes most significant at low absolute values of the dispersion parameter D [24].

Finally, there are other major non-linear effects including Stimulated Brillouin Scattering (SBS) and Stimulated Raman Scattering (SRS) [24], where photons of the incident field get annhilated in both cases. In other words, optical energy is transferred from a signal propagating at a particular optical frequency to a signal at a lower frequency. SBS occurs in the backward direction, where the lower frequency optical signal propagates in a direction that is opposite to that of the incident higher frequency signal, while SRS can occur in both directions [24].

Now that we have discussed both optical modulation and fiber based transmission, we will continue our discourse by considering optical photo-detection.

C. *Photo-detector*

Photo-detection is the process of detecting an optical signal using a photo-diode (PD), where a PD generates an electronic current that is proportional to the incident optical power. This process is referred to as square-law photo-detection, where the responsivity R of a PD is the ratio of the output photo-current to the incident optical power. The basic types of photo-detection are direct photo-detection [22] and coherent photo-detection [24]. In the direct photo-detection of 13(a), if $E_s(t)$ is the optical field of the received signal, then the generated photo-current $I(t)$ is $I(t) = R|E_s(t)|^2$ [22]. Thus, in direct photo-detection, the intensity $|E_s(t)|^2$ of the received optical signal should be modulated by electronic modulating signal in order to enable the reconstruction of the modulating signal using direct photo-detection in the receiver. On the other hand, in coherent photo-detection, the received optical signal is mixed with the output of a laser that serves as a local oscillator, followed by their joint photo-detection. Mathematically, this can be represented as $I(t) = R|E_s(t) + E_{lo}(t)|^2$, where $E_s(t)$ and $E_{lo}(t)$ are the optical fields of the received optical signal and the local oscillator signal, respectively. Expanding this expression would result in one of the terms being a product of the two fields, which is referred to as the beat signal. In heterodyne photo-detection, the optical frequency of the $f_{lo} = \frac{\omega_{lo}}{2\pi}$ Hz local oscillator is different from the carrier frequency $f_s = \frac{\omega_s}{2\pi}$ Hz of the incident optical signal. In this scenario, the photo-detected signal $I(t)$ is given by:

$$\begin{aligned} I(t) &= R|A_s e^{j\omega_s t + \phi_s} + A_{lo} e^{j\omega_{lo} t + \phi_{lo}}|^2 \\ &= R[A_s^2 + A_{lo}^2 + 2|A_s||A_{lo}| \cos(\omega_{diff} t + \phi_s - \phi_{lo})], \end{aligned} \tag{13}$$

where $f_{diff} = f_s - f_{lo}$, A_s and A_{lo} are the amplitudes of the received optical signal and the local oscillator signal, respectively, while ϕ_s and ϕ_{lo} are the phases of the two optical fields. Fig. 13(b) shows how heterodyne photo-detection can be carried out for the upconversion of the BB/IF signal to an RF frequency of f_{rf} Hz, which can be done by ensuring that we have $f_{diff} = f_{rf}$ and then filtering the photo-detected signal to retain the beat signal.

Direct photo-detection is simpler and hence more cost-effective than coherent photo-detection, while coherent photo-detection provides a better performance, thereby giving rise to the cost versus performance trade-off seen in Fig. 5.

The discussions so far assumed a noise-free optical link, while the next section details the various sources of noise in a ROF link.

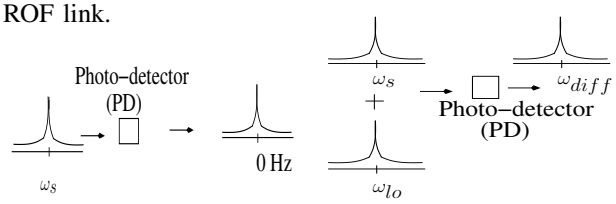

(a) Direct photo-detection (b) Heterodyne photo-detection

Fig. 13. Basic types of photo-detection (PD- Photo-diode)

D. *Noise in a ROF link*

There are various sources of noise in a ROF link, including the Relative Intensity Noise (RIN), Amplified Spontaneous Emission (ASE) noise, shot noise and the receiver's thermal noise, where Δf is the bandwidth over which the noise power is measured at the receiver [24]. The output of a laser that is driven using a constant current exhibits certain fluctuations in the output phase, frequency and intensity [24],

This article has been accepted for publication in a future issue of this journal, but has not been fully edited. Content may change prior to final publication. Citation information: DOI 10.1109/COMST.2015.2394911, IEEE Communications Surveys & Tutorials

which constitutes the above-mentioned **RIN**. The primary source of this is the spontaneous emission of photons, where the intensity noise results in a SNR degradation, while the phase/frequency noise leads to a non-zero spectral linewidth (splillage) around the output frequency [24]. Mathematically, the RIN noise power is formulated as follows [24]:

$$\sigma^2_{RIN} = K_{RIN} I^2_{dc} \Delta f, \tag{14}$$

where K_{RIN} is a device dependent value, which is usually expressed in dB/Hz and I_{dc} is the average photo-current value. Typically K_{RIN} has values around -150 dB/Hz. It can be seen from Equation (14) that the RIN is proportional to the square of the mean optical power. However, when the depth of optical modulation is high, especially in a ROF link that employs the subcarrier multiplexing of several RF signals, an improved expression for RIN was derived in [31], which reflected the enhanced presence of RIN owing to its dependence on the depth of optical modulation [31]. The concept of subcarrier multiplexing will be discussed in Section IV-A. Additionally, the **ASE** noise alluded to above is produced by spontaneous emission in an optical amplifier, which is then amplified by the amplifier's gain mechanism [24]. Furthurmore, **Shot Noise** is a quantum noise effect that is present in the photo-detected signal, which arises from the fact that the optical field and the electric current consists of discrete entities referred to as photons and electrons, respectively [24]. Mathematically, the shot noise power is given by [24]:

$$\sigma^2_{shot} = 2eI_{dc}\Delta f, \tag{15}$$

where e is the charge carried by an electron. Finally, the load resistor and the electronic amplifiers in the optical receiver impose **Thermal Noise**, owing to the temperature-dependent random Brownian motion of the electrons [24]. Mathematically, the thermal noise power can be expressed as [24]:

$$\sigma^2_{thermal} = \frac{4k_b T}{R_L}\Delta f, \tag{16}$$

where k_b is the Boltzmann constant, T is the abolute temperature, R_L is the load resistance, while F_n is the amplifier noise figure.

E. Wireless channel

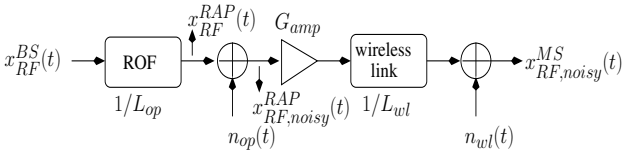

Fig. 14. **Block diagram of losses/gains in ROF enabled DL wireless transmission, as discussed in [32]**

The wireless channel is normally modelled using Gaussian, Rayleigh or Rician distributions, where the signal y received over a wireless channel H can me modelled as [15]:

$$y = Hx + n, \tag{17}$$

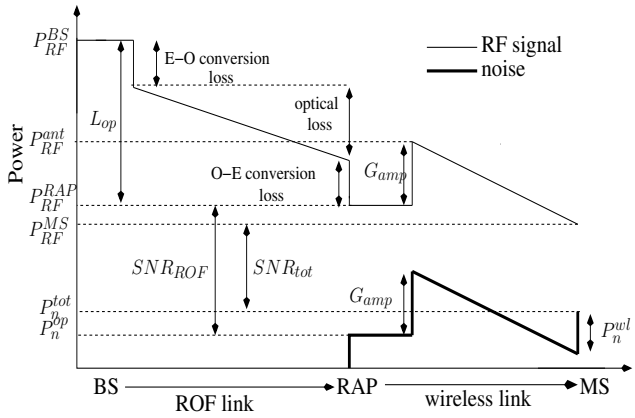

Fig. 15. **power budgeting as discussed in [32]**

where$x$ is the transmitted symbol matrix, n is the Gaussian noise matrix, while H is the channel matrix. H is unitary for a Gaussian wireless channel, while it consists of Rayleigh and Rician distributed channel co-efficients for a fading channel obeying a Rayleigh and Rician distribution, respectively [15]. In the case of millimeter wave communications, the wireless channel has a higher free-space pathloss, which can however be overcome by employing beamforming using directional antennas. Directional antennas consist of an array of antennas, whose outputs constructively interfere in some directions, while destructively interfering in other directions. For a detailed study of the millimeter-wave wireless channel and beamforming, the reader is referred to [21] and [33]. Futhermore, for a comprehensive study of the wireless channel, the reader is referred to [15], since this paper focuses on the optical aspects of the ROF link. Nevertheless, in this section we focus on radio-communication issues, which have a direct bearing on the ROF backhaul design, including power budgeting and the presence of accumulating noise [32], [31]. The significance of these issues are illustrated by considering the simple case of a ROF DL that does not employ optical amplification and has a Gaussian wireless channel. Fig. 14 and Fig. 15 portray a diagrammatic representations of the gains and losses in such an ROF link. The RF signal $x^{BS}_{RF}(t)$ having a power of P^{BS}_{RF} is attenuated by a factor of L_{op} by the ROF link, resulting in the photo-detected signal $x^{RAP}_{RF}(t)$ having a power of P^{RAP}_{RF}. The attenuation L_{op} includes that arising from the E-O conversion, fiber propagation, insertion loss of optical components and the O-E conversion. Using Equations (14), (15) and (16), the noise $n_{op}(t)$ imposed by the ROF link has a power of:

$$P^{op}_n = \sigma^2_{RIN} + \sigma^2_{shot} + \sigma^2_{thermal}. \tag{18}$$

It is worth noting here that when spread spectrum wireless techniques like Code Division Multiple Access (CDMA) are employed, a larger wireless bandwidth is desired. However, this also increases P^{op}_n. The optical noise is accounted for in Fig. 14 by adding it to $x^{RAP}_{RF}(t)$ for generating $x^{RAP}_{RF,noisy}(t)$, as shown in Fig. 14. As shown in Fig. 14 and Fig. 15, the

This article has been accepted for publication in a future issue of this journal, but has not been fully edited. Content may change prior to final publication. Citation information: DOI 10.1109/COMST.2015.2394911, IEEE Communications Surveys & Tutorials

noise contaminated photo-detected signal is then amplified by a factor of G_{op}, where P_{RF}^{ant} is the power of the signal (without noise) that is transmitted from the antenna. The transmitted signal undergoes a wireless pathloss induced attenuation of L_{wl}, as shown in Fig. 14, and is finally received at the MS, where the noise $n_{wl}(t)$ having a power of P_n^{wl} is added by the wireless link. The signal that is finally employed in the MS is $x_{RF,noisy}^{MS}(t)$. It must be noted that in Fig. 14, L_{wl} and G_{amp} are amplitude attenuation and amplification values, while power attenuation/amplification refers to their squared values.

Radio cell size calculations based on cumulating noise and fiber attenuation is derived in [32] and [9]. Following that model, Equation (27) can be obtained as follows.

It can be seen from Fig. 15 that the Signal to Noise Ratio (SNR) of the ROF link (measured after photo-detection in RAP) as well as that of the total link including the optical and wireless transmission (measured in the MS), are as follows [32]:

$$SNR_{ROF} = \frac{P_{RF}^{RAP}}{P_n^{op}}, \tag{19}$$

$$SNR_{tot} = \frac{P_{RF}^{MS}}{P_n^{tot}}, \tag{20}$$

where P_{RF}^{RAP} depends on the operating laser power, on the depth of optical modulation and on L_{op} [32]. Furthermore, the following is evident from Fig. 15 [32]:

$$P_{RF}^{MS} = P_{RF}^{RAP}\left(\frac{G_{amp}}{L_{wl}}\right)^2 \tag{21}$$

$$P_n^{tot} = P_n^{op}\left(\frac{G_{amp}}{L_{wl}}\right)^2 + P_n^{wl}. \tag{22}$$

Assuming that the wireless noise power is k times that of the optical noise power, Equation (22) can be written as:

$$P_n^{tot} = P_n^{op}\left(\frac{G_{amp}}{L_{wl}}\right)^2 [1 + k\left(\frac{L_{wl}}{G_{amp}}\right)^2], \tag{23}$$

where $k \approx 1$ correponds to both the wireless and optical noise having similar powers, while $k \gg 1$ or $k \ll 1$ correponds to the wireless noise being much stronger or much weaker than the optical noise, respectively. In the following analysis, we focus our attention on the scenario, where $k \approx 1$, because the other scenarios can be analysed in a similar manner. Furthermore, as stated earlier, L_{wl} is the signal amplitude attenuation of wireless propagation. However, the wireless path loss L_{db} is usually specified in decibels and it refers to the power attenuation during wireless propagation, i.e. $L_{wl}^2 = 10^{\frac{L_{dB}}{10}}$. Using this relation as well as substituting Equations (19), (21) and (23) into Equation (20), we arrive at [32]:

$$SNR_{tot} = SNR_{ROF}\frac{1}{1 + k\frac{10^{\frac{L_{dB}}{10}}}{G_{amp}^2}} \tag{24}$$

$$= SNR_{ROF}\frac{1}{1 + \frac{10^{\frac{L_{dB}}{10}}}{G_{amp}^2}} \text{ for k} \approx 1. \tag{25}$$

Equation (25) helps us understand the limitations imposed on the design of the ROF link by the requirements of the wireless link, as discussed in terms of the minimum RAP amplifier gain and maximum cell size in the following sections.

a) Minimmum RAP amplifier gain: Given a ROF link having a SNR of SNR_{ROF}, Equation (25) allows us to calculate the minimum gain G_{amp}^{min} of the electronic amplifier in the RAP, which is necessary for supporting a cell size that correponds to a maximum loss of L_{dB}^{max} at the cell boundary, where $SNR_{tot} \geq SNR_{tot}^{worst}$ always has to be maintained in the MS. Using Equation (25), G_{amp}^{min} is formulated as follows [32]:

$$G_{amp}^{min} = \sqrt{\frac{\frac{L_{dB}^{max}}{10}}{\frac{SNR_{ROF}}{SNR_{tot}^{worst}} - 1}} \text{ for k} \approx 1. \tag{26}$$

A fundamental design limitation that can be observed from Equation (26) is that SNR_{ROF} should be higher than the worst-case SNR expected at the cell boundary [32].

b) Cell size: Assuming that the electronic amplifier in the RAP has a gain of G_{amp} and that a worst-case SNR of SNR_{tot}^{worst} has to be maintained at the cell boundary using a ROF link having a SNR of SNR_{ROF}, we can calculate the maximum affordable wireless pathloss to be [32]:

$$L_{dB}^{max} = 10\log([\frac{SNR_{ROF}}{SNR_{tot}^{worst}} - 1]G_{amp}^2) \text{ for k} \approx 1. \tag{27}$$

It can be observed from Equation (27) that a larger cell, i.e. a larger L_{dB}^{max}, requires a larger SNR_{ROF}, i.e. a lower fiber length.

It can be concluded from the above discussion that SNR_{ROF} maximization is critical for the design of a ROF link. It can be seen from Fig. 15 that SNR_{ROF} is maximized by limiting the length of the fiber used. Alternatively, it can be improved by reducing the E-O and O-E conversion losses through the use of reactive matching circuits instead of resistive matching circuits. However, this would limit the RF bandwidth of the ROF link [32].

Our discourse on modulation techniques in Section II-A introduced the various optical modulators, while the discussion in Section III will cover the commonly employed modulation schemes.

III. Common ROF Optical Modulations Schemes

ROF systems may rely on modulating either the intensity or the angle, i.e. phase/frequency, of the optical carrier. In the following sections we will describe the optical intensity modulation and the optical angle modulation.

A. *Optical Intensity Modulation*

By definition, Intensity Modulation (IM) involves the modulation of the intensity[1] of the optical signal by the modulating electronic signal, where detection can be carried out by using both the direct or coherent photo-detection schemes discussed

[1]The intensity of an optical signal is the square of its amplitude.

This article has been accepted for publication in a future issue of this journal, but has not been fully edited. Content may change prior to final publication. Citation information: DOI 10.1109/COMST.2015.2394911, IEEE Communications Surveys & Tutorials

in Section II-C. Intensity modulation may be of single-sideband or double-sideband nature or may result in a carrier suppressed output. The corresponding Optical Double Side Band (ODSB), Optical Single Side Band (OSSB) and Optical Carrier Suppression (OCS) intensity modulation schemes are described in the following sections.

*1) **Optical Double Side Band Intensity Modulation**:* Fig. 16(a) shows the stylized spectrum of an ODSB signal, which consists of the optical carrier frequency f_c as well as of the lower and upper optical sidebands. If the centre frequencies of the lower and upper optical sidebands are f_{lower} and f_{upper} respectively, then in Fig. 16(a) we have $f_c - f_{lower} = f_{upper} - f_c = f_{rf}$ [34], where f_{rf} is the center frequency of the modulating RF signal. Direct modulation of lasers and external modulation using an EAM can be invoked for generating an ODSB signal [23]. Additionally, an ODSB signal may be generated by the single-drive MZM of Fig. 8(a), by setting $V_{bias} = V_\pi/2 + m2V_\pi$ or $V_{bias} = -V_\pi/2 + m2V_\pi$ in Equations (5), where m is an integer [25], [35] and $V(t)$ is the RF signal to be transmitted. The specific bias condition employed for generating ODSB signals is referred to as quadrature biasing. The same condition is true for the dual-drive MZM of Fig. 8(b), along with the additional condition that there should be a phase difference of π between the RF signals $V_1(t)$ and $V_2(t)$ in Equation (5).

While the ODSB signal of Fig. 16(a) has two modulation sidebands, the OSSB signal to be discussed in the next section has a single modulation sideband.

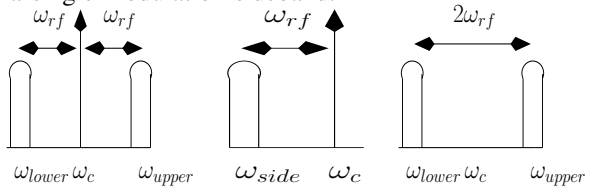

(a) ODSB signal (b) OSSB signal (c) OCS signal

Fig. 16. Optical modulation formats (ODSB- Optical Double Side Band; OSSB- Optical Single Side Band; OCS- Optical Carrier Suppression)

*2) **Optical Single Side Band Intensity Modulation**:* Fig. 16(b) shows the stylized spectrum of an OSSB signal, which consists of the optical carrier frequency f_c and only one of the two possible sidebands at $f_{sideband}$ Hz. As seen from Fig. 16(b), we have $f_c - f_{sideband} = f_{RF}$, where f_{RF} is the frequency of the modulating RF signal. There are several techniques that can be employed for generating OSSB signals, including the employement of the Fiber Bragg Gratings (FBGs) [36] and the Dual-Drive MZM of Fig. 8(b).

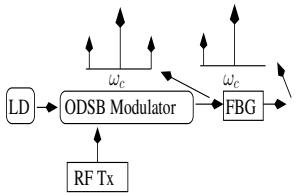

Fig. 17. OSSB generation using a Fiber Bragg Grating (FBG) (LD-Laser Diode; RF Tx- RF Transmitter)

A FBG can be used for filtering out one of the sidebands of an ODSB signal, as shown in Fig. 17 [36]. A FBG filter

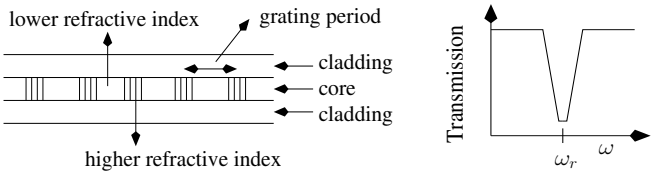

(a) A FBG filter (b) FBG transmission

Fig. 18. Structure and transmission spectrum of a Fiber Bragg Grating

consist of a periodic perturbation of the effective refractive index along the length of the fiber core, as shown in Fig. 18(a) [37]. The length of one period of this perturbation is referred to as the grating period [37]. A FBG filter has a transmission profile as shown in Fig. 18(b), where the signal at frequency f_r is reflected. The value of f_r depends on both the periodicity of the perturbation and on the effective refractive index of the fiber core. This technique conceived for OSSB signal generation needs high-selectivity filters for retaining only the desired sideband, especially when the RF carrier involved is not high. Moreover, the temperature-dependent variations of the refractive index results in the reflected wavelength value being temperature-sensitive [38]. Furthermore, an OSSB signal can also be generated by the **Dual-Drive MZM** of Fig. 8(b), when it is quadrature biased by setting $V_{bias} = V_\pi/2 + m2V_\pi$ or $V_{bias} = -V_\pi/2 + m2V_\pi$ in Equation (5), where m is an integer, whilst simultaneously ensuring that a phase shift of 90^o is maintained between the RF signals applied to its two arms seen in Fig. 8(b) [35], [27], [39].

Recall that the ODSB and OSSB signals of Figures 16(a) and 16(b), respectively, include the optical carrier, but this is not the case for the OCS signal discussed in the next section.

*3) **Optical Carrier Suppression Modulation**:* As seen from Fig. 16(c), an Optical Carrier Suppression (OCS) based signal consists of a suppressed optical carrier frequency at f_c Hz and two sidebands at $f_c \pm f_{rf}$ Hz, where the frequency of the RF signal employed is f_{RF} Hz. An OCS signal can be generated by the MZM of Fig. 8, when it is MITP biased, as illustrated in Fig. 9. This is achieved by setting $V_{bias} = V_\pi + m2V_\pi$ in Equation (5), where m is an integer [40]. The photo-detection of the OCS signal generates a signal at $2f_{rf}$ Hz, which is a result of the above-mentioned beating between the two optical sidebands during photo-detection [41].

Employing the ODSB modulation of Fig. 16(a), especially when using the direct modulation of Fig. 6(a), requires a simple [34] and inexpensive [23] set-up. Even when employing the external modulators of Fig. 8, the ODSB signals can be generated using a single-drive MZM, while OSSB signal generation requires the more sophisticated dual-drive MZM. However, ODSB signals suffer from a higher chromatic dispersion-induced power penalty than OSSB signals. This is because the phase-change imposed by chromatic dispersion is frequency-dependent, thereby resulting in a phase-difference between the upper and lower sidebands in the ODSB signal of Fig. 16(a). The photo-detected signal is proportional to the optical power $P(t) = |E(t)|^2$, with $E(t)$ being the optical field-strength of the ODSB signal, where the optical power

This article has been accepted for publication in a future issue of this journal, but has not been fully edited. Content may change prior to final publication. Citation information: DOI 10.1109/COMST.2015.2394911, IEEE Communications Surveys & Tutorials

is attenuated owing to the destructive interference between the beating sidebands [34]. This phenomenon is discussed in greater detail in Section V-K. Moreover, OSSB signals have a higher optical spectral efficiency. The OCS signals too are tolerant to chromatic dispersion, but they have a frequency doubled output. Thus, there is a cost vs. performance trade-off, which was alluded to in Fig. 5

Now that we have become familiar with the basic intensity modulation techniques, we move on to discussing optical angle modulation in the next section.

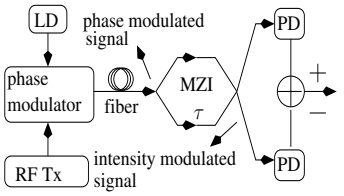

Fig. 19. Phase modulation using a Mach-Zehnder delay Interferometer (MZI) (LD- Laser Diode; RF Tx- RF Transmitter; PD- Photo-diode)

B. Optical Angle Modulation

Optical angle modulation involves the modulation of the phase or frequency of the optical signal, which are typically referred to as optical Phase Modulation (PM) and Frequency Modulation (FM), respectively. Optical angle modulated signals can be detected coherently, as shown in Fig. 13(b) or directly, as shown in Fig. 13(a), where coherent detection is straight-forward, while direct detection requires a prior conversion of the angle modulated signal to an intensity modulated signal using a discriminator in the O-E blocks of Fig. 3. A discriminator is an optical component which has a frequency/phase dependent output intensity. Mach-Zehnder delay interferometers of Fig. 19 [42] are the most commonly employed discriminators, as detailed below.

Again, the **Mach-Zehnder delay Interferometer (MZI)** is shown in Fig. 19, where the ouput of a laser operating at a frequency of f_c Hz and at an optical power of P_{in} is phase modulated and transmitted over the fiber. The angle modulated signal entering the MZI is $E_{in}(t) = \sqrt{2P_{in}}e^{j\omega_c t+\phi(t)}$, where $\phi(t)$ depends on the modulating electronic signal and the intensity $|E_{in}(t)|^2$ of the angle modulated signal is constant. The incoming angle modulated signal is then fed into the two arms of the MZI of Fig. 19, where the signal in one of the arms experiences a delay of τ seconds with respect to the other. The outputs of the two arms are combined to generate an optical field E_{out}, whose intensity P_{out} is as follows [42]:

$$P_{out} = |E_{out}|^2 = \frac{P_{in}}{2}\left|e^{j\omega_c t+\phi(t)} + e^{j\omega_c(t-\tau)+\phi(t-\tau)}\right|^2 = \frac{P_{in}}{2}[1+1+2\cos(\omega_c\tau+\Delta\phi(t))], \quad (28)$$

where we have $\Delta\phi(t) = \phi(t) - \phi(t-\tau)$ and the MZI is quadrature biased with $\omega_c\tau = -\pi/2$. Subsequently, using the small-signal approximation that $\sin(\Delta\phi(t)) \approx \Delta\phi(t)$, we get [42], [43]:

$$P_{out} = P_{in}[1+\sin(\Delta\phi(t))] = P_{in}[1+\Delta\phi(t)] \quad (29)$$

Thus, the optical signal is now intensity modulated and can be detected by the direct photo-detection scheme of Fig. 13(a) [42]. Additionally, the MZI of Fig. 19 generates a complementary output, whose intensity is $P_{out,2} = P_{in}[1-\Delta\phi(t)]$ [42]. Balanced photo-detection can be achieved by subtracting the two photo-detected outputs, as shown in Fig. 19 [42], where the associated advantages of balanced photo-detection will be discussed in Section V-D. The dynamic range of an angle modulated link that relies on direct photo-detection, largely depends on both the non-linearity of the descriminator and on the residual IM present in the phase-modulated signal that is transmitted [44].

Intensity modulated signals can be detected using the simpler direct photo-detection discussed in Section II-C, while angle modulated signals require an additional discriminator for direct photo-detection or they employ the more complex coherent photo-detection discussed in Section II-C. On the other hand, the cross-talk level in multi-channel systems is lower, when employing phase modulation than upon employing intensity modulation [42]. Moreover, optical intensity modulation using the MZMs of Fig. 8 or EAM of Fig. 10(a) requires biasing, while the phase modulator of Fig. 11 is not biased. Hence, intensity modulation suffers from the drifting bias voltage and hence needs bias stabilization circuits [45]. Thus, there is a cost versus performance trade-off, which was portrayed in the stylized illustration of Fig. 5.

Having covered the basics of a single ROF link, we now discuss the various ROF multiplexing techniques in Section IV.

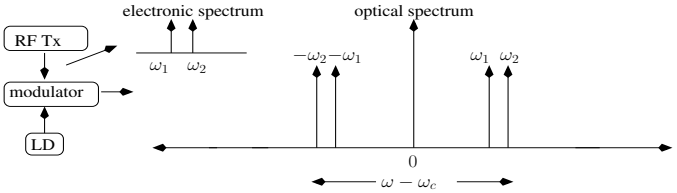

Fig. 20. A Sub Carrier Multiplexing (SCM) transmitter model (LD- Laser Diode; RF Tx- RF Transmitter)

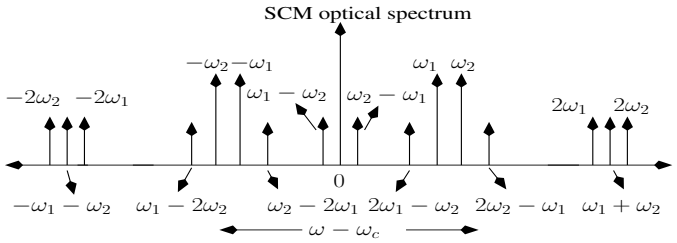

Fig. 21. Sub Carrier Multiplexing (SCM) optical spectrum

IV. MULTIPLEXING

Optical multiplexing employed in multi-user/multi-RAP scenarios allows us to increase the throughput of an optical fiber link. There are two basic types of optical frequency multiplexing schemes, which can be employed in ROF systems, namely Sub-Carrier Multiplexing (SCM) [46] and Wavelength Division Multiplexing (WDM) [47].

This article has been accepted for publication in a future issue of this journal, but has not been fully edited. Content may change prior to final publication. Citation information: DOI 10.1109/COMST.2015.2394911, IEEE Communications Surveys & Tutorials

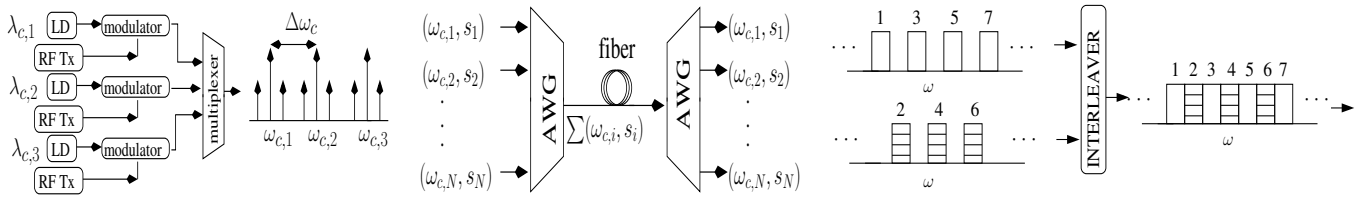

(a) A ODSB-WDM transmitter model (b) A basic MUX/DEMUX (c) An interleaver

Fig. 22. Wavelength Division Multiplexing (WDM) (LD- Laser Diode; RF Tx- RF Transmitter; AWG- Arrayed Waveguide Grating)

A. *Sub-Carrier Multiplexing*

Sub-Carrier Multiplexing (SCM) refers to the frequency-domain multiplexing of multiple modulating signals, which are termed as sub-carriers, for example signals at f_1 and f_2 Hz. The combined signal in then input to the direct modulation scheme [48] of 6(a) or to the external modulation [49] schemes of Fig. 8 and Fig. 10(a), as shown in Fig. 20. The spectrum of the modulating electronic signal and of the modulated optical signal is shown in Fig. 20, where the desired sidebands, also referred to as optical channels, of the ODSB modulated SCM signal are located at $f_c \pm f_1$ Hz and $f_c \pm f_2$ Hz.

The optical spectrum shown in Fig. 20 is an idealised representation, while that in Fig. 21 shows the optical harmonics and intermodulation products that are generated during SCM. If the number of SCM channels is $N = 2$, then the desired sidebands are at $f_c \pm f_1$ Hz and $f_c \pm f_2$ Hz. The spectrum of Fig. 21 also contains other sidebands, where the sidebands at $f_c \pm mf_1$ Hz and $f_c \pm mf_2$ Hz, with m being an integer, are referred to as optical harmonics. The sidebands located at $f_c \pm (2f_1 - f_2)$ Hz, $f_c \pm (2f_2 - f_1)$ Hz and $f_c \pm (f_1 \pm f_2)$ Hz in Fig. 21 are referred to as optical intermodulation products. Similarly, the harmonics in the photo-detected signal are located at mf_1 Hz and mf_2 Hz, while the second-order and third-order intermodulation products are located at $f_i \pm f_j$ Hz and $f_h \pm f_i - f_j$ Hz, respectively, where $h, i, j \in \{1, 2, ..N\}$, and h, i and j are SCM channel indices [50]. For example, the non-linearity in a ROF link that employs the SCM of two RF frequencies, namely the WCMDA frequency of $f_1 = 1.9$ GHz and the WLAN IEEE 802.11b frequency of $f_2 = 2.4GHz$, is discussed in [51]. As seen in Fig. 9 and Fig. 10(b), the intensity is modulated in a non-linear fashion around the bias point in external modulation, which creates harmonics and inter-modulation products.

B. *Wavelength Division Multiplexing*

While SCM employs a single optical carrier to transmit multiple modulating signals, Wavelength Division Multiplexing (WDM) involves the fiber-based transmission of multiple optical carrier frequencies. As shown in Fig. 22(a), each carrier frequency is modulated by an electronic signal, thereby generating sidebands around that carrier. Subsequently, the signals are multiplexed to generate the spectrum seen in Fig. 22(a), where the spectrum consists of three optical carriers. The corresponding sidebands appear on either side of each carrier. In **Dense Wavelength Division Multiplexing (DWDM)** [47], the channel spacing $\Delta\omega_c$ of Fig. 22(a) has standardized values of 12.5, 25, 50, 100 or 200 GHz [52]. Various optical components are employed in WDM based ROF networks, including a multiplexer /demultiplexer and Optical Add Drop Multiplexer (OADM), which are detailed below.

A Multiplexer (MUX) and a Demultiplexer (DEMUX) is used for combining and separating the optical signals appearing at different optical carrier frequencies, respectively. Most DEMUXs are also capable of operating as a MUX, when operated in the reverse direction, i.e. when light enters from the output ports. As seen in Fig. 22(b), the most basic MUX/DEMUX consists of a $(1 \times N)$ Arrayed Waveguide Grating (AWG), which relies on the principle of diffracting the light in order to separate/combine the wavelengths [53]. Each channel consists of the optical carrier along with its sidebands, as represented by $(\omega_{c,i}, s_i)$ in Fig. 22(b), while the multiplexed signal is indicated as $(\sum \omega_{c,i}, s_i)$. The MUX of Fig. 22(b) multiplexes individual frequency bands, while the interleaver of Fig. 22(c) is employed for bundling sets of even and odd indexed frequency bands. As shown in Fig. 24, the interleaver can be operated in the reverse direction to implement de-interleaving. The OADM of Fig. 25 is employed at the RAP to "drop", i.e. demultiplex, a downlink WDM channel, while "adding", i.e.multiplexing, an uplink signal at the same or possibly different optical frequency. Fig. 25 shows the block diagram of an OADM, where the downlink signal carried by the optical carrier at $f_{c,2} = \frac{\omega_{c,2}}{2\pi}$ Hz is dropped and an uplink signal at the same optical carrier frequency is added.

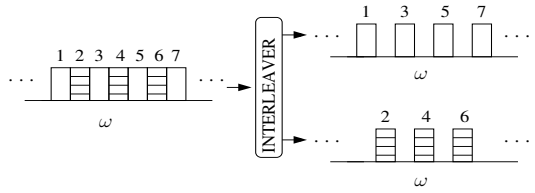

Fig. 24. An interleaver operated as a de-interleaver

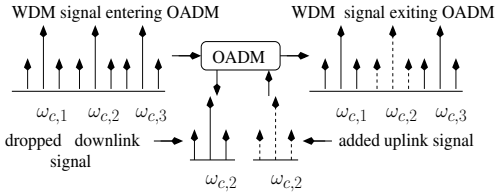

Fig. 25. Optical Add Drop Multiplexer (OADM)

The throughput that can be achieved using WDM is higher than that, which can be achieved using SCM. However, this comes at the cost of having to use multiple laser sources, MUXs, DEMUXs and OADMs, thereby giving rise to the cost versus performance trade-off indicated in Fig. 5. It is

This article has been accepted for publication in a future issue of this journal, but has not been fully edited. Content may change prior to final publication. Citation information: DOI 10.1109/COMST.2015.2394911, IEEE Communications Surveys & Tutorials

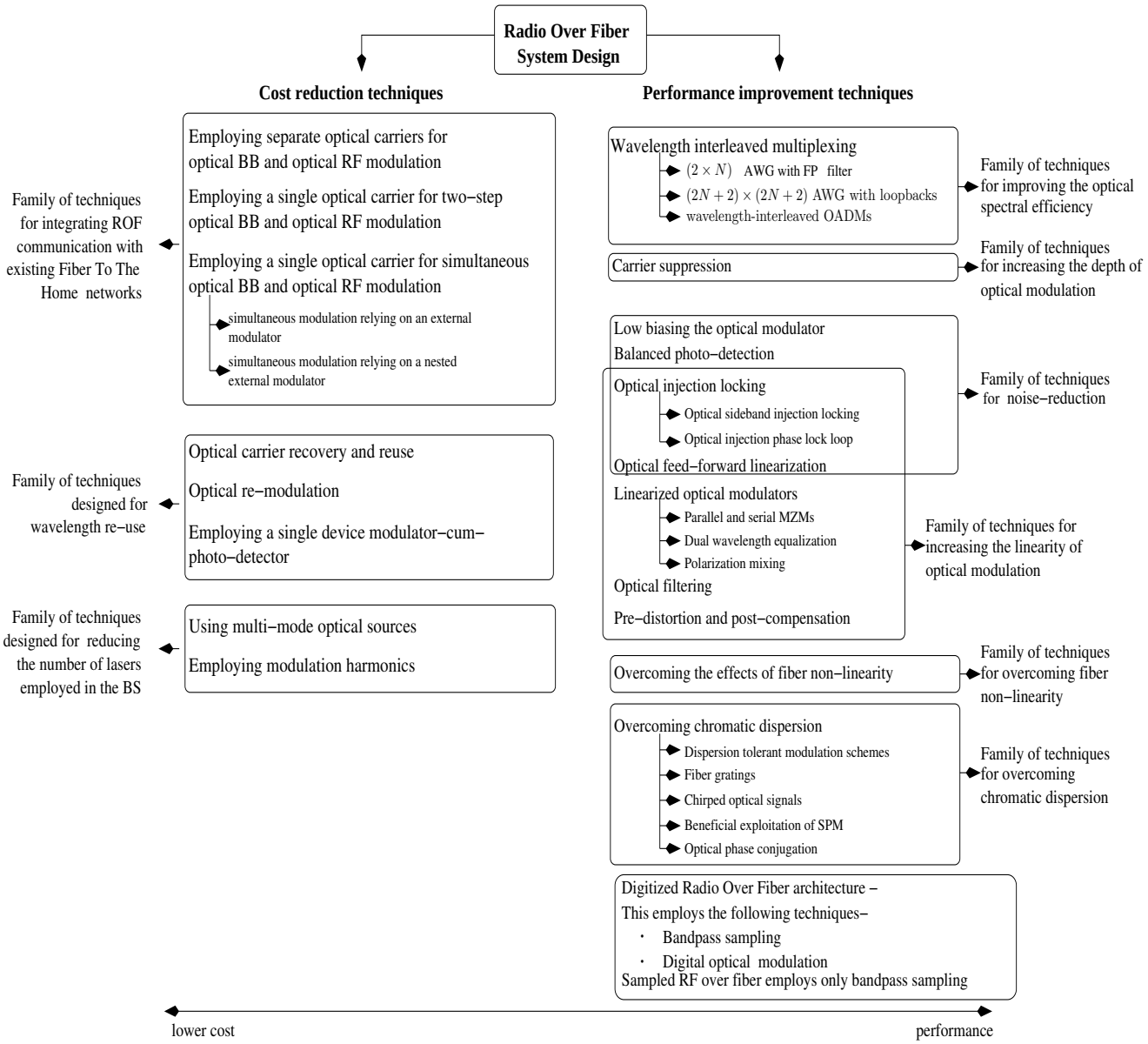

Fig. 23. The various cost reduction and performance improvement techniques for ROF communications (LD- Laser Diode; RF Tx- RF Transmitter)

also possible to combine and use both SCM and WDM simultaneously, as mentioned in Fig. 5.

Equipped with a basic understanding of the different components of a simple ROF link, we now move on to discussing a range of advanced performance improvement techniques in Section V.

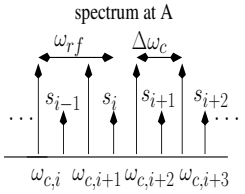

Fig. 26. WI-DWDM signal

V. ROF Performance Improvement Techniques

There are numerous challenges associated with efficient millimeter-wave ROF communication, including the generation and reliable transmission of the wireless signal over the optical channel. In this section we describe several techniques that may be employed for improving the ROF link's performance in terms of throughput, Noise Figure (NF) or dynamic range.

A. *Wavelength interleaved multiplexing*

As per definition, in a Wavelength Interleaved Wavelength Division Multiplexing (WI-WDM) system, the frequency spacing between the optical carrier at $f_{c,i} = \frac{\omega_{c,i}}{2\pi}$ Hz and its sideband at $\frac{s_i}{2\pi}$ Hz is higher than the frequency spacing $\Delta f_c = \frac{\Delta\omega_c}{2\pi}$ Hz between the adjacent optical carriers, which results in the interleaved spectrum shown in Fig. 26. The spectrum of Fig. 26 is generated by multiplexing signals that

This article has been accepted for publication in a future issue of this journal, but has not been fully edited. Content may change prior to final publication. Citation information: DOI 10.1109/COMST.2015.2394911, IEEE Communications Surveys & Tutorials

TABLE I

RADIO OVER FIBER (ROF) PERFORMANCE IMPROVEMENT TECHNIQUES (PART 1)

Technique	Year	Authors	Contribution
Wavelength Interleaved Wavelength Division Multiplexing (WI-WDM)	2001	Lim *et al.* [54]	Designed a WI-WDM system using Optical Add-Drop Multiplexers (OADMs).
	2003	Toda *et al.* [47]	Implemented of WI-WDM using a MUX/DEMUX that employed $(2 \times N)$ Arrayed Waveguide Grating (AWG) with a Fabry Perot (FP) filter.
	2006	Bakaul *et al.* [55]	Achieved simultaneous demultiplexing of the N downlink WI-WDM channels and multiplexing of the N uplink channels into a WI-WDM signal using an AWG with loopbacks.
Carrier Suppression	2002	Rongqing *et al.* [49]	A tunable Fabry-Perot (FP) filter was used for suppressing the optical carrier of an Optical Single Side Band (OSSB) signal in order to improve the receiver sensitivity.
	2005	Attygalle *et al.* [56]	A Fiber Bragg Grating (FBG) filter was used for suppressing the optical carriers of OSSB and Optical Double Side Band (ODSB) signals, which improved the receiver sensitivity by upto 7 dB.
	2005	Gu *et al.* [57]	A sub-picometer bandpass filter having a 3 dB bandwidth of 120 MHz was designed and fabricated. This was then used for implementing carrier suppression in a system employing low RF carriers.
Low biasing the optical modulator	1993	Farwell *et al.* [58]	Operated a Mach-Zehnder Modulator (MZM) at an optical bias below the quadrature biasing point to increase the linear dynamic range.
	2007	Ackerman *et al.* [59]	Operated a MZM at an optical bias below the quadrature biasing point to increase the Signal to Noise Ratio (SNR).
Balanced photo-detection	2007	McKinney *et al.* [60]	Designed a ROF link having a Noise Figure (NF) of less than 10 dB by relying on a dual-output MZM and differential detection.
Optical Injection Locking (OIL)	1998	Braun *et al.* [61]	A 64 GHz, 140 -155 Mbps signal having a low phase noise $<$-100 dBc/Hz and a bit rate of was generated using Optical Sideband Injection Locking (OSIL).
	2003	Johansson *et al.* [62]	A RF signal having a low phase noise and a data rate of 148 Mbps was generated in the 26-40 GHz range using an Optical Injection Phase Lock Loop (OIPLL) for transmission distances upto 65 Km.
	2006	Chrostowski *et al.* [63]	Presented the various advantages of using OIL in a ROF link, including higher laser power, higher bandwidth, lower noise and lower non-linearity.
	2010	Ng'oma *et al.* [64]	Direct modulation of the output of an optically injection locked laser was done to generate a multi-Gbps RF signal at 60 GHz.
Optical feed-forward linearization	2007	Ismail *et al.* [65]	Achieved simultaneous reduction of 3rd-order Intermodulation Distortion (IMD) by 26-dB and laser-noise by 7-dB at 5.2 GHz using feed-forward linearization.

are generated using the OSSB modulation schemes discussed in Section III-A.2 [47]. In other words, as shown in Fig. 26, we have $f_{rf} > \Delta f_c$, where f_{rf} is the frequency of the modulating RF signal. This technique is usually implemented along with the DWDM technique that was discussed in Section IV-B. WI-WDM results in a higher spectral efficiency than the conventional non-interleaved WDM, but requires more sophisticated techniques for multiplexing and demultiplexing the signals [47] [54]. In the following paragraphs we highlight some of these techniques, assuming OSSB modulation.

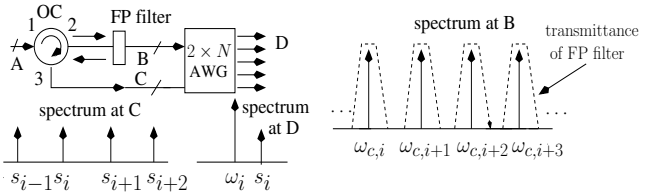

Fig. 27. Wavelength Interleaved Wavelength Division Multiplexing (WI-DWDM) Demultiplexer (DEMUX) using Fabry Perot (FP) filter (AWG- Arrayed Waveguide Grating; OC- Optical Circulator)

a) $(2 \times N)$ ***AWG with Fabry Perot (FP) filter*** *[47]:* A $(a \times b)$ AWG consists of a input ports and b output ports, while a Fabry Perot (FP) filter is an optical filter having alternating transmission and reflection bands. Hence, effectively it acts as a comb filter. The incident optical wave will be either transmitted through or reflected by the FP filter, depending on the optical frequency. A DEMUX and MUX pair using an AWG and a FP filter is shown in Figures 27 and 28,

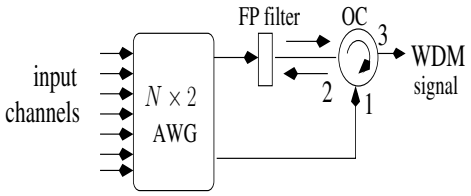

Fig. 28. Wavelength Interleaved Wavelength Division Multiplexing (WI-DWDM) Multiplexer (MUX) using Fabry Perot (FP) filter (AWG- Arrayed Waveguide Grating; WDM- Wavelength Division Multiplexing; OC- Optical Circulator)

respectively [47]. The corresponding spectra at points A, B, C and D of the DEMUX architecture using the FP filter are shown in Figures 26 and 27. In the DEMUX of Fig. 27, the WI-DWDM signal, whose spectrum is shown in Fig. 26, enters port 1 of the Optical Circulator (OC) and leaves from its port 2, where the set of sidebands seen in the WI-WDM signal of Fig. 26 are reflected, while the set of carriers are transmitted by the FP filter. The reflected sidebands re-enter port 2 of the OC and leave from port 3. The separated carriers-set and sidebands-set are then fed into the two input ports of the AWG of Fig. 27, whose output consists of the demultiplexed signals. As indicated by the spectrum at point D of Fig. 27, each separated signal contains the carrier ω_i and its corresponding sideband s_i [47].

The MUX of Fig. 28 operates in a similar fashion, except that the direction of signal-flow is reversed [47]. As shown in Fig. 28, the independent channels enter the MUX, while the

This article has been accepted for publication in a future issue of this journal, but has not been fully edited. Content may change prior to final publication. Citation information: DOI 10.1109/COMST.2015.2394911, IEEE Communications Surveys & Tutorials

set of carriers and the set of sidebands appear at the top and bottom output port of the AWG in Fig. 28, respectively. The top and bottom outputs of the AWG in Fig. 28 have stylized spectra similar to those seen at points B and C of Fig. 27, respectively. The set of sidebands then enter port 1 and exit from port 2 of the OC, where, as shown in Fig. 28, these sidebands are reflected by the FP filter, re-enter port 2 and finally exit from port 3 of the OC. On the other hand, the set of carriers that exited from the top port of the AWG of Fig. 28 are transmitted through the FP filter. Hence, they too exit from port 3 of the OC. Thus, the multiplexed signal becomes available from port 3 of the OC [47] of Fig. 28.

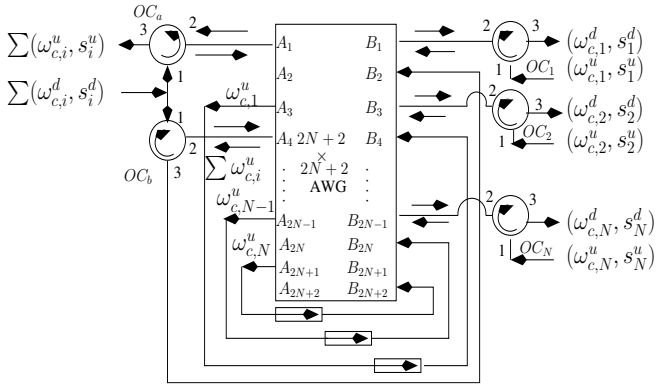

Fig. 29. Multiplexer/Demultiplexer (MUX/DEMUX) employing an Arrayed Waveguide Grating (AWG) in loopback configuration (OC- Optical Circulator)

b) $(2N+2)\times(2N+2)$ ***AWG with loopbacks****:* A loopback architecture is one in which the output ports are connected to the input ports of the AWG. The architecture shown in Fig. 29 implements simultaneous demultiplexing of the N downlink channels and multiplexing of the N uplink channels or vice-versa in a ROF system that employs WI-WDM. While the discussion below assumes a scenario in which the downlink channels are demultiplexed and uplink signals are multiplexed, the processs is similar for the case of uplink demultiplexing and downlink multiplexing.

In Demultiplexing [55], the downlink WI-DWDM signal, which consist of the N optical carriers and their corresponding single sidebands, is portrayed in Fig. 29 as $\sum(\omega^d_{c,i}, s^d_i)$. The downlink power is split by a coupler and it enters ports A_1 and A_4 of the AWG via the circulators OC_a and OC_b of Fig. 29, respectively. The optical carriers along with their respective sidebands exit from ports $B_1,\ B_3\ \cdots B_{2N-1}$ of Fig. 29. These are obtained from port 3 of OC_1 to OC_N and are indicated in Fig. 29 as $(\omega^d_{c,i}, s^d_i)$ [55].

In Multiplexing [55], the N uplink optical signals enter ports $B_1,\ B_3\ \cdots B_{2N-1}$ via the OCs and are represented as $(\omega^u_{c,i}, s^u_i)$ in Fig. 29. The optical carriers exit from port A_4 while the sidebands exit from port A_1 in Fig. 29. The output of port A_4 is indicated as $\sum\omega^u_{c,i}$ in Fig. 29, which are then looped back into port B_2. This results in the N separated optical carriers ω_i output at $A_3,\ A_5\ \cdots A_{2N+1}$, which are then again looped back to ports $B_4,\ B_6\ \cdots B_{2N+2}$. This results in the combined optical carriers $\sum\omega^u_{c,i}$ leaving from port A_1 of Fig. 29. Thus, both the optical carriers and their sidebands exit from port A_1. This WI-DWDM optical signal then exits from port 3 of OC_a and it is represented as $\sum(\omega^u_{c,i}, s^u_i)$ in Fig. 29 .

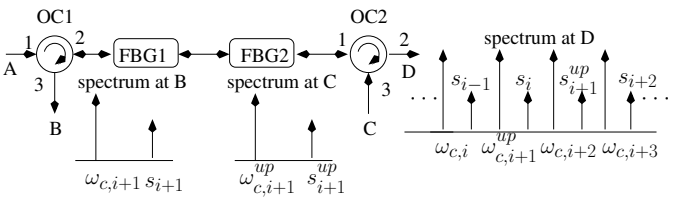

Fig. 30. Optical Add-Drop Multiplexer (OADM) (FBG- Fiber Bragg Grating filter; OC- Optical Circulator)

*c) **Wavelength-interleaved optical add-drop multiplexers**:* In Fig. 30, the optical OSSB-WDM signal of Fig. 26 enters into port 1 of OC1 and leaves from port 2 [54]. Subsequently, the optical carrier $\omega_{c,i+1}$, that is to be dropped, is reflected by the FBG filter 1 (FBG1), while the corresponding sideband s_{i+1} is reflected by FBG2 [54], as shown in Fig. 30. The rest of the signal enters port 1 of OC2 The reflectivity profile of the FBG1 and FBG2 filters is as shown in Fig. 18(b), where the centre frequency $f_r = \frac{\omega_r}{2\pi}$ has values of $f_{c,i+1} = \frac{\omega_{c,i+1}}{2\pi}$ Hz and $\frac{s_{i+1}}{2\pi}$ Hz, respectively. The signals that are reflected by FBG1 & FBG2 back-propagate and re-enter port 2 of OC1 and they are dropped from port 3, where the spectrum of the signal exiting from port 3 is shown at point B of Fig. 30. The uplink signal, whose spectrum is shown at point C of Fig. 30, enters port 3 of OC2 and exits from port 1. This uplink signal having a carrier $\omega^{up}_{c,i+1}$ and sideband s^{up}_{i+1} gets reflected by the FBG filters, because they are at the same frequencies as the previously dropped signal and they re-enter port 1 of OC2. Hence, the total signal entering port 1 of OC2 includes the channels within the signal at point A, which were not reflected by the FBG filters, along with the added uplink channel. The signal entering port 1 finally exits from port 2 of OC2, where the spectrum exiting from port 2 is shown at point D of Fig. 30. Thus, a downlink channel is dropped from the spectrum of Fig. 26 and replaced by the uplink channel to obtain the spectrum at point D of Fig. 30.

Upon concluding our discussion on WI-WDM, recall that the first MUX/DEMUX architecture relies on a $(2\times N)$ AWG, a Fabry Perot (FP) filter as well as on an Optical Circulator (OC) and can either perform multiplexing or demultiplexing. On the other hand, the second MUX/DEMUX architecture employs the more complex $(2N+2)\times(2N+2)$ AWG with loopbacks along with several OCs, but can achieve simultaneous multiplexing and demultiplexing of the signals. However, none of these MUX/DEMUX architectures permits access to an individual channel or to a set of channels within the multiplexed signal without having to demultiplex all the channels. This can be implemented using the OADM alluded to in the previous discussion. Fig. 31 shows some commonly used ROF network topologies along with the BSs, Remote Nodes (RNs) and RAPs, where the MUX/DEMUX and OADMs are employed assuming that duplex communication with each RAP is achieved using a unique wavelength. Fig. 31 also shows the operations that MUX/DEMUXs and

This article has been accepted for publication in a future issue of this journal, but has not been fully edited. Content may change prior to final publication. Citation information: DOI 10.1109/COMST.2015.2394911, IEEE Communications Surveys & Tutorials

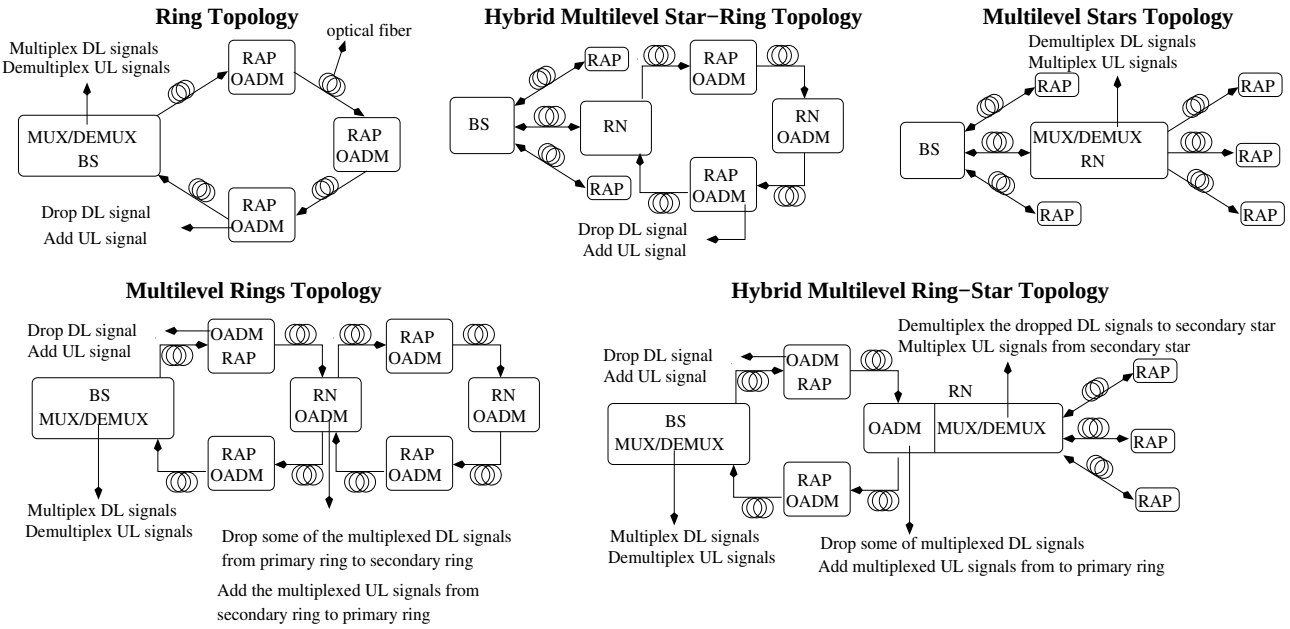

Fig. 31. Use of Multiplexers/Demultiplexers (MUXs/DEMUXs) and Optical Add Drop Multiplexers (OADMs) in different ROF topologies (BS- Base Station; RN- Remote Node; RAP- Radio Access Point; DL Downlink; UL- Uplink

OADMs perform on both the Downlink (DL) and Uplink (UL) ROF signals.

Let us now move on from the family of techniques conceived for improving optical spectral efficiency to carrier suppression techniques, which are capable of increasing the depth of optical modulation, thereby improving the receiver sensitivity.

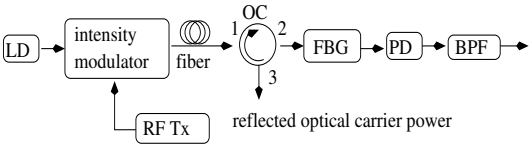

Fig. 32. Carrier suppression (LD- Laser Diode; RF Tx- RF Transmitter; FBG- Fiber Bragg Grating; PD- Photo-diode; BPF- Band Pass Filter)

B. Carrier Suppression

Suppressing the optical carrier with respect to the modulation sidebands increases the depth of optical modulation, thereby beneficially improving the attainable receiver sensitivity [56], [66], [67], [49], where the typical value of the optimum Carrier to Sideband Ratio (CSR) is 0 dB. Fig. 32 portrays an architecture that implements carrier suppression, where the output of the laser is intensity modulated using the RF signal and transmitted over the fiber to the RAP. In the RAP, the modulated optical signal enters port 1 of the OC of Fig. 32 and then exits from port 2, where it enters the FBG filter that implements carrier suppression. The FBG filter, originally discussed in Fig. 18, reflects a portion of the optical carrier power corresponding to the desired suppression, but ideally allows 100 % transmission of the optical sidebands. The reflected optical carrier power enters port 2 and then exits from port 3 of the OC, where it can be re-used for uplink modulation. The FBG filter of Fig. 32 can also be employed before fiber transmission in order to simplify the RAP architecture [56]. However, this latter technique would prevent the implementation of wavelength re-use, since the reflected carrier power would no longer be available at the RAP but only at the BS.

Following this rudimentary introduction to the pertinent issues of carrier suppression, we now consider the family of techniques designed for reducing the noise imposed by the ROF link, which in turn improves both the optical receiver sensitivity as well as the dynamic range. These techniques include low-biasing the optical modulator, balanced photo-detection as well as Optical Injection Locking (OIL) and optical feed-forward linearization.

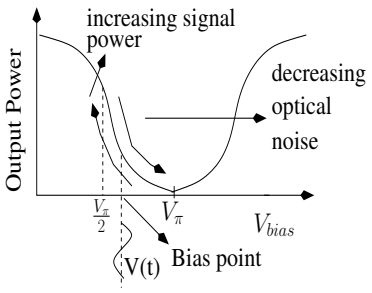

Bias point	V_{bias}
QP	$\frac{V_\pi}{2}$
MITP	V_π

Fig. 33. Biasing the optical modulator at an optical power below that of Quadrature Point (QP) biasing (MITP- Minimum Transmission Point)

C. Low-biasing the optical modulator

As discussed in Section III, if the ODSB/OSSB modulation of Fig. 16 was carried out at the transmitter using a RF signal at f_{RF} Hz, then the desired photo-detected signal is also generated at f_{RF} Hz. However, no signal is generated at f_{RF} Hz for the OCS modulation scheme of Fig. 16, where a frequency-doubled photo-detected signal is generated at $2f_{RF}$ Hz instead. ODSB/OSSB modulation requires a QP biased

This article has been accepted for publication in a future issue of this journal, but has not been fully edited. Content may change prior to final publication. Citation information: DOI 10.1109/COMST.2015.2394911, IEEE Communications Surveys & Tutorials

MZM that is associated with $V_{bias} = V_\pi/2$, while OCS modulation requires a MITP biased MZM with $V_{bias} = V_\pi$. If no frequency doubling is desired then, the QP biased MZM of Fig. 8 is employed. Fig. 33 shows the trade-off between the optical noise and optical signal power, when the bias point indicated by an arrow moves from the QP towards the MITP of Fig. 33 [58]. It can be seen from Equations (6) and (7) that unlike in the QP biased scenario of Fig. 33, the MITP biased scenario of Fig. 33 has a suppressed first harmonic, which implies that the power of the photo-detected f_{RF} Hz RF signal decreases, when the bias point indicated by the arrow moves from the QP towards the MITP. However, it can be seen from Equations (6) and (7), that the DC value in the photo-detected signal is higher for the case of QP biasing than for MITP biasing. Thus, observe from Equations (14) and (15) that the shot noise, RIN and signal-ASE beat noise level, which together constitute the optical noise, decrease at a faster rate, when the bias point moves from the QP towards MITP [59] [58], as shown in Fig. 33. If the dominant source of noise in an optical link that employs a QP biased MZM is the optical noise, then the output SNR increases as the bias is shifted from the QP towards the MITP, which can be deduced from Fig. 33. The SNR increases till the photo-detector's thermal noise becomes the dominant source of noise, beyond which the SNR starts to decrease. Therefore, the optimum bias value corresponding to the maximum SNR lies between the QP and MITP, where its actual value depends on the optical power at the MZM's input. The expression for the Noise Figure (NF) and its relation to the Spurious Free Dynamic Range (SFDR) of an optical link is as follows on a decibel (dB) scale [59], [68]:

$$NF[dB] = SNR_{in}[dB] - SNR_{out}[dB], \quad (30)$$

$$SFDR[dB] = \frac{2}{3}\{IP3[dB] - (-174 + NF[dB])\}, \quad (31)$$

where IP3 is the level of the third-order inter-modulation products. Hence, optimising the bias point not only reduces the noise figure, but also results in an increase of the link dynamic range. A similar performance improvement can be achieved by low-biasing the EAM of Fig. 10(a) [69] [70] to an optical power level below that shown in Fig. 10(b).

However, the limitation of this technique is that it assumes that the effect of the stronger second-order distortion, including harmonics and intermodulation distortion, generated by low-biasing can be neglected. It can be seen from Equation (6) and Equation (7) that unlike in the QP biased scenario, the MITP biased scenario has a strong second order harmonic. In a SCM system having N channels, the second order hamonics do not lie within the transmission bandwidth if we have $2f_i > f_N \ \forall \ i$, where f_i is the electronic frequency of the i^{th} channel being modulated onto the optical carrier. The non-linearity that generates second-order harmonics also results in the generation of second-order intermodulation products of the form of $f_i \pm f_j$, where $i, j \in \{1, 2, ...N\}$. Second-order intermodulation products can be neglected if they do not lie within the SCM signal'a bandwidth i.e. $(f_i \pm f_j) < f_1$ *or* $(f_i \pm f_j) > f_N \ \forall \ i, j$. The conditions for neglecting the second-order harmonic and intermodulation distortion are met, if the SCM signals are within an octave, i.e. $f_N < 2f_1$ [58].

Let us now discuss a second technique that assists in reducing the noise imposed by the optical link, namely balanced photo-detection.

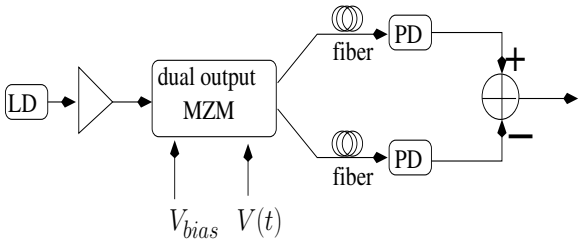

Fig. 34. Balanced photo-detection (LD- laser Diode; PD- Photo-diode; MZM- Mach-Zehnder Modulator)

D. *Balanced photo-detection*

Balanced photo-detection schemes involve the subtraction of two received signals, which results in the desired components in those signals being added, while the noise being mitigated. Fig. 34 shows the block diagram of balanced photo-detection, where the laser output is fed to the dual-output MZM that generates a pair of modulated outputs [60]. The first output is the standard output of an MZM with an intensity of $P_1(t) = P_{in}[1 + \cos(\frac{\pi V_{bias}}{V_\pi} + \frac{\pi V(t)}{V_\pi})]$, while the other output has an intensity of [71]:

$$P_2(t) = |E(t)|^2 = \left| \sin(\frac{\pi V_{bias}}{2V_\pi} + \frac{\pi V(t)}{2V_\pi})\sqrt{2P_{in}}e^{j\omega_c t} \right|^2$$
$$= P_{in}[1 - \cos(\frac{\pi V_{bias}}{V_\pi} + \frac{\pi V(t)}{V_\pi})], \quad (32)$$

Both outputs are photo-detected after transmission through the fiber and as shown in Fig. 34, balanced photo-detection involves the subtraction of the two photo-detected signals, where the balanced photo-detector output is given by [60]:

$$I_{balanced} = I_1(t) - I_2(t)$$
$$= R \cdot P_1(t) - R \cdot P_2(t)$$
$$= 2R \cdot P_{in} \cdot \cos(\frac{\pi V_{bias}}{V_\pi} + \frac{\pi V(t)}{V_\pi}), \quad (33)$$

where R is the responsivity of the photo-diode. Again, it can be seen from Equation (33) that the desired signals are added, while the intensity noise that is common to the two photo-detected signals is suppressed by the difference operation [60]. A link that has a sub-10 dB NF can be achieved using balanced photo-detection [60].

The next two techniques belonging to the family of optical noise-reduction techniques, namely Optical Injection Locking (OIL) and optical feed-forward linearization, also belong to the family of techniques designed for increasing the linearity of optical modulation. We now discuss OIL, which assists in generating high-power, low-noise laser outputs.

This article has been accepted for publication in a future issue of this journal, but has not been fully edited. Content may change prior to final publication. Citation information: DOI 10.1109/COMST.2015.2394911, IEEE Communications Surveys & Tutorials

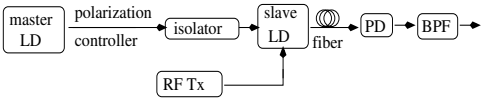

Fig. 35. Optical Injection Locking (LD- Laser Diode; PD- Photo-diode; RF Tx- RF Transmitter; BPF- Band Pass Filter)

E. Optical Injection Locking

Optical Injection Locking (OIL) is a technique conceived for generating a high-power laser output that has both a low intensity noise and a low phase noise. Fig. 35 shows the schematic of OIL, where the output of the low-power, low-noise master-laser of Fig. 35 is injected into a high-power slave-laser. The slave-laser is constrained to operate at the frequency of the injected laser, provided that this frequency is sufficiently close to its own free-running frequency. The difference between the free-running frequency and the injection-locked frequency of the slave-laser is referred to as the frequency detuning, where using a higher injected power results in a higher allowable frequency detuning. As shown in Fig. 35, the output of the slave-laser is directly modulated by the electronic RF transmitter before transmission over the fiber, while the isolator ensures that no reflected signals enter the master-laser.

OIL has several advantages [63]. For example, when using OIL, the laser's relaxation oscillation frequency f_r, as shown in Fig. 7, increases. Hence, direct modulation results in weaker dynamic non-linearity induced harmonics and inter-modulation [72]. Additionally, it can be seen from Fig. 7 that the increase in f_r is accompanied by an increase in the modulation bandwidth of the laser [64]. Furthermore, it is possible to directly modulate the laser using frequencies that are close to its relaxation oscillation frequency without the usual increase in the RIN noise [64]. When OIL is used, it becomes possible to generate a high-fidelity, high-power optical signal, which enables the designer to achieve a high link-SNR. Finally, OIL can also be employed for generating OSSB signals [73].

Two variations of OIL that employ heterodyne photo-detection are discussed in the following sub-sections, including Optical Sideband Injection Locking and Optical Injection Phase Locked Loops. These techniques result in performance improvements at the cost of an increased transmitter complexity.

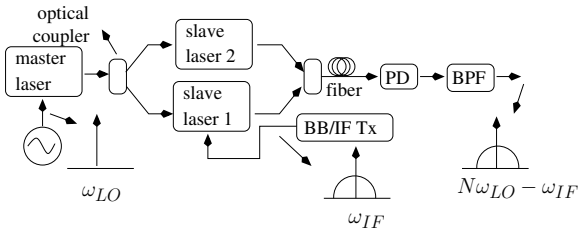

Fig. 36. Optical Sideband Injection Locking (BB- Baseband; IF - Intermediate Frequency; PD- Photo-diode; BPF- Band Pass Filter)

a) ***Optical Sideband Injection Locking****:* A so-called dual-mode signal consists of two optical frequencies, where heterodyne detection may be used for generating a RF signal, as discussed in Section II-C. The performance of a link that employs this technique can be improved by additionally invoking the concept of OIL. Typically, it is the slave laser's output that is RF modulated during OIL. However, as shown in Fig. 36, it is also possible to injection-lock two -rather than just one- slave lasers to different sidebands of a master-laser [74] that has been modulated using a RF tone at $f_{LO} = \frac{\omega_{LO}}{2\pi}$ Hz. This OIL operation is then followed by the modulation of either one or of both sidebands using the BB/IF signal at $f_{IF} = \frac{\omega_{IF}}{2\pi}$ Hz. As shown in Fig. 36, the subsequent heterodyne photo-detection of these high-power sidebands generates the high-fidelity upconverted RF signal appearing at $]N \cdot f_{LO} - f_{IF}]$ Hz. More explicitely, Optical Sideband Injection Locking (OSIL) facilitates the injection locking of the slave-lasers to higher-order optical sidebands, i.e to harmonics that are present within the output of the RF-modulated master-laser [61], where the upconverted photodetected signals can be generated at $[N \cdot f_{LO} \pm f_{IF}]$ Hz with N being an integer.

The optical phase noise can be further reduced by amalgamating OIL with Optical Phase Lock Loops (OPLLs), which however results in added transmitter complexity. This hybrid technique is discussed in the next section.

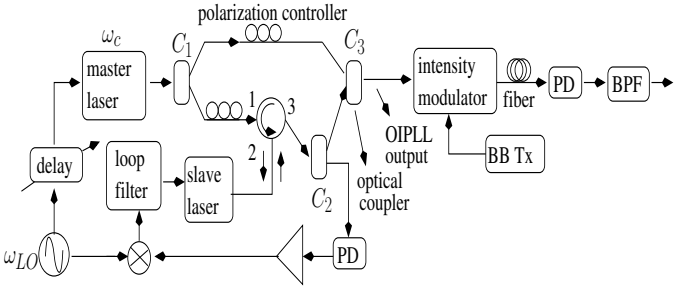

Fig. 37. Optical Injection Phase Locked Loop(OIPLL) (PD- Photo-diode; BB Tx- Baseband Transmitter; BPF- Band Pass Filter)

b) ***Optical Injection Phase Locked Loop****:* The OPLL relies on an architecture designed for maintaining phase coherence between the signals that are employed in coherent photo-detection. An OPLL reduces the optical phase noise imposed on the signal transmitted over a ROF link. OIL can be combined with the OPLL technique in order to amalgamate the benefits of both techniques. Such a transmitter is referred to as an Optical Injection Phase Locked Loop (OIPLL) [75], [62], which is shown in Fig. 37. The master-laser operating at an optical frequency of $f_c = \frac{\omega_c}{2\pi}$ Hz, is modulated by a RF tone at $f_{LO} = \frac{\omega_{LO}}{2\pi}$ Hz, as shown in Fig. 37. The master-laser output is split by the coupler C_1 into two parts, one of which enters port 1 and exits via port 2 of the OC, where this signal is employed in injection locking. The slave-laser in Fig. 37 is injection locked to one of the first-order ($N = 1$) or higher-order sidebands ($N > 1$) in the output of the master-laser. The slave-laser in Fig. 37 generates the injection locked output at $[f_c + N \cdot f_{LO}]$ Hz and also reflects the output of the master-laser. As shown in Fig. 37, the output of the slave-laser exits from port 3 of the OC, followed by a splitting operation by the coupler C_2 [75]. The upper output of C_2 in Fig. 37 is combined with the upper output of C_1 to generate the OIPLL output, while the lower output of C_2 is locally

This article has been accepted for publication in a future issue of this journal, but has not been fully edited. Content may change prior to final publication. Citation information: DOI 10.1109/COMST.2015.2394911, IEEE Communications Surveys & Tutorials

heterodyne photo-detected to generate a RF tone at $N \cdot f_{LO}$ Hz, which is then input to the feedback loop. In the feedback loop, output of the f_{LO} Hz oscillator is frequency-multipled by N and mixed with the photo-detected $N \cdot f_{LO}$ Hz RF tone. The mixer output depends on the phase difference between the two signals. As shown in Fig. 37, this mixer output is fed to a loop filter which generates a feedback that modulates the slave-laser. Hence, the loop-filter assists in phase-matching. Meanwhile, the OIPLL output is intensity modulated by the Baseband Transmitter (BB Tx), then transmitted over the fiber and finally photo-detected to generate an upconverted signal at $N \cdot f_{LO}$ Hz [75].

In addition to noise reduction, OIL also resulted in the enhanced linearity of the direct optical modulation scheme of Fig. 6(a) [63]. We now move on to another technique, namely optical feed-forward linearization, that helps enhance the linearity of both direct as well as external optical modulation, apart from suppressing the optical noise.

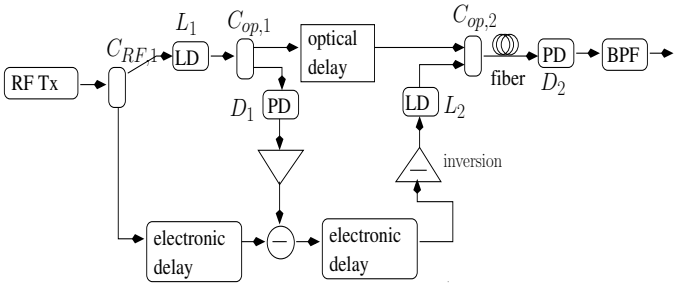

Fig. 38. Optical feed-forward linearization (RF Tx- RF transmitter; LD- Laser Diode; PD- Photo-diode; BPF- Band Pass Filter)

F. Optical feed-forward linearization

Optical feed-forward linearization is a technique that may be employed at the transmitter for pre-compensating the non-linear effects of optical modulation. This technique is implemented using the architecture seen in Fig. 38 [65]. As seen in Fig. 38, the input RF signal power is split into two branches by the RF coupler $C_{RF,1}$, where the upper branch modulates the optical carrier generated by laser L_1, while the lower branch is used as an uncorrupted reference signal. The modulated optical output of L_1 seen in Fig. 38 contains both the RF signal as well as the inter-modulation and harmonic distortion terms, which are additionally corrupted by RIN noise. This optical signal from L_1 is then split using a 50:50 optical coupler $C_{op,1}$, as seen in Fig. 38, where the lower-branch output of $C_{op,1}$ is photo-detected by the photo-diode D_1, amplified and then subtracted from the lower branch output of the RF coupler $C_{RF,1}$. The output of the RF coupler $C_{RF,1}$ does not suffer from the degradations and noise imposed by optical modulation, because it is generated by the electronic RF transmitter and not by photo-detecting the modulated optical signal [65]. Hence, the subtraction operation generates a difference signal that ideally contains only the distortion terms imposed by optical modulation and the RIN noise [65]. This electronically delayed difference signal is then inverted in Fig. 38 and modulated onto the output of laser the L_2. Note that the laser L_2 operates at an optical frequency $f_{L2} = \frac{\omega_{L2}}{2\pi}$, which is significantly different from the optical frequency $f_{L1} = \frac{\omega_{L1}}{2\pi}$ of L_1. As seen in Fig. 38, the modulated output of laser L_2 is then combined with the optically delayed modulated output of laser L_1 using the 90:10 optical coupler $C_{op,2}$ and transmitted over the fiber. If $A_1(t)e^{j\omega_{L1}t}$ and $A_2(t)e^{j\omega_{L2}t}$ are the optical signals received at photo-detector D_2 from lasers L_1 and L_2, respectively, then their coherent photo-detection by photo-detector D_2 results in the signal:

$$\begin{aligned} P_{linear} &= R|A_1(t)e^{j\omega_{L1}t} + A_2(t)e^{j\omega_{L2}t}|^2 \\ &= R|A_1(t)|^2 + R|A_2(t)|^2 \\ &\quad + 2R|A_1(t)||A_2(t)|\cos[j(\omega_{L1} - \omega_{L2})t], \end{aligned} \tag{34}$$

where again, R is the photo-diode's responsivity. Since the operating frequencies of the two lasers are significantly different, i.e. $(\omega_{L1} - \omega_{L2})$ is large, the third term of Equation (34) would be located within the electronic spectrum at a frequency that is far higher than that of the first two terms. The first two terms represent the coherent addition of the two signals. Since $R|A_2(t)|^2$ carries an inverted replica of the distortion plus RIN noise in $R|A_1(t)|^2$, this addition results in the cancellation of the distortion plus RIN noise term [65]. Hence, as per Equation (31), the SFDR will be significantly improved, because the feed-forward linearization technique of Fig. 38 suppresses the both inter-modulation products as well as the laser RIN over a large bandwidth.

We now conclude our discussions on the family of noise-reduction techniques. Low-biasing of the optical modulator is simpler than the subsequently discussed balanced photo-detection, but the former technique constrains the usable SCM signals to be within an octave. While the extent of noise-reduction obtained from the various noise-reduction techniques discussed in this paper depends on the specifications of the components used, OIL in general provides a much higher performance improvement than the rest. However, this comes at the cost of a higher transmitter complexity.

As mentioned previously, the last two techniques in the family of optical noise-reduction techniques, namely OIL and optical feed-forward linearization, also assist in increasing the linearity of optical modulation. Let us now continue our discourse by moving on to another subset of techniques that help increase the linearity of optical modulation, namely to the family of linearized optical modulators.

G. Linearized optical modulators

There are several architectures that linearize the transfer-characteristics of the MZM of Fig. 9(a), which result in the efficient suppression of the even-order and third-order inter-modulation products in the photo-detected signal. As a result of linearization, the SFDR of the links employing these architectures is maximised, since the SFDR of Equation (31) now depends on the much weaker fifth-order inter-modulation products, rather than on the third-order inter-modulation products. Some of the architectures within this subset include both the parallel and serial MZMs architectures, as well as the dual

This article has been accepted for publication in a future issue of this journal, but has not been fully edited. Content may change prior to final publication. Citation information: DOI 10.1109/COMST.2015.2394911, IEEE Communications Surveys & Tutorials

TABLE II

RADIO OVER FIBER (ROF) PERFORMANCE IMPROVEMENT TECHNIQUES (PART 2)

Technique	Year	Authors	Contribution
Linearized optical modulators	1990	Korotky *et al.* [76]	Two parallely connected modulators increased the linearity of modulation at the cost of a tolerable increase in the optical power and drive voltage employed.
	1991	Skeie *et al.* [77]	The cascading of modulators ensured 95 dB suppression of the 3rd harmonic when using a single tone modulating signal at a modulation depth of 20%.
	1999	Ackerman *et al.* [78]	Simultaneous modulation of optical carriers at two wavelengths achieved a dynamic range of 74 dB in 1 MHz over a bandwidth higher than an octave.
	2009	Masella *et al.* [79]	A linear polarizer was employed both before and after a mixed-polarization MZM to achieve 13 dB increase in the Spurious Free Dynamic Range (SFDR) when employing Optical Single Side Band (OSSB) modulation.
Optical filtering	2007	Lim *et al.* [80]	The optical sidebands that contribute most to the 3rd-order IMD in the photo-detected RF signal were filtered out using an optical filter to obtain an increase of 9 dB in the IMD suppression.
	2007	Hatice *et al.* [81]	An optical filter having a 3 dB bandwidth of 120 MHz was presented, which could separate two RF signals spaced as close as 50 MHz without significant distortion.
Pre-distortion and post-compensation	2002	Fernando *et al.* [82]	Pre-distortion in the downlink and post-compensation in the uplink using high-order adaptive filters linearized the ROF link, while keeping the RAP simple.
	2003	Roselli *et al.* [83]	Low cost pre-distortion circuits were designed for compensating 2nd and 3rd order distortions that arise from direct modulation of lasers.

wavelength equalization and polarization mixing to be detailed below.

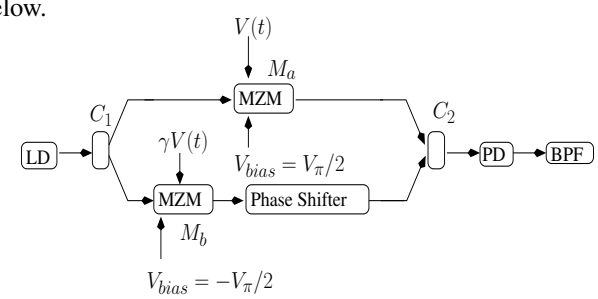

Fig. 39. Linearization using dual parallel MZMs (LD- Laser Diode; MZM- Mach-Zehnder Modulator; PD- Photo-diode; BPF- Band Pass Filter)

a) ***Parallel and serial MZMs****:* It can be observed from Equation (6) that the Quadrature Point (QP) biasing of a MZM results in negligible second-order distortions, but significant third-order distortions in the photo-detected signal, where the polarity of the third-order distortion depends on the quadrature bias voltage that is applied in Fig. 8. Dual-parallel linearization draws its motivation from the fact that the third-order distortions can be suppressed by superimposing signals in which the polarity of the third-order distortion is opposite [76]. As shown in Fig. 39, the output of the LD is fed to the coupler C_1 having a power splitting ratio of η_1, where the pair of outputs gleaned from the coupler C_1 are fed to the MZMs M_a and M_b, which are QP biased at $V_\pi/2$ and $-V_\pi/2$, respectively [76]. As shown in Fig. 39, the pair of MZMs are driven by the same RF signal $V(t)$, which have a voltage ratio of γ. The outputs of the pair of MZMs are combined by the coupler C_2 of Fig. 39 having a power combining ratio of η_2. Using Equation (3), the expression describing the photo-detected signal becomes:

$$I(t) = I_0|\sqrt{1-\eta_1}\sqrt{1-\eta_2}\cos(\frac{\pi}{4}+\frac{V(t)}{2V_\pi})e^{j\phi_a} + \sqrt{\eta_1}\sqrt{\eta_2}\cos(-\frac{\pi}{4}+\frac{\gamma V(t)}{2V_\pi})e^{j\phi_b}|^2, \quad (35)$$

where I_0 is the photo-detected signal, if there was no dual-parallel modulation. The optical phase shifter of Fig. 39 ensures that the phase-difference of the optical fields at the output of the pair of modulators is $\phi_a - \phi_b = \pi/2$. Then, the expression of Equation (35) becomes [76]:

$$\begin{aligned} I(t) &= I_0[(1-\eta_1)(1-\eta_2)\cos^2(\frac{\pi}{4}+\frac{V(t)}{2V_\pi}) \\ &\quad + \eta_1\eta_2\cos^2(-\frac{\pi}{4}+\frac{\gamma V(t)}{2V_\pi})] \\ &= I_0[(1-\eta_1)(1-\eta_2)(1-\sin(\frac{V(t)}{2V_\pi})) \\ &\quad + \eta_1\eta_2(1+\sin(\frac{\gamma V(t)}{2V_\pi}))] \\ &= \sum_{k=0}^{\infty} c_k[V(t)]^k. \end{aligned} \quad (36)$$

Using the Taylor series expansion of the $\sin(x)$ in the Equation (36), it may be readily shown that there are no even harmonics in the photo-detected signal at all. Hence, naturally there would be no second-order or fourth-order distortions in the photo-detected signal either. The third-order inter-modulation product I_{IM3} and the desired RF signal I_{signal} is proportional to the Taylor series coefficients c_3 and c_1, respectively. Hence [76], we have

$$I_{IM3} \propto c_3 \propto \left[(1-\eta_1)(1-\eta_2) - \eta_1\eta_2\gamma^3\right] \quad (37)$$

$$I_{signal} \propto c_1 \propto \left[(1-\eta_1)(1-\eta_2) - \eta_1\eta_2\gamma\right]. \quad (38)$$

It may be observed from Equation (37) that if the condition of $(1-\eta_1)(1-\eta_2) = \eta_1\eta_2\gamma^3$ is satisfied, then this would ensure having $c_3 = 0$ and hence we suppress the third-order inter-modulation products. However, this would also reduce the value of c_1 in Equation (38), which would attenuate the desired signal. Hence, this linearization comes at the cost of a weaker desired signal, which would in turn result in a reduced output SNR and an increased NF.

This article has been accepted for publication in a future issue of this journal, but has not been fully edited. Content may change prior to final publication. Citation information: DOI 10.1109/COMST.2015.2394911, IEEE Communications Surveys & Tutorials

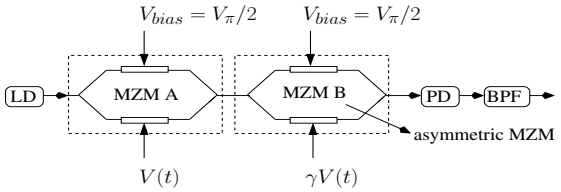

Fig. 40. Linearization using serial MZMs (LD- Laser Diode; MZM- Mach-Zehnder Modulator; PD- Photo-diode; BPF- Band Pass Filter)

This concept of using those values of power-splitting ratio and drive-voltage ratio that suppress the third-order distortion can be extended to the architecture of Fig. 40 as well, where two dual-drive MZMs, namely MZM-A and MZM-B, are connected in series and are QP biased with $V_{bias} = V_\pi/2$ [77]. The splitter as well as the coupler of MZM-B has an asymmetric power coupling ratio of η, while the ratio of the RF drive voltages to the MZMs is γ. Assuming the MZMs of Fig. 40 operate in the push-pull mode of operation discussed in Section II-A, the photo-detected signal is:

$$
\begin{aligned}
I(t) &= I_o \left| \frac{1}{2} e^{j(\frac{\pi V_{bias}}{2V_\pi} + \frac{\pi V(t)}{2V_\pi})} + \frac{1}{2} e^{-j(\frac{\pi V_{bias}}{2V_\pi} + \frac{\pi V(t)}{2V_\pi})} \right|^2 \\
&\times \left| \sqrt{\eta}\sqrt{\eta} e^{j(\frac{\pi V_{bias}}{2V_\pi} + \frac{\pi \gamma V(t)}{2V_\pi})} + \sqrt{1-\eta}\sqrt{1-\eta} e^{-j(\frac{\pi V_{bias}}{2V_\pi} + \frac{\pi \gamma V(t)}{2V_\pi})} \right|^2 \\
&= 0.25 I_o [1 + \cos(\frac{\pi V_{bias}}{V_\pi} + \frac{\pi V(t)}{V_\pi})] \\
&\times [0.5\eta^2 + 0.5(1-\eta)^2 + \eta(1-\eta)\cos(\frac{\pi V_{bias}}{V_\pi} + \frac{\pi \gamma V(t)}{V_\pi})] \\
&= 0.25 I_o [1 - \sin(\frac{\pi V(t)}{V_\pi})] \\
&\times [0.5\eta^2 + 0.5(1-\eta)^2 - \eta(1-\eta)\sin(\frac{\pi \gamma V(t)}{V_\pi})] \qquad (39) \\
&= \sum_{k=0}^{\infty} c_k (V(t))^k. \qquad (40)
\end{aligned}
$$

Using the Taylor series expansion of Equation (39) we get $c_k = 0$ for all even k in Equation (40), while those values of γ and η are chosen which would result in $c_3 = 0$, thereby suppressing the third-order distortions.

It is seen from Fig. 39 and Fig. 40 that linearizing the optical modulation using parallely or serially connected MZMs relies on a single laser and on multiple MZMs. We now discuss an alternate technique designed for linearizing optical modulation, namely dual-wavelength equalization, which relies on multiple lasers and on a single MZM.

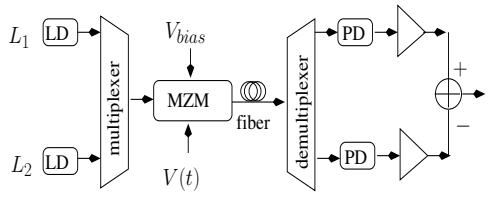

Fig. 41. Dual-wavelength equalization (LD- Laser Diode; MZM- Mach-Zehnder Modulator; PD- Photo-diode)

*b) **Dual-wavelength equalization**:* The strength of both the required signal and of the intermodulation products in the photo-detected signal depend on the switching voltage V_π of the MZM in Fig. 8. If two optical signals modulated by the same data are photo-detected and subtracted from each other, as seen in Fig. 41, then it is possible to suppress the third-order intermodulation products without totally suppressing the required signal, provided that the switching voltages employed in the two modulations schemes are different [78]. To expand a little further, Fig. 41 shows the block diagram of an architecture that implements dual-wavelength equalization, where the outputs of two laser diodes L_1 and L_2 are multiplexed using the WDM scheme of Fig. 22(b) and fed into a MZM modulator that is driven by the RF signal $V(t)$ and biased at V_{bias} Volts. Each of the two laser diodes operates at different wavelengths, where we set the ratio of the MZM switching voltages V_π of Equation (5) at these wavelengths to r [78]. As shown in Fig. 41, after transmission through the fiber, the signal is demultiplexed using the scheme of Fig. 22(b) and the two wavelengths are separately photo-detected, amplified and then subtracted. The ratio of the photo-detected signals after amplification is A, when there is no optical modulation. The mathematical expression of the difference signal is as follows:

$$
\begin{aligned}
I(t) &= I_o[1 + \cos(\frac{\pi V_{bias}}{V_\pi} + \frac{\pi V(t)}{V_\pi})] \\
&\quad - A I_o[1 + \cos(\frac{\pi V_{bias}}{V_\pi} + \frac{\pi V(t)}{r V_\pi})] \\
&= \sum_{k=0}^{\infty} c_k [V(t)]^k. \qquad (41)
\end{aligned}
$$

Using the Taylor series expansion of the $\cos(x)$ terms and exploiting the fact that the desired RF component I_{signal} as well as the third-order inter-modulation product I_{IM3} are proportional to the co-efficients c_1 and c_3, respectively, we arrive at [78]:

$$I_{signal} \propto c_1 \propto \left[\sin(\frac{\pi V_{bias}}{V_\pi}) - \frac{A}{r}\sin(\frac{\pi V_{bias}}{r V_\pi}) \right] \qquad (42)$$

$$I_{IM3} \propto c_3 \propto \left[\sin(\frac{\pi V_{bias}}{V_\pi}) - \frac{A}{r^3}\sin(\frac{\pi V_{bias}}{r V_\pi}) \right]. \qquad (43)$$

The bias voltage V_{bias} is chosen so that the MZM is QP biased or at least near-QP biased for both wavelengths, where we have $\frac{\pi V_{bias}}{V_\pi} = \frac{2m+1}{2}\pi$ and $\frac{\pi V_{bias}}{r V_\pi} = \frac{2n+1}{2}\pi$ with m and n being integers. When this specific biasing is used, we have $c_2 = [\cos(\frac{\pi V_{bias}}{V_\pi}) - \frac{A}{r^2}\cos(\frac{\pi V_{bias}}{r V_\pi})] \approx 0$, i.e. the photo-detected signal would only contain highly suppressed second-order inter-modulation products. When the MZM is QP biased, I_{IM3} of Equation(43) becomes [78]: $I_{IM3} \propto \left[1 - \frac{A}{r^3}\right]$. Hence, the third-order inter-modulation products can be suppressed, provided that the condition of $A = r^3$ is maintained [78]. However, maintaining this would reduce the strength of I_{signal} in Equation(42) and hence would increase the NF.

This article has been accepted for publication in a future issue of this journal, but has not been fully edited. Content may change prior to final publication. Citation information: DOI 10.1109/COMST.2015.2394911, IEEE Communications Surveys & Tutorials

The techniques conceived for linearizing the MZM transfer curve of Fig. 9(a) that have been discussed so far either employed multiple MZMs, as seen from Fig. 39 and Fig. 40, or employed multiple lasers, as seen from Fig. 41. We now continue our discourse about linearized optical modulators by discussing a technique that relies on a single MZM and a single laser to linearize optical modulation, but requires a polarizer.

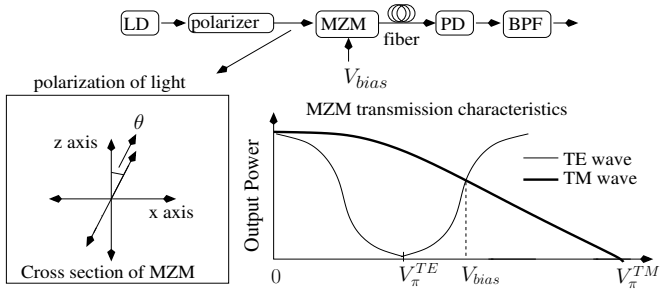

Fig. 42. Linearization using polarization mixing (LD- Laser Diode; MZM- Mach-Zehnder Modulator; PD- Photo-diode; TE- Transverse Electric; TM- Transverse Magnetic)

*c) **Polarization Mixing**:* The polarizarion of light characterizes the direction of its electric field vector. If an optical signal that is propagating along the y-axis and is polarized at an angle θ with respect to the z axis, as seen from Fig. 42, enters the modulator, then it results in a super-position of a pair of waves within the MZM that have orthogonal polarizations, which are typically referred to as the Transverse Electric (TE) and the Transverse Magnetic (TM) waves [84]. Since the MZMs are sensitive to the polarization of the optical signal, the switching voltages V_π^{TE} and V_π^{TM} are different for each of these polarizations, as shown in the MZM transfer characteristics of Fig. 42. The switching voltages and the bias voltage V_{bias} applied satisfy the following conditions:

$$\frac{\pi V_{bias}}{V_\pi^{TE}} = \frac{\pi(4m+1)}{2} \text{ and } \frac{\pi V_{bias}}{V_\pi^{TM}} = \frac{\pi(4n+3)}{2}, \quad (44)$$

where m as well as n are integers and $\gamma = \frac{V_\pi^{TE}}{V_\pi^{TM}}$ may be used for denoting the ratio of V_π^{TE} and V_π^{TM}. It can be seen from the MZM transfer characteristics of Fig. 42 that for a bias voltage of V_{bias} both waves experience QP biased modulation, and that the transfer characteristics have opposite slopes at this bias voltage. The pair of waves can be mathematically described by the orthogonal components of a vector. Hence, the photo-detected signal becomes:

$$\begin{aligned} I(t) &= I_0|\sin(\theta)\cos(\frac{\pi}{4}+\frac{V(t)}{2V_\pi})\hat{x} \\ &+ \cos(\theta)\cos(-\frac{\pi}{4}+\frac{\gamma V(t)}{2V_\pi})\hat{z}|^2 \\ &= I_0[\sin^2(\theta)\cos^2(\frac{\pi}{4}+\frac{V(t)}{2V_\pi}) \\ &+ \cos^2(\theta)\cos^2(-\frac{\pi}{4}+\frac{\gamma V(t)}{2V_\pi})] \\ &= I_0[\sin^2(\theta)(1-\sin(\frac{V(t)}{2V_\pi})) \\ &+ \cos^2(\theta)(1+\sin(\frac{\gamma V(t)}{2V_\pi}))] = \sum_{k=0}^{\infty} c_k (V(t))^k. \end{aligned} \quad (45)$$

Here I_0 is the unmodulated photo-detected signal. Using the Taylor series expansion of the trignometric terms in Equation (45), it may be readily observed that there are no even harmonics (i.e. we have $c_k = 0$ for k being even) in the photo-detected signal. This is because the MZM is QP biased for both modes. The third-order inter-modulation I_{IM3} and the desired RF signal I_{signal} are proportional to the Taylor series coefficients c_3 and c_1, respectively. Hence from Equation (45) we have,

$$I_{IM3} \propto c_3 \propto \left[\sin^2(\theta) - \cos^2(\theta)\gamma^3\right] \quad (46)$$

$$I_{signal} \propto c_1 \propto \left[\sin^2(\theta) - \cos^2(\theta)\gamma\right] \quad (47)$$

If the condition of $\frac{\cos^2(\theta)}{\sin^2(\theta)} = \frac{1}{\gamma^3}$ is satisfied, then this would ensure $c_3 = 0$ in Equation (46) and hence we would suppress third-order inter-modulation products in the photo-detected signal $I(t)$ of Equation (45) [84], where physically $\frac{\cos^2(\theta)}{\sin^2(\theta)}$ is the ratio of the optical power in the TE and TM modes of Fig. 42. However, according to Equation (47), this would also reduce the value of c_1, i.e. it would reduce the desired signal. On the other hand, unlike the architecture of Fig. 42 discussed here, the one in [79] did not rely on the TE and TM modes having opposite slopes at the QP of the MZM transfer curves in Fig. 42. Instead, it relied on two linear polarizers for suppressing the non-linear sidebands within the optical field. Explicitely, the authors of [79] cancelled some of the optical sidebands that contribute to the third-order distortion of the photo-detected signal, namely the sidebands at $f_c + 2f_1 - f_2$ Hz and $f_c + 2f_2 - f_1$ Hz. Here, f_c Hz is the optical frequency of the laser whose output was externally modulated using a dual-tone RF signal at f_1 Hz and f_2 Hz by the linearized modulator. Finally, similar polarization mixing techniques may also be employed for linearizing a phase modulator [85].

Having studied the subset of linearized modulators within the family of techniques designed for increasing the linearity of optical modulation, we now study how optical and electrical filtering can be invoked for increasing the linearity of optical modulation in the next two techniques to be discussed below.

This article has been accepted for publication in a future issue of this journal, but has not been fully edited. Content may change prior to final publication. Citation information: DOI 10.1109/COMST.2015.2394911, IEEE Communications Surveys & Tutorials

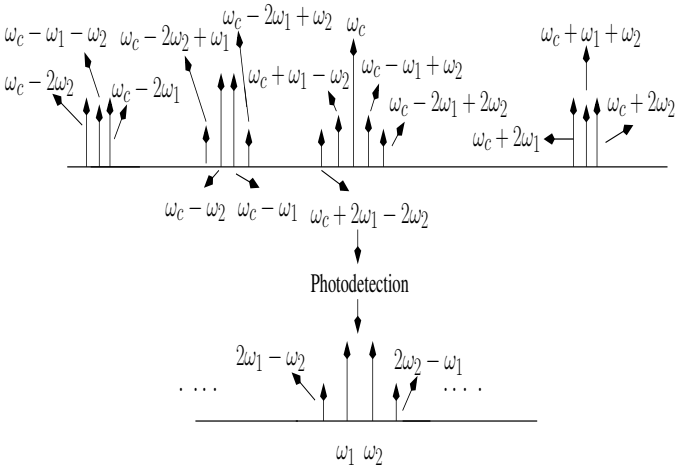

Fig. 43. Optical spectrum of non-linear OSSB modulation

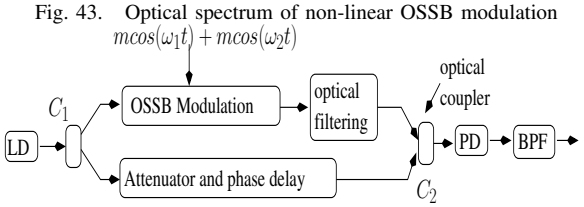

Fig. 44. Linearization using optical filtering (LD- Laser Diode; PD- Photodiode; BPF- Band Pass Filter)

H. Optical filtering:

Fig. 43 [80] shows the optical spectrum after an optical carrier at $f_c = \frac{\omega_c}{2\pi}$ Hz has been OSSB modulated by two RF tones having frequencies of $f_1 = \frac{\omega_1}{2\pi}$ Hz and $f_2 = \frac{\omega_2}{2\pi}$ Hz. Fig. 43 [80] also shows the spectrum of the photo-detected signal. As shown in Fig. 43, the most significant inter-modulation products in the photo-detected signal are the third-order inter-modulation products which are located at $(2\omega_1 - \omega_2)$ and $(2\omega_2 - \omega_1)$. The major pairs in the optical spectrum of Fig. 43 that beat together during photo-detection and generate the third-order inter-modulation product at $(2\omega_1 - \omega_2)$ are those at $\{\omega_c, \omega_c - 2\omega_1 + \omega_2\}$ and $\{\omega_c - \omega_1, \omega_c + \omega_1 - \omega_2\}$. Similarly, the major pairs in the optical spectrum of Fig. 43, that beat together during photo-detection and generate the inter-modulation product at $(2\omega_2 - \omega_1)$ are those at $\{\omega_c, \omega_c - 2\omega_2 + \omega_1\}$ and $\{\omega_c - \omega_2, \omega_c - \omega_1 + \omega_2\}$. While the sidebands at $(\omega_c - \omega_1)$ and $(\omega_c - \omega_2)$ in Fig. 43 are the required modulation sidebands, those at $(\omega_c - 2\omega_1 + \omega_2)$ and $(\omega_c - 2\omega_2 + \omega_1)$ are too close to the required sidebands to be easily filtered out using low-cost optical filters. By contrast, the sidebands at $(\omega_c + \omega_1 - \omega_2)$ and $(\omega_c - \omega_1 + \omega_2)$ may be readily filtered out using inexpensive optical filters. The architecture that implements this filtering technique is shown in Fig. 44, where the unmodulated laser output power is split into two halves using the coupler C_1. One of the outputs of C_1, namely the upper branch, is OSSB modulated followed by optical filtering for removing the sidebands at $(\omega_c + \omega_1 - \omega_2)$ and $(\omega_c - \omega_1 + \omega_2)$ in Fig. 43. The optical filter also filters out the optical carrier at ω_c. Then, after accurate attenuation and phase-shift, the optical carrier is re-introduced using the other output of coupler C_1, namely the lower branch of Fig. 44. This technique can also be extended to three-tone modulation by filtering out the components at $(\omega_c \pm \omega_m \mp \omega_n)$ for $m, n \in \{1, 2, 3\}$.

We now study the final technique designed for increasing the linearity of optical modulation, namely pre-distortion and post-compensation. These techniques, unlike the previous techniques of the family, are implemented in the electronic domain, rather than in the optical domain.

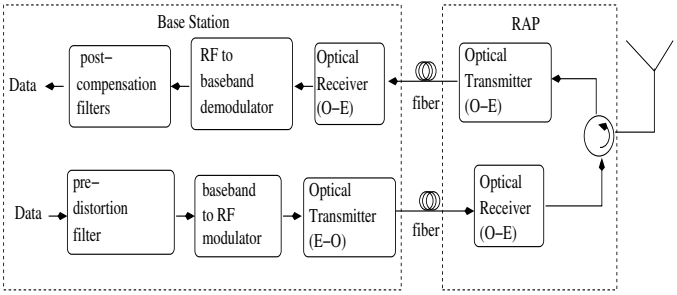

Fig. 45. **Linearization using pre-distortion and post-compenasation filters, as discussed in [82]** (RAP- Radio Access Point; O-E- Optical to Electronic; E-O- Electronic to Optical)

I. Pre-distortion and post-compensation

The non-linearities encountered in optical modulation can be compensated for at the optical transmitter and receiver by pre-distortion and post-compensation, respectively, using electronic filters. Fig. 45 of [82] shows the block diagram of an architecture that employs transmitter pre-distortion and receiver post-compensation filters in the BS, where again, the pre-distortion filter compensates for the non-linear effects of the ROF Downlink (DL) prior to the actual transmission, while the post-compensation filter removes the higher order sidebands generated by the non-linear effects after the ROF Uplink (UL) transmission [82]. Both these filters are located at the BS and hence have the advantage of centralised signal processing. This filter-based compensation technique may be used in ROF links employing both the direct [83] as well as the external modulation schemes of Fig. 6(a) and Fig. 8, respectively.

During DL transmission, the data signal is firstly pre-distorted using the non-linear characteristic of the filter, then upconverted to RF and finally employed in modulating the DL optical carrier, as seen in Fig. 45. This DL optical signal is transmitted to the RAP, where it is photo-detected and then wirelessly transmitted to the MS. The UL wireless signal received at the RAP of Fig. 45 is employed for modulating the UL optical carrier followed by transmission to the BS, where the UL ROF signal is photo-detected and then downconverted. Finally, the signal is fed to the post-compensation filter of Fig. 45 and then decoded. These filters can also be made adaptive, since the modulated response varies significantly between various lasers [82]. The sinusoidal transfer function of a MZM shown in Fig. 9(a) can be compensated by applying a arcsine filter[1] to the modulating signal prior to optical modulation [86].

[1]A filter in which the ouput is related to the input through a inverse sine function.

This article has been accepted for publication in a future issue of this journal, but has not been fully edited. Content may change prior to final publication. Citation information: DOI 10.1109/COMST.2015.2394911, IEEE Communications Surveys & Tutorials

We now conclude our discussions on the family of techniques conceived for increasing the linearity of optical modulation. While the OIL techniques of Fig. 35, Fig. 36 and Fig. 37 significantly increase the linearity of direct optical modulation, they cannot be used for increasing the linearity of the external optical modulation of Fig. 8. Moreover, they significanlty increase the complexity of the optical transmitter. It requires polarization matching between the master- and slave-laser, which are connected using sophisticated polarization maintaining fibers. Unlike OIL, the optical feed-forward linearization technique of Fig. 38 may be beneficially applied for eliminating the distortions in the case of both direct as well as external modulation [65]. However, this technique requires both accurate amplitude and phase matching for attaining a beneficial distortion and noise reduction, which may be achieved by using the amplifiers and delay elements of Fig. 38. The phase-mismatch introduced by the chromatic dispersion of the fiber may be compensated, provided that the transmitter is designed for a fixed fiber length, which would however relatively limit the employement of such a transmitter. Additionally, it is worth noting that this linearization technique is also associated with a relatively high implementational cost [83]. Employing the linearized MZMs of Fig. 39, Fig. 40, Fig. 41 and Fig. 42 results in the suppression of the distortion, but it is accompanied by the suppression of the desired signal as well. The subsequently discussed optical filter-based linearization of optical modulation. as shown in Fig. 44, results in significant performance improvements. However, this scheme relies on the filtered sidebands found at $(\omega_c + \omega_1 - \omega_2)$ and $(\omega_c - \omega_1 + \omega_2)$ in the optical spectrum of Fig. 43 being sufficiently far from the desired sidebands at $(\omega_c - \omega_1)$ and $(\omega_c - \omega_2)$, thereby imposing restrictions on the usable RF frequencies. We finally discussed the electronic filter-based technique of Fig. 45, which is effective in the case of external modulation, but cannot easily suppress both the higher harmonics and the inter-modulation products in direct modulation [65]. Moreover, the operational bandwidth of these electronic techniques is limited [65]. Nevertheless, their strength is their relatively low implementational cost, when compared to other optical techniques [83].

Having focussed our attention on the benefits of increasing the linearity of optical modulation, let us now concentrate our attention on the family of techniques that help in overcoming fiber-nonlinearity.

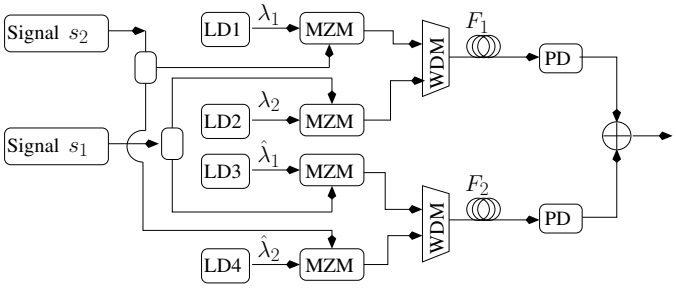

Fig. 46. Multiple fiber transmission for overcoming the effects of fiber non-linearity (LD-Laser Diode; MZM- Mach Zehnder Modulator; PD- Photodiode; WDM- Wavelength Division Multiplexing)

J. Overcoming the effects of fiber non-linearity

As was discussed in Section II-B, XPM and SPM are the undesired consequences of the fiber's non-linearity. The detrimental effects of these phenomena can be greatly reduced by using constant-amplitude optical modulation schemes like optical frequency and optical phase modulation, which however requires additional components for photo-detection, as was discussed in Section III-B. Additionally, two basic techniques have been proposed in the literature for suppressing the effects of fiber non-linearity, including multiple fiber transmission [87] and carrier suppression [87]. Multiple fiber transmission is similar to the balanced photo-detection technique of Fig. 34, since both techniques involve the removal of the undesired components by adding two replicas of the same signal. However, multiple fiber transmission requires the transmission of the signals through a pair of identical fibers at different wavelengths. For example, as seen in Fig. 46, a pair two signals s_1 and s_2 may be modulated onto the wavelengths λ_1 generated by laser LD1 and λ_2 generated by laser LD2, respectively and then transmitted through the fiber F_1 for photo-detection. Similarly, these signals are also modulated onto the wavelengths $\hat{\lambda}_2$ generated by laser LD4 and $\hat{\lambda}_1$ generated by laser LD3 and then transmitted through the fiber F_2 for photo-detection, as portrayed in Fig. 46. The specific choice of these four wavelengths should meet the following criteria [87]: $\lambda_1 - \lambda_2 = \hat{\lambda}_1 - \hat{\lambda}_2$ and $D_1 = -D_2$, where D_1 and D_2 are the dispersion parameters of the fibers F_1 and F_2, respectively, as defined in Section II-B. In such a scenario the XPM crosstalk contamination imposed on the received signals in the pair of optical fibers are 180^0 out of phase and hence they would cancel out each other after their addition [87]. The disadvantage of this technique is the need to transmit the same signal through multiple fibers, thereby reducing the achievable throughput.

On the other hand, as discussed in Section V-B, carrier suppression improves the receiver sensitivity of the link, which implies that the transmitter can operate at a lower transmit power, thereby reducing the effects of fiber non-linearity.

Let us now continue our discourse by considering the family of techniques designed for overcoming chromatic dispersion.

K. Overcoming Chromatic Dispersion

Chromatic dispersion, originally discussed in Section II-B, results in symbol-broadening [24] and an associated power-reduction penalty [34], and hence increases the BER of the ROF link. A ROF link that employs the ODSB modulation technique of Fig. 16(a) along with the direct photo-detection technique of Fig. 13(a) constitutes the most common ROF implementation, which is a direct consequence of its low cost as well as low complexity. However, the disadvantage of employing ODSB modulation is the above-mentioned chromatic dispersion-induced power penalty, where the chromatic dispersion imposes a phase-shift of the optical signal propagating through the fiber. The frequency-dependent phase-change imposed by chromatic dispersion results in a phase-difference between the upper and lower sidebands in the ODSB signal

This article has been accepted for publication in a future issue of this journal, but has not been fully edited. Content may change prior to final publication. Citation information: DOI 10.1109/COMST.2015.2394911, IEEE Communications Surveys & Tutorials

TABLE III
RADIO OVER FIBER (ROF) PERFORMANCE IMPROVEMENT TECHNIQUES (PART 3)

Technique	Year	Authors	Contribution
Overcoming fiber non-linearity	2000	Yang *et al.* [87]	Signal transmission using 2 parallel fibers reduced the crosstalk by 15 dB over 200 MHz, while carrier suppression reduced the crosstalk by 20 dB over 2 GHz.
Overcoming Chromatic Dispersion	1997	Marti *et al.* [88]	Chromatic dispersion was overcome by compensating the differential delay between the optical frequencies using a Tapered Linearly Chirped Grating (TLCG).
	1997	Smith *et al.* [39]	An OSSB signal was generated using a dual-drive MZM and was shown to suffer from a lower dispersion-induced power penalty than ODSB modulation.
	1997	Smith *et al.* [27]	It was shown that the deteriorating effects of chromatic dispersion can be reduced by using chirped OSSB signals.
	1998	Ramos *et al.* [89]	Fiber non-linearity induced Self-Phase Modulation (SPM) was gainfully used for generating chirp having polarity that is opposite to the dispersion-induced chirp.
	1999	Sotobayashi *et al.* [90]	The dispersion-induced power penalty inflicted on an ODSB signal carrying a 60 GHz RF signal was reduced by using mid-way Optical Phase Conjugation (OPC).
	2006	Yu *et al.* [91]	It was shown that Optical Carrier Suppression (OCS) modulation has a high spectral efficiency and receiver sensitivity and small dispersion-induced power penalty.
Digitized Radio Over Fiber (DROF)	2009	Nirmalathas *et al.* [92]	It was shown that DROF ensured greater link linearity and exhibited the performance advantages of a digital optical link.
	2014	Yang *et al.* [93]	

of Fig. 16(a). The photo-detected signal is proportional to the optical power $P(t) = |E(t)|^2$, with $E(t)$ being the optical field-strength of the ODSB signal, where the optical power is attenuated owing to the destructive interference between the beating sidebands. Hence, this optical power-attenuation is referred to as dispersion-induced power-penalty. The attenuation of the optical power results in the attenuation of the electronic power P_{rf} of the photo-detected signal at f_{rf} Hz, where the extent of attenuation is given by [34]:

$$P_{rf} \propto \cos^2\left[\frac{\pi \cdot L \cdot D \cdot \lambda_c^2 \cdot f_{rf}^2}{c \cdot [1 - \frac{2}{\pi} \cdot \arctan(\alpha_{chirp})]}\right], \qquad (48)$$

where D is the chromatic-dispersion parameter (also called GVD parameter) of Equation (10) discussed in Section II-B, L is the length of the fiber, λ_c is the wavelength of the optical carrier, c is the speed of light in vacuum and α_{Chirp} is the chirp parameter of the signal. Chirping in an intensity-modulated optical signal refers to a time-dependent variation of the instantaneous optical frequency from its ideal value of $f_c = \frac{c}{\lambda_c}$ Hz. Thus, chromatic dispersion limits the both the affordable fiber lengths L and the modulating-signal frequencies f_{rf}, when ODSB modulation is employed [94]. Chromatic dispersion can be compensated by using specialised fibers called Dispersion Compensation Fibers (DCF) [24]. If D_{comp} is the dispersion parameter of the DCF, then chromatic dispersion can be overcome by propagating the optical signal through L_{comp} meters of the DCF, after it has propagated through L meters of the standard SMF, provided that the following condition is met [24]:

$$D_{comp} \cdot L_{comp} = -D \cdot L. \qquad (49)$$

The compensation of non-linearity in optical modulation using electronic filters was discussed in Section V-I. Similarly, even chromatic dispersion can be compensated using electronic equalisers [10].

Additionally, other techniques that have been proposed in the literature for overcoming chromatic dispersion include employing dispersion-tolerant schemes like the OSSB and OCS modulation schemes of Fig. 16(b) and Fig. 16(c), apart from employing the fiber-gratings of Fig. 49, chirped optical signals, the optical phase conjugation technique of Fig. 53 and the exploitation of SPM [89], which are detailed below.

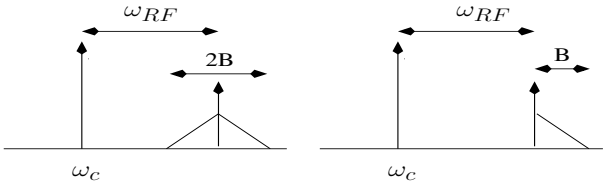

(a) Using Electronic Double Side Band (EDSB) signal (b) Using Electronic Single Side Band (ESSB) signal

Fig. 47. Optical Single Side Band (OSSB) signal spectrum

*a) **Dispersion-tolerant modulation schemes**:* Employing the OSSB and OCS optical modulation formats of Fig. 16(b) and Fig. 16(c), respectively, results in a high degree of immunity to the dispersion-induced power penalty [39], [91]. Additionally, the BS transmitter may modulate a BB signal onto the optical carrier, while, at the RAP, the heterodyne photo-detection technique of Fig.13(b) would ensure the generation of an up-converted RF signal that does not suffer from the dispersion-induced power penalty.

The detrimental effect of chromatic dispersion increases as the optical bandwidth of the signal increases. Hence, the resilience of OSSB modulation to chromatic dispersion can be further improved by employing electronic single-sideband modulating signals during optical modulation, instead of the usual electronic double-sideband signal [34]. Fig. 47(a) and Fig. 47(b) illustrate the optical spectra of OSSB signals that have been generated using electronic double-sideband and single-sideband signals, respectively [34]. Even when OSSB modulation is employed, some residual chromatic dispersion persists because the modulating signal has a finite bandwidth of $2B$ around the RF carrier f_{RF}, as seen in Fig. 47(a). As seen from Fig. 47(b), the excess-bandwidth can be eliminated by employing an electronic single-sideband signal during optical modulation, instead of the usual electronic DSB signal [34], which leads to a further reduction of the detrimental effects of chromatic dispersion.

However, unlike the ODSB modulation, the OSSB and

This article has been accepted for publication in a future issue of this journal, but has not been fully edited. Content may change prior to final publication. Citation information: DOI 10.1109/COMST.2015.2394911, IEEE Communications Surveys & Tutorials

OCS modulations, primarily rely on the external modulation technique of Fig. 8(b) that employs a dual-drive MZM [34]. Thus, if we are constrained to employ ODSB modulation, then we may overcome the limitations imposed by chromatic dispersion by relying on the techniques discussed below, where employing fiber-gratings is discussed first.

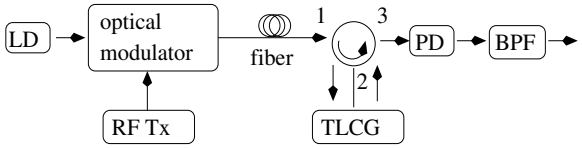

Fig. 48. Chromatic dispersion compensation using a Tapered Linearly Chirped Grating (TLCG)(LD- Laser Diode; RF Tx- RF Transmitter; PD- Photo-diode; BPF- Band Pass Filter)

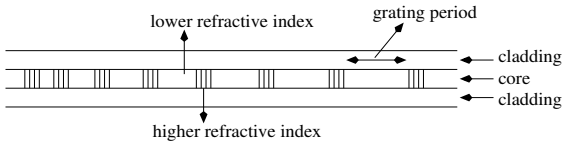

Fig. 49. Linearly chirped Fiber Bragg Grating (FBG)

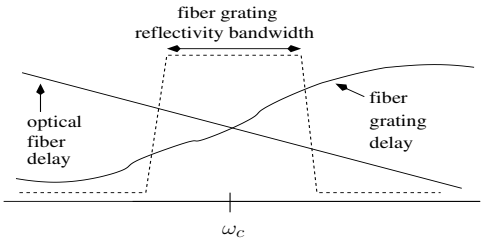

Fig. 50. Optical delay of Tapered Linearly Chirped Grating (TLCG)

b) ***Fiber gratings****:* As discussed in Section II-B, chromatic dispersion occurs because the propagation velocity of the different frequencies contained in the optical signal are different. Thus, chromatic dispersion manifests itself in the form of the various frequency components having different delays. This delay difference can be equalized by using the technique of Fig. 48 that relies on the Tapered Linearly Chirped Grating (TLCG)[1] optical filter [88], where the ouput of a laser operating at an optical frequency of $f_c = \frac{\omega_c}{2\pi}$ Hz is modulated using a RF signal and then transmitted over the fiber. At the receiver of Fig. 48, the optical signal enters port 1 and exits from port 2 of the optical circulator (OC). The signal then enters the TLCG and it is reflected back into port 2 of the OC. Finally, the signal exits from port 3 and then it is photo-detected. As seen from Fig. 50, within its reflectivity bandwidth[2] that is centered around the optical carrier of ω_c, the TLCG introduces an optical delay that is a near-linear function of the optical frequency. Thus, as seen from Fig. 50, the frequency-dependent dispersion-induced delay introduced by the optical fiber can be compensated by using a TLCG [88].

[1]The linearly chirped FBG of Fig. 49, unlike the conventional FBG of Fig. 18(a), has a linear increase/decrease of the otherwise constant grating period. The TLCG consists of a linearly chirped fiber grating that is implemented in a tapered fiber.

[2]Band of frequencies pre-dominantly reflected by the optical filter.

While this technique is potentially capable of compensating the effects of chromatic dispersion, it also requires an additional optical filter with a carefully designed optical delay profile. In the next section, we discuss a technique, namely the employement of chirped optical signals, that is easier to implement.

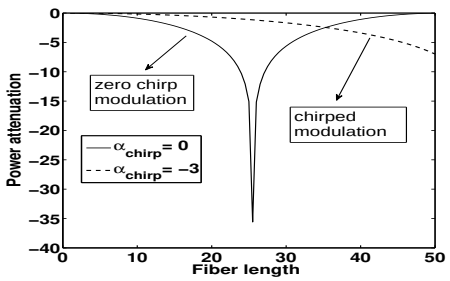

Fig. 51. Power attenuation induced by chromatic dispersion [27]

c) ***Chirped optical signals****:* The dispersion-induced power-reduction of ODSB signals was formulated in Equation (48), where it can be observed that the extent of power-reduction depends on both the magnitude and polarity of the chirp parameter α_{chirp} of the transmitted signals. Fortunately, the power-reduction could be lessened by introducing chirp in the transmitted signal, as shown in Fig. 51, while ensuring that this chirp has the reverse polarity with respect to the chirp induced by the chromatic dispersion [27]. It can be seen from Equation (3) that the dual-drive MZM of Fig. 8(b) introduces an adjustable chirp, where the value of α_{chirp} depends on the amplitudes of both the drive voltages that are applied to the arms of the dual-drive MZM, i.e. on $V_1(t)$ and $V_2(t)$. As discussed in Section II-A, zero-chirp operation is possible, if the dual-drive MZM of Fig. 8(b) operates in the push-pull mode. If $V_1(t)$ and $V_2(t)$ are sinusoidal signals associated with amplitudes of V_1 and V_2, respectively, then we have [27]:

$$\begin{aligned}\alpha_{chirp} &= \frac{V_1+V_2}{V_1-V_2}\tan\left(\frac{\pi(V_{bias}-V_\pi)}{2V_\pi}\right)\\ &= \pm\frac{V_1+V_2}{V_1-V_2} \quad \text{(ODSB signal)},\end{aligned} \tag{50}$$

where $V_{bias} = \frac{(2n+1)V_\pi}{2}$ for ODSB modulation for $n = 0, 1, ...$ The dual-drive MZM typically has a non-ideal extinction ratio of $\gamma \neq 1$, where for the case of ODSB signal transmission we have $\alpha_{chirp} = \frac{V_1+\gamma^2 V_2}{\gamma(V_1-V_2)}$ [95]. As discussed in Section II-A, the ideal value of γ is 1. Fig. 51 compares the dispersion-induced power attenuation when using unchirped and chirped optical signals, where the dispersion-induced power attenuation is shown for the case of ODSB transmission, that employs an optical wavelength of 1550 nm, a sinusoidal RF modulating signal of 12 GHz and a fiber having a dispersion parameter of $D = 17ps/nm/km$ [27]. It can be seen from Fig. 51, that using negative values of α_{chirp} reduces the dispersion-induced power attenuation [27].

While the above techniques rely on a MZM for generating a chirp that compensates the dispersion-induced chirp, the technique discussed in the next section relies on the otherwise

This article has been accepted for publication in a future issue of this journal, but has not been fully edited. Content may change prior to final publication. Citation information: DOI 10.1109/COMST.2015.2394911, IEEE Communications Surveys & Tutorials

undesired effect of SPM for compensating the the dispersion-induced chirp.

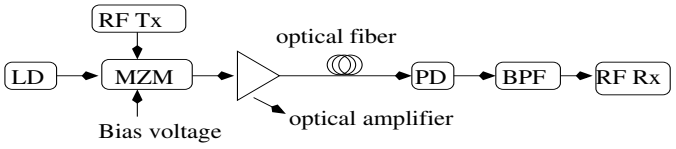

Fig. 52. Chromatic dispersion compensation using Self-Phase Modulation (SPM) (LS- laser Diode; RF Tx- RF Transmitter; PD- Photo-diode; BPF- Band Pass Filter; RF Rx- RF Receiver)

*d) **Beneficial exploitation of SPM**:* As discussed in Section II-B, SPM is imposed by the fiber's non-linearity and it becomes significant, when a high optical transmit-power is employed. This is the case in the architecture of Fig. 52 owing to inserting an optical amplifier in the transmitter. SPM introduces a chirp that has the opposite polarity to the chirp that is introduced by chromatic dispersion [89]. Thus, SPM can be employed for reducing the effects of chromatic dispersion [89], where the extent of SPM-induced chirp depends both on the optical power levels and on the fiber length. However, the technique of Fig. 52 may need the use of an additional optical equipment, namely an optical amplifier, which also adds ASE noise. The main limitation of this technique is the inevitable accompanying non-linear phenomenon of Stimulated Brillouin Scattering (SBS), which was discussed in Section II-B. Hence, the resultant SBS must be suppressed using other techniques. Additionally, the high optical power levels used in this technique may result in fiber's non-linearity inducing significant inter-modulation in SCM systems and XPM in WDM systems.

We now continue our discourse on the family of techniques designed for overcoming chromatic dispersion by considering the optical phase conjugation technique that aims for eliminating the dispersion-induced phase-difference between the upper and lower sidebands in the ODSB signal of Fig. 16(a).

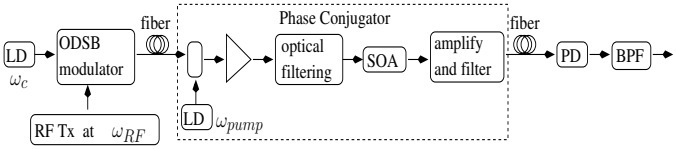

Fig. 53. Chromatic dispersion compensation using Optical Phase Conjugation (LS- laser Diode; RF Tx- RF Transmitter; PD- Photo-diode; BPF- Band Pass Filter)

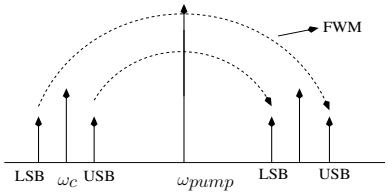

Fig. 54. Optical phase conjugation using Four Wave Mixing (FWM) (LSB- Lower Side Band; USB- Upper Side Band)

*e) **Optical Phase Conjugation**:* An ODSB signal suffers from the dispersion-induced power-reduction imposed by the phase-difference between the upper and lower sidebands. This power-penalty can be avoided by swapping the two sidebands midway through the fiber-length [90]. This would ensure a similar dispersion-induced phase-shift in both the upper and the lower sidebands, which eliminates the detrimental phase-difference. This technique is referred to as Optical Phase Conjugation (OPC). Fig. 53 shows the block diagram of optical phase conjugation, where an ODSB signal is generated by modulating an optical carrier at ω_c using a RF signal at ω_{RF}. The ODSB signal consists of the optical carrier along with lower and upper sidebands at $\omega_c - \omega_{RF}$ and $\omega_c + \omega_{RF}$, respectively. The signal enters the phase conjugator of Fig. 53 after propagating half-way through the fiber length. As shown within the phase conjugator of Fig. 53, a high-power optical carrier at ω_{pump}, that is referred to as the pump signal, is coupled with the optical signal being transmitted. This combined signal is optically amplified, followed by optical filtering to remove the optical amplifier's out-of-band ASE noise discussed in Section II-D and it then enters a Semiconductor Optical Amplifier (SOA). The FWM process originally introduced in Section II-B, that occurs within the SOA between the pump signal ω_{pump} and the modulated signal, generates an additional signal as per Equations (11) and (12) [90], where the signal-spectrum at the output of the conjugator is shown in Fig. 54. It should be noted that the wavelength-conversion efficiency is polarization sensitive and hence the modulated signal and pump signal must be polarization matched using a polarization controller, prior to their coupling. It can be seen from Fig. 54 that the lower sideband of the original signal correponds to the upper sideband in the new signal and vice-versa. The resultant optical signal is then filtered, amplified and transmitted over the remaining half of the fiber link. Additionally, the effect of SPM, originally introduced in Section II-B, is partially compensated by OPC [90]. Naturally, perfect compensation of the power-dependent SPM would have been possible only if the power variation along the fiber length was perfectly symmetric with respect to the position of the phase conjugator [90]. However in reality, the optical power gradually reduces as the signal propagates through both the fiber segments in Fig. 53.

We now conclude our discussions on the family of techniques conceived for overcoming chromatic dispersion and move on to the next performance improvement technique, namely Digitized Radio Over Fiber (DROF). The digital optical link used in long-distance wired optical communication provides a better performance than the ROF link of Fig. 3. Hence, DROF aims for incorporating the advantages of a digital optical link in ROF communication.

L. DROF architecture

All the ROF architectures discussed so far modulate the analog RF signal onto the optical carrier, as seen from Fig. 3, which, for the sake of contrast, we refer to as Analog Radio Over Fiber (AROF). By contrast, in Digitized ROF (DROF), the RF signal is sampled, digitized and then is used for modulating the optical carrier. The main motivation behind the design of the DROF architecture is the desire to have a digital optical link and at the same time rely on

This article has been accepted for publication in a future issue of this journal, but has not been fully edited. Content may change prior to final publication. Citation information: DOI 10.1109/COMST.2015.2394911, IEEE Communications Surveys & Tutorials

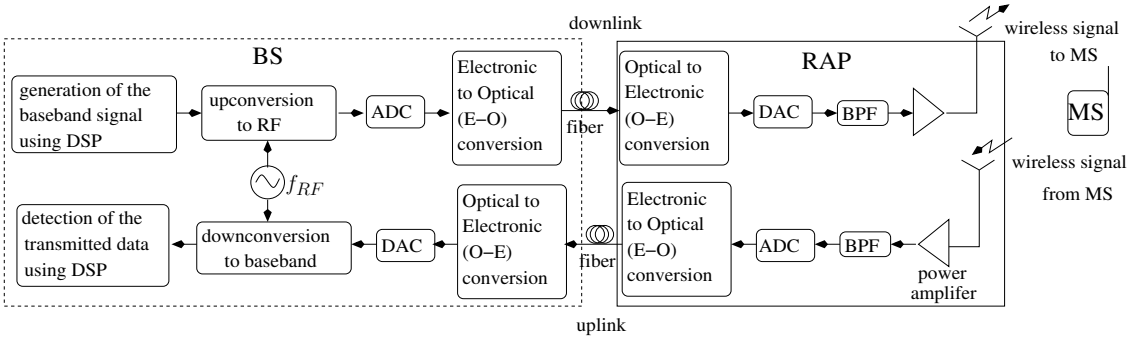

Fig. 56. DROF link block diagram

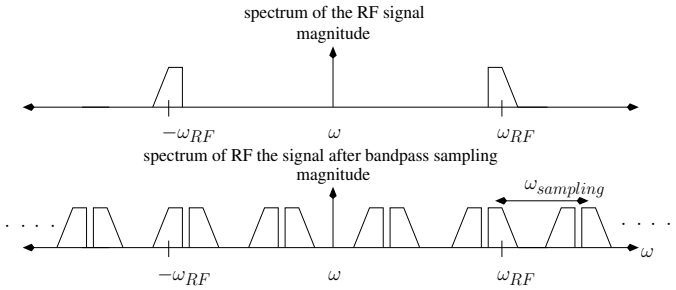

Fig. 55. Bandpass sampling

centralised signal processing at the BS [92]. In the DROF architecture of Fig. 56, the signal processing required for generating the DL RF signal is carried out at the BS, where the RF signal is digitized before modulating the optical carrier [92]. Conventional sampling of the RF signal at a rate higher than twice the highest frequency present in the signal using the Nyquist Theorem is not practically feasible, because of the high values of the wireless carrier frequency. Hence, typically critical bandpass sampling is used [92], which is illustrated in Fig. 55, where the sampling frequency is chosen to satisfy the aliasing-free condition, so that the original analog RF signal can be reconstructed by using a bandpass filter centered at $f_{RF} = \frac{\omega_{RF}}{2\pi}$ Hz and having a bandwidth of B Hz. The valid bandpass sampling rates for a bandwidth of B are [92]:

$$\frac{2(f_{RF}+\frac{B}{2})}{k} \leq f_s \leq \frac{2(f_{RF}-\frac{B}{2})}{k-1} \; \forall \; 1 \leq k \leq \lfloor \frac{f_{RF}+\frac{B}{2}}{B} \rfloor, \quad (51)$$

where $\lfloor w \rfloor$ represents the integer part of w and k is an integer. Thus, when employing bandpass sampling, the sampling rate depends on the bandwidth of the signal, rather than, on the highest frequency present in the signal [92].

Fig. 56 illustrates the block diagram of a DROF architecture [92], where the DL BB signal is generated, upconverted and digitized using an Analogue to Digital Convertor (ADC) at the BS. The digitized signal is then employed in modulating the optical carrier. At the RAP, the photo-detected BB signal is fed to a Digital to Analogue Convertor (DAC) and the RF signal is reconstructed. The reconstructed RF signal is then amplified using a power amplifier and transmitted over the wireless channel. As shown in Fig. 56, the UL signal received at the RAP is amplified, bandpass filtered, digitized and employed for modulating the optical carrier. At the BS, the photo-detected signal is fed to a DAC, followed by down-conversion to a BB signal. The transmitted UL bits are then detected from the BB signal, by employing Digital Signal Processing (DSP) techniques [92].

The advantage of employing optical BB modulation is that one can use inexpensive direct modulation [92] or an external modulator having a low-modulation bandwidth [96]. Furthermore, typically a performance improvement is achieved by employing a digital optical link. Employing a DROF architecture, that involves the transmission of optical signals carrying BB digital data, has a high degree of tolerance to the previously mentioned dispersion-induced power-penalty [3] and also ensures a higher degree of linearity of the optical-link. Hence, DROF provides a better performance than the conventional ROF architecture of Fig. 3 [92], [93]. However, the trade-off in this case is the need for using ADCs and DACs and hence DROF has a more complex and costly RAP than the conventional ROF link of Fig. 3. Furthermore, BB optical modulation is also employed in fiber-based wired optical communication and has been extensively dealt with in various tutorials [97] and books [24].

At this point it is worth mentioning that despite the low sampling rate achieved using bandpass sampling, the bit rate of the DROF link may still be high, because it is the product of the sampling rate and the ADC's bit-resolution. Recently, a variant of the DROF technique, namely sampled RF-over-fiber, was proposed to overcome this challenge [93]. The solution in [93] had a similar architecture as Fig. 56, with the difference that the ADC only samples the RF signal using a sample-and-hold circuit without quantizing or encoding the sampled values. The sampled baseband signal is then transmitted over the ROF link. In the UL, the BS's receiver filters out the down-converted version of the RF signal from the spectrum of the baseband sampled signal, while in the DL, the RAP's receiver filters the image at the RF frequency. However, in the DL, employing a higher carrier frequency results in a weaker filtered image.

We now conclude our discussions on the performance improvement techniques designed for ROF communications by referring back to Fig 4 and Fig. 23. It becomes plausible from our discussions on the performance improvement techniques that while the designer has access to the plethora of techniques listed in Fig. 23 to choose from, there is also a cost to be

This article has been accepted for publication in a future issue of this journal, but has not been fully edited. Content may change prior to final publication. Citation information: DOI 10.1109/COMST.2015.2394911, IEEE Communications Surveys & Tutorials

paid, as seen from Fig 4. The higher the implementational cost and complexity of the technique, the better the performance improvement is expected to be. Hence, we complete our discourse with a discussion of the various cost-reduction techniques designed for ROF communications, as listed in Fig. 23.

VI. Cost Reduction Techniques

The various cost reduction technqiues proposed for ROF communications, as seen from Fig. 23, include the family of techniques designed for integrating ROF communication with the existing Fiber To The Home (FTTH) optical networks, the family of techniques conceived for implementing wavelength reuse and the set of techniques proposed for reducing the number of lasers, which will be discussed in Sections VI-A, VI-B and VI-C, respectively.

A. Integration with existing FTTH optical networks

The penetration of the optical fiber to the end user is increasing at a rapid rate, because the telecommunication service providers are attempting to support increased wired data rates for their customers. These networks are referred to as *Fiber To The Home* (FTTH) networks. It should be noted here that wired signals in this manuscript refer to the fiber signals for stationary devices like personal-computers, while wireless signals refers to the signals for mobile devices. The wired signal that is carried by the FTTH networks is of baseband (BB) nature, while the ROF signal is of RF nature. Hence, transmitting the ROF signals over both the existing FTTH networks [103] and indoor optical networks [104] would result in significant cost advantages and in efficiently exploiting the bandwidth of the existing fibers. This kind of integration can be achieved in the following ways:

1) Employing separate optical carriers for optical BB and optical RF modulation [105];
2) Employing a single optical carrier for two-step optical BB and optical RF modulation;
3) Employing a single optical carrier for simultaneous optical BB and optical RF modulation.

Note that the terms optical BB modulation and optical RF modulation in this manuscript refer to the modulation of electronic BB and electronic RF signals onto the optical carrier, respectively.

*1) **Employing separate optical carriers for optical baseband and optical RF modulation**:* Separate optical carriers can be employed at the BS for transmitting the BB wired signal and the ROF wireless signal. As shown in Fig. 57, lasers operating at optical frequencies of $f_{baseband} = \frac{\omega_{baseband}}{2\pi}$ Hz and $f_{ROF} = \frac{\omega_{ROF}}{2\pi}$ Hz are modulated by the BB wired signal and the RF wireless signal, respectively. These two signals are then multiplexed for generating a signal, whose spectrum is shown in Fig. 57. As shown in Fig. 57, the multiplexed signal is transported over the FTTH network to the home of the end user, where it is demultiplexed. The optical signal carrying the BB data directly supports the wired devices, while the ROF signal is fed to a RAP that supports indoor wireless communication [103]. In this case the BS would be several kilometers away from the customer premises. In the case of larger houses/buildings the demultiplexed ROF signal would enter an in-building optical network that supports several RAPs [106].

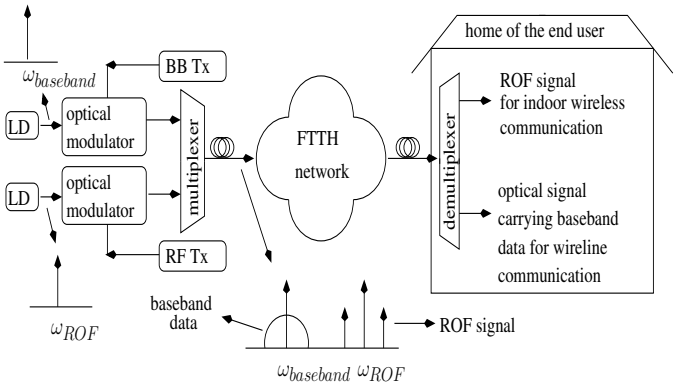

Fig. 57. Using separate optical carriers for optical baseband and optical RF modulation (LD- laser diode; RF Tx- RF transmitter; BB Tx- Baseband Transmitter; FTTH- Fiber To The Home)

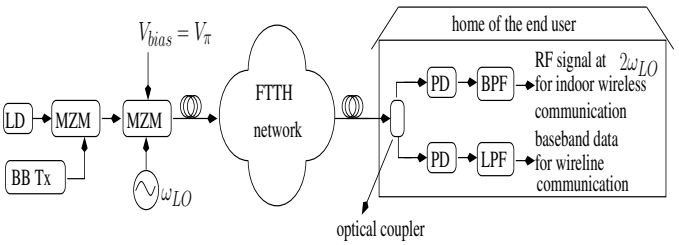

Fig. 58. Employing a single optical carrier for two-step optical baseband and RF modulation (LD- laser diode; MZM- Mach-Zehnder Modulator; BB Tx- Baseband Transmitter; PD- Photo-diode; BPF- Band Pass Filter; FTTH- Fiber To The Home; LPF- Low Pass Filter)

*2) **Employing a single optical carrier for two-step optical baseband and RF modulation**:* Instead of using separate optical carriers, the wired BB data and the wireless RF signal may be modulated onto the same optical carrier at the BS in two modulation steps and then transmitted to the RAP. Fig. 58 shows the block digram of a 2-step modulation for integrating ROF and FTTH transmission [101]. Observe in Fig. 58 that the output of the laser operating at an optical power of P_{in} is BB modulated by the bit stream $b(t)$ using an MZM having a switching voltage of V_π. Then, the BB modulated optical signal power P_{BB} is:

$$P_{BB} = P_{in}\left[1 - \cos(\frac{\pi b(t)}{V_\pi})\right], \tag{52}$$

where we have $b(t) = 0$ and $b(t) = V_\pi$ for bits '0' and '1', respectively. As shown in Fig. 58, the output of the BB modulation step is then OCS modulated using a RF tone $V_{LO}\cos(\omega_{LO}t)$ that drives a MITP biased MZM to generate

This article has been accepted for publication in a future issue of this journal, but has not been fully edited. Content may change prior to final publication. Citation information: DOI 10.1109/COMST.2015.2394911, IEEE Communications Surveys & Tutorials

TABLE IV
RADIO OVER FIBER (ROF) COST REDUCTION TECHNIQUES (PART 1)

Technique	Year	Authors	Contribution
Integration with existing Fiber To The Home (FTTH) networks	1997	Blumenthal *et al.* [98]	Simultaneous optical modulation of a 2.5 Gbps baseband (BB) signal and a 100 Mbps, 5.5 GHz RF signal on a single optical carrier was implemented using a Mach Zehnder Modulator (MZM).
	2001	Kamisaka *et al.* [99]	Simultaneous optical modulation of a 10 Gbps BB signal and a 155 Mbps, 60 GHz RF signal on a single optical carrier was done using an Electro-Absorption Modulator (EAM).
	2007	Jia *et al.* [100]	Simultaneous optical modulation of a 10 Gbps BB signal and a 2.5 Gbps, 20/30 GHz RF signal on a single optical carrier was implemented using a MZM and an interleaver. Frequency doubling ensured the generation of a 40/60 GHz RF signal at the optical receiver.
	2007	Jia *et al.* [101]	Designed a testbed setup for simultaneous delivery of wired and wireless data by using a single optical carrier in a two-step optical BB and RF modulation.
	2007	Lin *et al.* [102]	Simultaneous optical modulation of a 1.25 Gbps BB signal and a 622 Mbps, 10 GHz RF signal on a single optical carrier was implemented using a nested-MZM. Frequency doubling ensured the generation of a 20 GHz RF signal at the optical receiver.
	2008	Llorente *et al.* [103]	Proposed the distribution of high-definition audio/video content by transmitting Ultra Wide Band (UWB) RF signals over FTTH networks. A BER below 10^{-9} was achieved when transmitting 1.25 Gbps UWB RF signals over 50 kms of fiber.

a signal, whose optical power P_{total} is:

$$P_{total} = P_{BB}\left[1-\cos(\frac{\pi V_{LO}\cos(\omega_{LO}t)}{V_\pi})\right]$$
$$= P_{BB}\left[1 - J_0(\frac{\pi V_{LO}}{V_\pi}) - 2\sum_{n=1}^{\infty}(-1)^n J_{2n}(\frac{\pi V_{LO}}{V_\pi})\cos(2n\omega_{LO}t)\right]. \quad (53)$$

Then, as shown in Fig. 58, the signal is transmitted through the FTTH network and then fed to an optical coupler that splits the optical signal into two parts. The lower-branch is photo-detected using a low-bandwidth photo-detector for recovering the BB wired signal represented by $P_{BB}\left[1 - J_0(\frac{\pi V_{LO}}{V_\pi})\right]$ in Equation (53), while upper-branch of the coupler is photo-detected using a high-bandwidth photo-detector to recover a RF signal represented by $2P_{BB}J_2(\frac{\pi V_{LO}}{V_\pi})\cos(2\omega_{LO}t)$ in Equation (53) [101].

We now continue our discourse on the family of techniques designed for integratng ROF communication with the existing FTTH networks by considering simultaneous optical baseband and optical RF modulation.

*3) **Simultaneous optical baseband and optical RF modulation** :* Instead of using the two-step modulation of Fig. 58, the wired BB data and the wireless RF signal could be simultaneously modulated onto the same optical carrier at the BS and then transmitted to the customer premises. This can be achieved using several techniques, including the use of the conventional external modulator (i.e. MZM and EAM) and of the sophisticated nested-external modulators.

*a) **Simultanous optical baseband and optical RF modulation relying on an external modulator**:* Simultaneous modulation can be achieved using the MZM of Fig. 8 or the EAM of Fig. 10(a), where the architecure that achieves simultaneous optical baseband and RF modulation using an external modulator is shown in Fig. 59. Observe in Fig. 59 that the output of the laser is modulated by a MZM that is

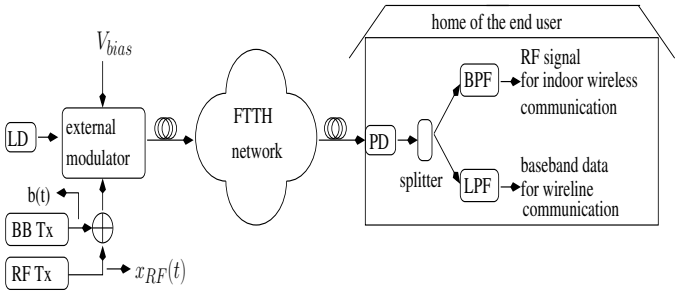

Fig. 59. Simultaneous optical baseband and optical RF modulation using an external modulator (LD- laser diode; RF Tx- RF transmitter;BB Tx- Baseband Transmitter; PD- Photo-diode; BPF- Band Pass Filter; FTTH- Fiber To The Home; LPF- Low Pass Filter)

biased at $V_{bias} = -V_\pi/2$ and driven by a combination of the BB wired data $b(t)$ and the wireless RF signal $x_{rf}(t)$. Subsequently, the modulated signal is transmitted from the BS to the end user over the FTTH network, where it is photo-detected and filtered to separate the BB wired and RF wireless data. Using Equation (5), the photo-detected signal $I(t) \propto P_{out}(t) = P_{in}[1+\sin(\frac{\pi(b(t)+x_{rf}(t))}{V_\pi})]$, which can be expanded using Taylor series [98] to:

$$\frac{P_{out}(t)}{P_{in}} = 1 + \sin(\frac{\pi b(t)}{V_\pi}) + \cos(\frac{\pi b(t)}{V_\pi})\frac{\pi x_{rf}(t)}{V_\pi} - \frac{1}{2}\sin(\frac{\pi b(t)}{V_\pi})\frac{\pi^2 x_{rf}^2(t)}{V_\pi^2} - \frac{1}{6}\cos(\frac{\pi b(t)}{V_\pi})\frac{\pi^3 x_{rf}^3(t)}{V_\pi^3}..., \quad (54)$$

where,

$$b(t) = \begin{cases} V \text{ for bit '1'} \\ -V \text{ for bit '0'} \end{cases}$$

In Equation (54), the first two terms contain the desired BB signal, i.e. $P_{BB}(t) = 1 + \sin(\frac{\pi b(t)}{V_\pi})$ and the third term has the desired RF signal, $P_{rf}(t) = \cos(\frac{\pi b(t)}{V_\pi})\frac{\pi x_{rf}(t)}{V_\pi}$, while the higher order terms produce intermodulation distortion both at the BB and RF frequencies. $\cos(\frac{\pi b(t)}{V_\pi})$ is the same for both values of $b(t)$, which implies that the desired RF signal in the third term of Equation (54) is not corrupted by the BB signal [98]. However, the BB transmission affects the power

This article has been accepted for publication in a future issue of this journal, but has not been fully edited. Content may change prior to final publication. Citation information: DOI 10.1109/COMST.2015.2394911, IEEE Communications Surveys & Tutorials

of the photo-detected RF signal. For the case of pure optical RF modulation, i.e. when $b(t) = 0$, the power in the desired third term of Equation (54) would be maximised, because we have $|\cos(\frac{\pi b(t)}{V_\pi})| = 1$, while for simultaneous optical modulation we have $|\cos(\frac{\pi b(t)}{V_\pi})| < 1$, because $b(t) \neq 0$. The performance of BB modulation is improved by using a larger difference between the optical power $P_{BB}(t)$ transmitted for bit '0' and bit '1'. This can be achieved by increasing the amplitude V of $b(t)$, which, however, reduces the value of $|\cos(\frac{\pi b(t)}{V_\pi})|$ and hence reduces $P_{rf}(t)$. Hence, the power in the detected RF signal is reduced when simultaneous optical BB and RF modulation is employed. For the case of pure optical BB modulation, i.e for $x_{RF}(t) = 0$ in Equation (54), we would have chosen $V = V_\pi/2$ to ensure that the MZM is operating at its mimimum and maximum $P_{BB}(t)$ for the bits '0' and '1', respectively. However, for the scenario that involves simultaneous BB and RF modulation, it is evident from Equation (54) that choosing $V = V_\pi/2$ would result in the desired third term $P_{rf}(t)$ going to zero, i.e. no RF transmission would occur. Thus, the BB optical modulation has to be carried out using non-optimum values of $P_{BB}(t)$ [98].

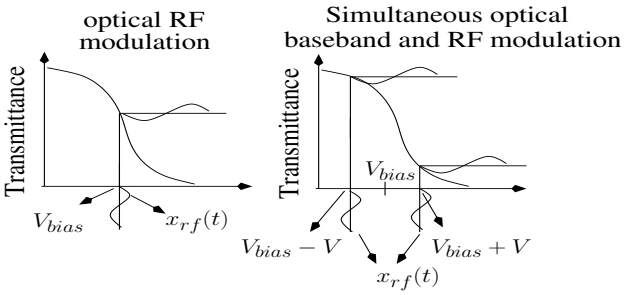

Fig. 60. Optical modulaton using the Electro-Absorption Modulator (EAM)

Additionally, the architecture of Fig. 59 can be implemented using the EAM of Fig. 10(a), where the condition of avoiding overmodulation imposes an upper limit on the total drive voltage that can be applied to the EAM [99]. The BB signal $b(t)$ is combined with the RF signal $x_{rf}(t)$ and the combined signal is then added to the bias voltage V_{bias} to generate the drive voltage, which is applied to the EAM. In this scenario, the output intensity that would be photo-detected is [99]:

$$I(t) \propto P(t) \propto T^2(V_{bias} + b(t) + x_{rf}(t)), \qquad (55)$$

where $T(v)$ is the transmittance of the EAM described in Section II-A. Expanding Equation (55) using Taylor series we get:

$$I(t) \propto T^2(V_{bias} + b(t)) + 2T(V_{bias} + b(t)) \left[\frac{d(T(v))}{dv}\right]_{v=V_{bias}+b(t)} x_{rf}(t) + ... \qquad (56)$$

In Equation (56), the first term contains the desired BB signal, while the second term has the desired RF signal [99]. The higher order terms would produce intermodulation distortion at both the BB and RF frequencies. The BB signal is represented by $b(t) = V$ for bit '1' and $b(t) = -V$ for bit '0'. For the case of pure optical RF modulation, i.e. for $b(t) = 0$, the power in the desired second term would be maximised because the slope of the transmission curve, i.e. $\left[\frac{d(T(v))}{dv}\right]$, is maximised at $V = V_{bias}$, which is evident in Fig. 60. However, for simultaneous optical modulation, the slopes at $V = V_{bias} \pm V$ become lower than that at $V = V_{bias}$, as seen from Fig. 60 and hence the photo-detected RF signal power drops [99]. The performance of BB modulation is improved by using a larger difference in the optical power transmitted for bits '0' and '1', which can be arranged by increasing the amplitude V of $b(t)$. However, this reduces the slope values at $V = V_{bias} \pm V$. Thus, BB modulation has to be carried out using non-optimum values in the EAM transmission curve of Fig. 60.

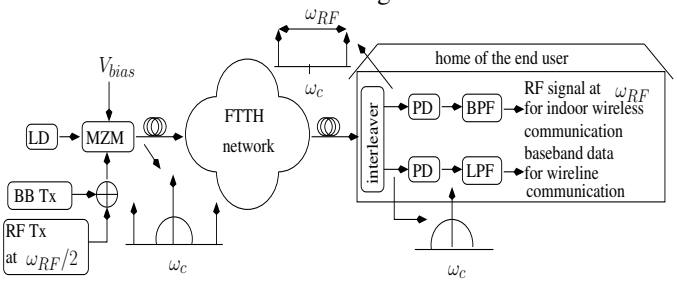

Fig. 61. Simultaneous optical baseband and optical frequency-doubled RF modulation (LD- laser diode; RF Tx- RF transmitter; BB Tx- Baseband Transmitter; PD- Photo-diode; BPF- Band Pass Filter; FTTH- Fiber To The Home; LPF- Low Pass Filter; MZM- Mach Zehnder Modulator)

In addition to the architecture of Fig. 59, the system shown in Fig. 61 also employs simultaneous optical BB and RF modulation with the additional advantage of being able to achieve frequency-doubling. Frequency-doubling helps generate high RF signals using lower electronic oscillator frequencies and optical modulators of lower electronic bandwidth. ROF transmission that implements frequency-doubling can be carried out along with simultaneous BB transmission, by using an interleaver [100]. In the architecture in Fig. 61, the output of the laser, operating at an optical frequency of $f_c = \frac{\omega_c}{2\pi}$ Hz, is modulated using a MZM that is driven by a combination of the wireless RF signal at $\omega_{RF}/2$ and the wired BB signal. As shown in Fig. 61 [100], the modulated BB data is present at the optical carrier ω_c, while the RF data is carried by the two first-order optical sidebands at $\omega_c \pm \omega_{RF}/2$. After transmission from the BS through the FTTH network, these optical sidebands are separated from the signal at the optical carrier frequency, by using an optical interleaver in the end user's home. Subsequently, as shown in Fig. 61, the sidebands are photo-detected to generate a frequency-doubled wireless RF signal at ω_{RF}, while the signal at the optical carrier frequency is photo-detected to retrieve the BB wired signal [100], [107].

It may be concluded that the cost of carrying out simultaneous optical BB and optical RF modulation, as opposed to separate modulations, is that of striking a performance trade-off. Explicitely, the amplitudes of $b(t)$ and $x_{RF}(t)$ in Fig. 59 have to be chosen in such a way that the required Quality of Service (QoS) can be achieved for both the BB and RF

This article has been accepted for publication in a future issue of this journal, but has not been fully edited. Content may change prior to final publication. Citation information: DOI 10.1109/COMST.2015.2394911, IEEE Communications Surveys & Tutorials

transmission [99]. A similar trade-off exists for the case of simultaneous modulation using a tri-band signal consisting of two RF signals at microwave and millimeter-wave frequencies along with a BB signal [29].

The stringency of this trade-off can be relaxed to some extent by using the more sophisticated nested-external modulator, as detailed in the next section.

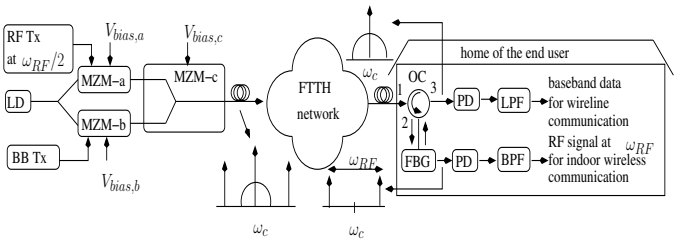

Fig. 62. Simultaneous optical baseband and optical frequency-doubled RF modulation using nested MZM (LD- laser diode; RF Tx- RF transmitter; BB Tx- Baseband Transmitter; PD- Photo-diode; BPF- Band Pass Filter; FTTH- Fiber To The Home; LPF- Low Pass Filter; MZM- Mach Zehnder Modulator)

*b) **Simultanous modulation relying on a nested-external modulator**:* Simultanous optical BB and optical RF modulation may also be implemented using the architecture of Fig. 62. that uses a nested-MZM instead of the conventional MZM, where the output of the laser diode operating at $f_c = \frac{\omega_c}{2\pi}$ Hz is split into two branches, which then modulate a nested MZM consisting of three MZMs referred to as MZM-a, MZM-b and MZM-c in Fig. 62. Specifically, MZM-a of Fig. 62 is biased at MITP and it is driven by the RF signal at a frequency of $f_{RF}/2 = \frac{\omega_{RF}/2}{2\pi}$ Hz to achieve OCS modulation. On the other hand, On OFF Keying (OOK) [97] optical BB modulation may be implemented using MZM-b, while MZM-c is biased at the MATP [102]. As seen in Fig. 62, the spectrum of the optical signal at the output of the nested MZM consists of the modulated BB data present at the optical carrier ω_c, while the RF data is carried by the two first-order optical sidebands at $\omega_c \pm \omega_{RF}/2$ [102]. After transmission from the BS to the customer premises through the FTTH network, the signal enters port 1 of the OC shown in Fig. 62 and exits from port 2, where the FBG filter of Fig. 18(a) reflects the signal at ω_c but lets the sidebands pass through. Subsequently, as shown in Fig. 62, the sidebands are photo-detected to generate a frequency-doubled wireless RF signal at $f_{RF} = \frac{\omega_{RF}}{2\pi}$ Hz, while the reflected optical signal enters port 2 and exits from port 3 of the OC in Fig. 62. This optical signal is then photodetected to retrieve the BB wired signal. The major advantage of this technique is that the two modulation schemes can be independently optimised [102]. However, for a fixed total optical power received at the photo-diode, increasing the modulation depth of one of the schemes increases its modulated optical power and hence improves this scheme's performance, while degrading the other scheme's performance [102].

Thus, the family of techniques proposed for integrating ROF communication with existing FTTH networks involves a trade-off between the performance of the ROF link and the baseband transmission. When designing the wireless networks, the effect of such a trade-off becomes important in the light of the limited power budget. It can be seen from the discussions in this section that the value of P_{RF}^{RAP} considered in Section II-E reduces, when the ROF link is integrated with the FTTH network. Thus, it can be concluded from Equation (19) that this reduction would degrade the SNR_{ROF} of the ROF link and hence would affect the wireless network parameters, like the cell-size and RAP amplifier gain, as discussed in Section II-E. We conclude our discussions on the family of techniques proposed for integrating ROF communication with existing FTTH networks by stating that they rely on infrastructure sharing to implement multiplexed optical communication. On the other hand, the techniques discussed in the next section, namely the family of techniques designed for wavelength reuse, relies on infrastructure sharing to implement duplexed optical communication.

B. Wavelength Re-use

Wavelength re-use is an optical duplexing technique, where Uplink (UL) communication is achieved by re-using the Downlink (DL) optical signal at the RAP. This leads to significant cost advantages, because the RAPs do not need to have their own optical sources, when wavelength re-use is employed. However, allocating a portion of the DL optical power to UL communication results in the degradation of the DL performance. The various ways of achieving wavelength re-use include Optical Carrier Recovery and Re-use (OCRR), Optical Re-Modulation (ORM) and employing a modulator-cum-photo-detector, which will be discussed in Sections VI-B.1, VI-B.2 and VI-B.3, respectively.

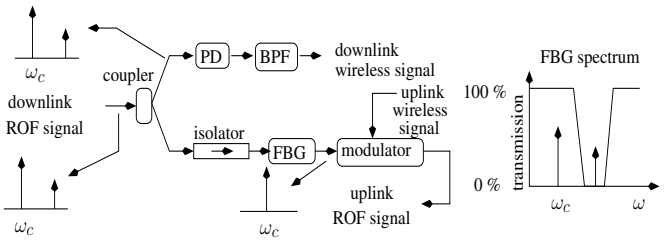

Fig. 63. Optical Carrier Recovery and Re-use (OCRR) in the RAP employing an optical coupler and FBG (PD- Photo-diode; BPF- Band Pass Filter; FBG- Fiber Bragg Grating)

*1) **Optical Carrier Recovery and Re-use (OCRR)**:* The techniques that involve the separation of the total or a fraction of the DL optical carrier power from the DL sidebands, for its reuse in UL communication, are referred to as OCRR techniques.

In the RAP of Fig. 63 [115], the DL OSSB signal power is split using an optical coupler, where the signal of the upper branch is photo-detected, while the lower branch-signal is fed to a FBG filter, whose transmission spectrum is also shown in Fig. 63. The FBG passes the optical carrier but reflects 100% of the sideband power. An isolator is incorporated at the input of the FBG filter to prevent the back propagation of the reflected sideband. The separated optical carrier that becomes available at the output of the FBG filter is then modulated by

This article has been accepted for publication in a future issue of this journal, but has not been fully edited. Content may change prior to final publication. Citation information: DOI 10.1109/COMST.2015.2394911, IEEE Communications Surveys & Tutorials

TABLE V
RADIO OVER FIBER (ROF) COST REDUCTION TECHNIQUES (PART 2)

Technique	Year	Authors	Contribution
Wavelength Re-use	1994	Wu *et al.* [108]	Introduced the concept of wavelength re-use by proposing the Optical Re-Modulation (ORM) arcitecture of Fig. 68.
	1998	Wu *et al.* [109]	
	1996	Welstand *et al.* [110]	The bias voltage was switched to obtain half-duplex operation when using a modulator-cum -photodetector, as shown in Fig. 72.
	1996	Westbrook *et al.* [111]	A single bias voltage was employed by the modulator-cum-photodetector, as shown in Fig. 73, at the cost of a downlink (DL) versus uplink (UL) performance trade-off.
	1997	Noel *et al.* [112]	
	1997	Wake *et al.* [113]	
	1999	Stohr *et al.* [114]	A pair of lasers were used at the Base Station (BS) along with a modulator-cum- photodetector at the Radio Access Point (RAP), as shown in Fig. 74, to implement wavelength re-use.
	2000	Kitayama *et al.* [11]	
	2001	Nirmalathas *et al.* [115]	Presented the Optical Carrier Recovery and Reuse (OCRR) techniques of Fig. 63 & Fig. 64.
	2003	Kuri *et al.* [116]	Employed the ORM architecture of Fig. 67, that relied on EAM-assisted intensity modulation in the DL as well as the UL.
	2005	Bakaul *et al.* [117]	Presented the OCRR technique of Fig. 66, which enables the implementation of OCRR in Wavelength-Interleaved Wavelength Division Multiplexing (WI-WDM) signals.
	2006	Kaszubowska *et al.* [118]	The OCRR technique of Fig. 64 was employed for remote delivery of the RF tone from the BS to the RAP.
	2006	Jia *et al.* [40]	The OCRR technique of Fig. 64 helped generate a frequency doubled RF signal.
	2006	Chen *et al.* [119]	The OCRR technique of Fig. 65 was employed in congugation with DL frequency doubling.
	2007	Yu *et al.* [120]	
	2007	Won *et al.* [121]	Implemented the ORM technique of Fig. 70 by using a gain saturated Reflective Semiconductor Optical Amplifier (RSOA),
	2008	Huang *et al.* [122]	The OCRR technique of Fig. 65 was employed in conjugation with DL frequency quadrupling.
	2008	Yu *et al.* [123]	Implemented ORM by employing optical phase modulation in the DL, while employing optical intensity modulation in the UL.
	2009	Ji *et al.* [124]	
	2013	Thomas *et al.* [3]	Implemented wavelength re-use by incorporating the performance improving Digitized ROF (DROF) technique in the UL of Fig. 68.

the UL RF signal and transmitted from the RAP to the BS over the fiber [115], hence achieving wavelength re-use.

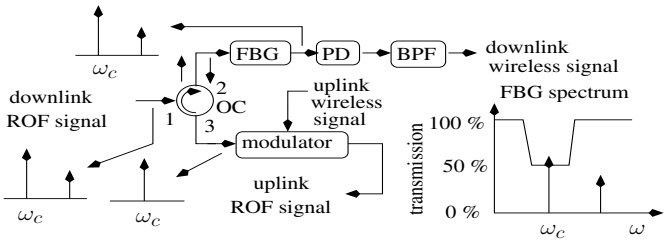

Fig. 64. Optical Carrier Recovery and Re-use (OCRR) in the RAP using an OC and FBG (FBG- Fiber Bragg Grating; OC- Optical Circulator; PD- Photo-diode; BPF- Band Pass Filter)

In the RAP of Fig. 64 [115], [118], the DL OSSB signal enters port 1 of the OC and exits from port 2, where a FBG filter, whose spectrum is also shown in Fig. 64, reflects 50% of the optical carrier's power. The remaining 50 % of the optical carrier's power along with 100% of the modulation sideband power propagates through the FBG filter and then it is photo-detected for generating the DL wireless signal. The reflected 50% of the optical carrier power enters the OC from port 2, exits from port 3 and then it is employed for optical UL modulation. For the case of an ODSB DL signal, the FBG filter of Fig. 64 can be designed for reflecting 100% of the optical carrier power, while the pair of sidebands propagate through the filter and are photo-detected for generating a frequency-doubled DL RF signal [40].

OCRR can also be achieved by employing an optical interleaver at the RAP [119]. As shown in the RAP of Fig. 65, the DL ODSB signal is fed to an interleaver that separates the optical carrier at ω_c from the pair of first-order sidebands at $\omega_c \pm \omega_{RF}/2$, where $f_{RF}/2 = \frac{\omega_{RF}/2}{2\pi}$ is the frequency of the

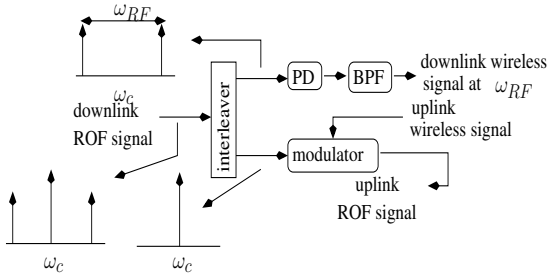

Fig. 65. Optical Carrier Recovery and Re-use (OCRR) in the RAP using an interleaver (PD- Photo-diode; BPF- Band Pass Filter)

RF signal generated in the BS. The optical sidebands are then photo-detected to generate a frequency-doubled signal at f_{RF} Hz [119] [119], [120]. As shown in Fig. 65, the separated optical carrier of the lower branch can then be employed for wavelength re-use. If second-order optical sidebands at $\omega_c \pm \omega_{RF}$ are generated instead of the first-order ones, for example by using a MATP biased MZM at the BS, then, in the RAP, their separation from the optical carrier followed by the subsequent photo-detection yields a frequency-quadrapled signal [122].

As mentioned previously in Section V-A, a commonly employed WDM ROF signal is the WI-DWDM signal of Fig. 26. The architecure of Fig. 66 [117] may also be employed to implement wavelength re-use in the RAP of a ROF system employing WI-WDM signals, where again, the input DL WI-DWDM spectrum shown in Fig. 66 was discussed in Section V-A. The WI-DWDM signal enters port 1 of the OC and exits from port 2. The channel that is to be dropped at the RAP is $\{\omega_{c,i+1}, s_{i+1}\}$. Hence, as shown in Fig. 66, the signal exiting port 2 is passed through the filter FBG A, that reflects

This article has been accepted for publication in a future issue of this journal, but has not been fully edited. Content may change prior to final publication. Citation information: DOI 10.1109/COMST.2015.2394911, IEEE Communications Surveys & Tutorials

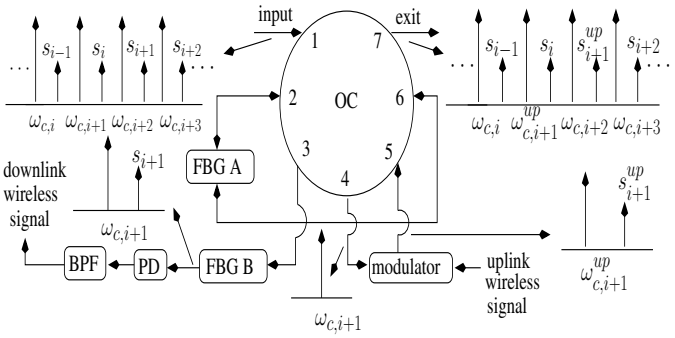

Fig. 66. Optical Carrier Recovery and Re-use (OCRR) in the RAP of a ROF system employing WI-WDM signals (FBG- Fiber Bragg Grating; OC- Optical Circulator; PD- Photo-diode; BPF- Band Pass Filter)

both the optical carrier $\omega_{c,i+1}$ and the corresponding sideband s_{i+1}, which therefore may be referred to as a double-notch filter. The rest of the WDM signal is fed into port 6 and it finally leaves from port 7. Both the optical carrier $\omega_{c,i+1}$ and the sideband s_{i+1}, that were reflected by FBG A, enters port 2 and exits from port 3, where it encounters the second filter FBG B, as shown in Fig. 66. The FBG B filter is a notch-filter that reflects 50% of the optical carrier $\omega_{c,i+1}$. The remaining 50% of the optical carrier power and 100% of the sideband power is passed through and employed in DL photo-detection [117]. The reflected 50% of the optical carrier power re-enters port 3 and leaves from port 4, where is it employed in UL modulation. As shown in Fig. 66, the UL signal enters port 5 and exits via port 6, where it encounters FBG A, that has been designed to reflect both the optical carrier at $\omega_{c,i+1}$ and the corresponding sideband. Hence, the UL signal is reflected by FBG A, enters port 6 of the OC and exits via port 7. Thus, the optical signal exiting port 7 consists of the UL signal at $\omega_{c,i+1}$ and s_{i+1}, instead of the DL signal at that frequency [117]. It also contains the other carriers and sidebands of the input WI-DWDM signal.

The advantage of the design of Fig. 63 is its simplicity [115]. However, it wastes 50% of the modulated sideband power. This disadvantage is circumvented by the design of Fig. 64 [115], which can also be extended to the SCM transmission regime of Fig. 20, regardless of the number of RF signals involved, since the FBG filter of Fig. 64 only has to reflect the optical carrier from the spectrum of Fig. 20. However, this design requires an OC, which is more complex and hence more expensive than an optical coupler. The design of Fig. 66 can be simultaneosly used as an OADM and a wavelength re-use module in a bus- or ring-based ROF network. Again, the disadvantage of this design is its complexity. A common design challenge in the architectures of Figures 64 and 66 is the fact that the imperfect isolation of the OC ports and variations in the transmittance-reflectance characteristics of the temperature-sensitive FBG filters result in cross-talk between the DL and UL signals [117]. The design of Fig. 65 employs an optical interleaver, which is not as sensitive to temperature variations as a FBG filter [38]. However, in the design of Fig. 65, the weaker second-order optical sidebands at $\omega_c \pm \omega_{RF}$ have to be filtered out at the BS, otherwise they will be passed along with the separated optical carrier. This occurs because the transfer function of the interleaver consists of alternating passbands and stopbands.

Let us now continue our discussions on the the family of techniques invented for wavelength-reuse by considering the arrangements that implement Optical Re-Modulation (ORM), which, unlike the above OCRR techniques, do not entail the separation of the optical carrier from its sidebands using high-selectivity optical filtering, but involve other constraints.

*2) **Optical Re-Modulation (ORM)**:* In ORM, the DL optical signal is remodulated by the UL data at the RAP, without relying on filtering for recovering the optical carrier. This can be achieved in a number of ways, as described below.

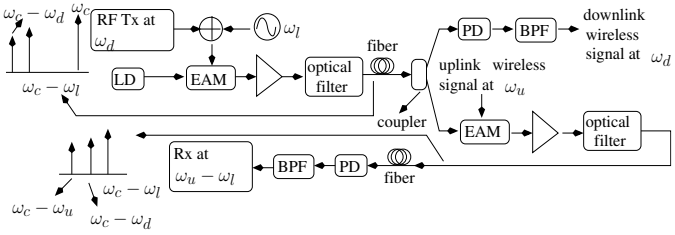

Fig. 67. Optical Re-Modulation (ORM) using an Electro-Absorption Modulator (RF Tx- RF Transmitter; LD- Laser Diode; PD- Photo=diode; BPF- Band Pass Filter)

Fig. 67 [116] illustrates an architecture that employs the EAM of 10(a) to achieve ORM. In Fig. 67, the downlink signal at $f_d = \frac{\omega_d}{2\pi}$ Hz and a local oscillator tone at $f_l = \frac{\omega_l}{2\pi}$ Hz are combined with the aid of the SCM technique of Fig. 20 and the resultant signal is then used for modulating the DL optical carrier generated by the LD at $f_c = \frac{\omega_c}{2\pi}$ Hz. The ODSB modulated signal is then optically filtered for generating an OSSB signal, whose spectrum is also shown in Fig. 67 [116]. After transmission of this signal from the BS to the RAP over the fiber, as shown in Fig. 67, half of the signal power is photo-detected and bandpass filtered in the upper branch of the Fig. 67 for removing the local oscillator tone and then transmitted to the MS, On the other hand, the other half of the signal power in the lower branch is additionally remodulated using an EAM by the UL signal at $f_u = \frac{\omega_u}{2\pi}$ Hz. It is then amplified and optically filtered for ensuring that the UL optical signal consist of a tone at $(\omega_c - \omega_l)$, an UL sideband at $(\omega_c - \omega_u)$ and a residual DL sideband at $(\omega_c - \omega_d)$ [116]. The UL optical signal is then transmitted from the RAP to the BS over the fiber, where it is photo-detected and bandpass filtered for removing the DL downlink signal. Finally, the downconverted uplink signal at $\omega_u - \omega_l$ is detected [116].

Another ORM architecture is shown in Fig. 68, where the output of a LD is modulated by the DL RF signal and it is then transmitted from the BS to the RAP. Then, a part of the DL signal power is separated using an optical coupler and additionally remodulated by the UL signal, using the MZM of the lower-branch in Fig. 68. The remodulated UL signal is transmitted from the RAP to the BS. Meanwhile, the signal in the upper-branch of Fig. 68 is photo-detected to generate the DL wireless signal. If the width of the UL and DL RF

This article has been accepted for publication in a future issue of this journal, but has not been fully edited. Content may change prior to final publication. Citation information: DOI 10.1109/COMST.2015.2394911, IEEE Communications Surveys & Tutorials

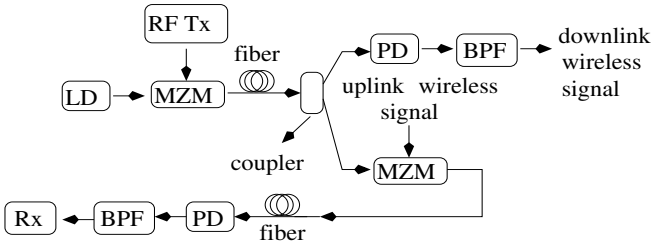

Fig. 68. Optical Re-Modulation (ORM) with constraints on uplink/downlink frequency allocation (RF Tx- RF Transmitter; LD- Laser Diode; PD- Photo=diode; BPF- Band Pass Filter; MZM- Mach-Zehnder Modulator; Rx- Receiver)

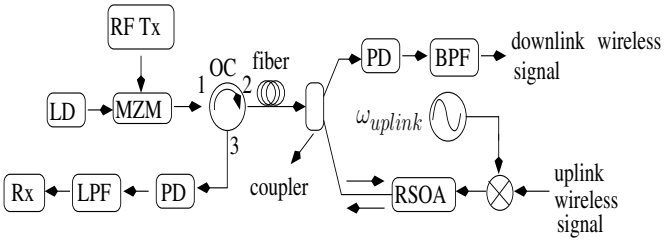

Fig. 70. Optical Re-Modulation (ORM) using a Reflective Semiconductor Optical Amplifier (RSOA) (RF Tx- RF Transmitter; LD- Laser Diode; PD- Photo=diode; BPF- Band Pass Filter; LPF- Low Pass Filter)

bands is less than an octave[1] and the frequency separation between the bands is more than the width of the bands, then the further modulated UL signal remains uneffected by the inter-modulation products between the DL and UL signals [109]. Thus, the UL signal can be filtered out from the signal that is photo-detected at the BS.

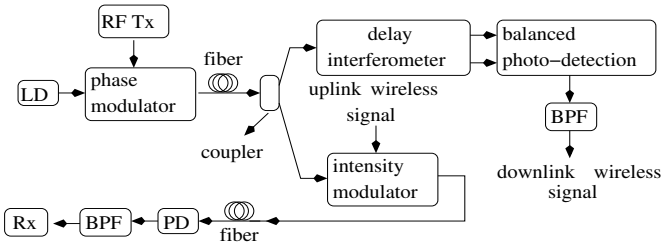

Fig. 69. Optical Re-Modulation (ORM) using phase modulation and intensity modulation for downlink and uplink optical communication, respectively (RF Tx- RF Transmitter; LD- Laser Diode; PD- Photo=diode; BPF- Band Pass Filter; Rx- Receiver)

Furthermore, it is possible to phase-modulate the optical carrier during its DL transmission and then intensity modulate the same optical carrier for its UL transmission as detailed below [123], [124], [6]. As shown in Fig. 69 [124], the output of the LD is phase-modulated by the RF signal and transmitted from the BS to the RAP over the fiber, where it was split into two branches by a coupler. The DL signal in the upper-branch of Fig. 69 is balanced photo-detected after performing a phase to intensity conversion using a delay interometer (DI) such as the MZI of Fig. 19, as discussed in Section III-B [124]. An MZI assists in employing balanced photo-detection, as discussed in Section V. It is worth mentioning that instead of performing phase-to-intensity conversion followed by direct balanced photo-detection, the coherent photo-detection of the phase-modulated signal may also be employed, as discussed Section II-C. The lower branch of the coupler of Fig. 69 is intensity-modulated by the UL RF signal using an external modulator. Afterwards, the UL optical signal is transmitted from the RAP to the BS over the fiber, where it is photo-detected to generate the UL RF signal, which is subsequently bandpass filtered and fed to the RF receiver.

Additionally, the architecture of Fig. 70 can also be used, where the output of a laser source is modulated by the DL RF signal using a MZM. Subsequently, the DL optical signal enters port 1 and exits from port 2 of the OC. This signal is then transmitted from the BS to the RAP over the fiber, where the signal is split into two branches. The upper branch is photo-detected to generate the DL wireless signal [121], while the lower branch is fed to a gain-saturated Reflective Semiconductor Optical Amplifier (RSOA) in order to suppress the DL optical sidebands. As shown in Fig. 70, the optical carrier is simultaneously modulated by the UL BB data that is generated by down-converting the $f_{uplink} = \frac{\omega_{uplink}}{2\pi}$ Hz wireless signal from the MS, which is received at the RAP [121]. Hence, the UL transmission requires the ocillator operating at ω_{uplink} in the RAP. The UL optical signal exits the RSOA and then it is transmitted from the RAP to the BS through the optical fiber, where it enters port 2 and exits from port 3 of the OC. As shown in Fig. 70, the UL signal is then photo-detected and the resultant BB UL signal is filtered and detected [121].

Let us now briefly contrast the solutions in Figures 67 to 70. The design of Fig. 67 requires the UL signal to be amplified using Erbium Doped Fiber Amplifiers (EDFAs) which add ASE optical noise, as discussed in in Section II-D. On the other hand, the design of Fig. 68 is simple, but it imposes certain conditions on the wireless frequency assignment. The design of Fig. 69 does not impose such restrictions, but requires either the phase-to-intensity conversion discussed in prior to the DL direct photo-detection or it has to employ the DL coherent photo-detection. Also, fiber dispersion converts the DL phase-modulation to intensity modulation, thereby corrupting the intensity modulation based UL transmission of Fig. 69. Moreover, any residual intensity-modulation of the DL transmission would degrade the UL transmission of the system in portrayed Fig. 69. Finally, the design of Fig. 70, unlike the designs of Figures 67 to Fig. 69, employs an oscillator for the down-conversion of the uplink wireless signal received from the MS, which may become a disadvantage in the case of high-RF frequencies, like millimeter-wave signals. However, the design of Fig. 70 has the advantage that the uplink optical modulator of the RAP performs the additional function of an amplifier as well, thereby improving the attainable BER [121].

All the wavelength re-use techniques described so far, namely the OCRR and ORM techniques, employ a separate optical UL modulator and DL photo-detector in the RAP. However, in the next section we discuss wavelength re-use techniques that employ a single modulator-cum-photo-detector, thereby reducing the RAP complexity.

[1]A frequency band from f_1 Hz to f_2 Hz is equal to an octave if $f_2 = 2f_1$

This article has been accepted for publication in a future issue of this journal, but has not been fully edited. Content may change prior to final publication. Citation information: DOI 10.1109/COMST.2015.2394911, IEEE Communications Surveys & Tutorials

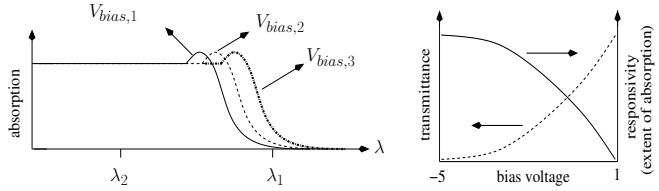

(a) EAM absorption at different optical wavelengths

(b) EAM absorption or transmission vs. bias voltage at λ_1

Fig. 71. EAM absorption characteristics

*3) **Employing a single device modulator-cum-photo-detector**:* The wavelength re-use techniques of Sections VI-B.1 and VI-B.2 need a photo-detector for detecting the DL optical signal and a separate modulator for transmitting the UL optical signal. However, it is possible to employ an EAM as a modulator-cum-photo-detector[1]. Both the operating optical wavelength and the bias-voltage has an influence on the transmission characteristics of the EAM. Fig. 71(a) illustrates the dependence of the EAM absorption on the operating wavelength [11]. As shown in Fig. 71(a), an optical input signal at a wavelength of λ_2 would be largely absorbed, i.e. it is largely photo-detected, regardless of the bias voltage, while an optical input signal at a wavelength of λ_1 would experience a bias-voltage-dependent aborption, i.e. a bias-voltage-dependent photo-detection, or transmittance level, as shown in Fig. 71(b) and discussed in Section II-A. As shown in Fig. 71(b), a low level of transmittance corresponds to a high level of absorption, i.e a high level of photo-detection of the optical input signal by the EAM [112]. On the other hand, a high-level of transmittance would enable the modulation of the input optical signal by the electronic signal applied to the EAM. This property has been exploited for designing the following EAM-based optical transceivers.

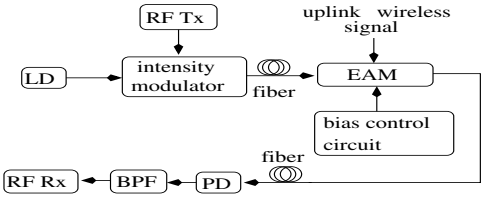

Fig. 72. Half-duplex operation of Electro-Absorption Modulator (EAM) as modulator-cum-photo-detector (LD- Laser Diode; RF Tx- RF Transmitter; PD- Photo-diode; BPF- Band Pass Filter; RF Rx- RF Receiver)

Single-wavelength half-duplex operation can be achieved using the EAM. When light at a wavelength λ_1 of Fig. 71(a) enters an EAM, achieving a high RF modulation efficiency requires the EAM to be biased at a point, where the slope of the transmission characteristics of Fig. 71(b) is maximum. This is true for moderate values of the reverse bias voltage, as seen from Fig. 71(b) [110]. On the other hand, it can also be seen from Fig. 71(b) that the optical input signal is largely absorbed, i.e. it is photo-detected, when a high reverse bias voltage is employed [112]. Thus, the EAM can be operated both as a modulator and a photo-detector by appropriately switching the bias voltage applied to it [110], as shown in the architecture of Fig. 72, where the bias voltage applied to the EAM in the RAP is switched based on whether photo-detection of the DL optical signal from the BS or transmission of the UL optical signal to the BS is taking place. The major drawback of this technique is however that the bi-directional communication is half-duplex, because simultaneous photo-detection and modulation is not possible. Additionally, the need for employing bias control circuits is another complexity-related drawback.

[1]A single device that is capable of photo-detecting the DL optical signal as well as modulating it with the electronic UL signal.

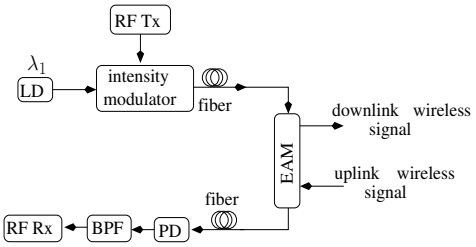

Fig. 73. Full-duplex operation of Electro-Absorption Modulator (EAM) as modulator-cum-photo-detector (LD- Laser Diode; RF Tx- RF Transmitter; PD- Photo-diode; BPF- Band Pass Filter; RF Rx- RF Receiver)

In contrast to Fig. 72 relying on a half-duplex operation, single-wavelength full-duplex operation can be used, as in the architecture of Fig. 73, where the operating wavelength is chosen to be λ_1 of Fig. 71(a) and the bias voltage is not switched. In the architecture of Fig. 73, the EAM bias voltage of Fig. 71(b) is adjusted to a specific value that would strike the desired compromise between the UL modulation efficiency and the DL photo-detection efficiency, along with the UL modulation non-linearity being at an acceptable level [111]. Hence, the EAM in the RAP is not operating in the ideal photo-detection region of Fig. 71(b) and it photo-detects the DL optical signal, while also modulating the UL wireless signal onto the optical carrier. It is possible to operate the EAM in a bias-free scenario, i.e. when a bias of zero volts is appled, but it can be seen from Fig. 71(b) that choosing a bias voltage of zero volts would result in the EAM becoming less efficient as a photo-detector than as a modulator. Hence different antenna gain values would have to be applied to the UL and DL signal at the mobile device to ensure a similar performance [113].

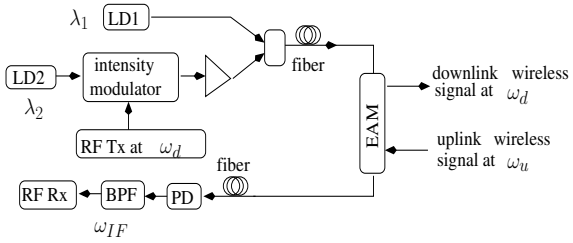

Fig. 74. Full-duplex operation of Electro-Absorption Modulator (EAM) as modulator-cum-photo-detector (LD- Laser Diode; RF Tx- RF Transmitter; PD- Photo-diode; BPF- Band Pass Filter; RF Rx- RF Receiver)

Finally in contrast to Fig. 72 and Fig. 73, dual-wavelength full-duplex operation may also be employed. The need to strike a compromise between the modulation efficiency and the photo-detection efficiency can be circumvented by adopting a dual-wavelength operation. In the architecture of Fig. 74 [114], the output of the laser LD2, operating at λ_2 of Fig.

This article has been accepted for publication in a future issue of this journal, but has not been fully edited. Content may change prior to final publication. Citation information: DOI 10.1109/COMST.2015.2394911, IEEE Communications Surveys & Tutorials

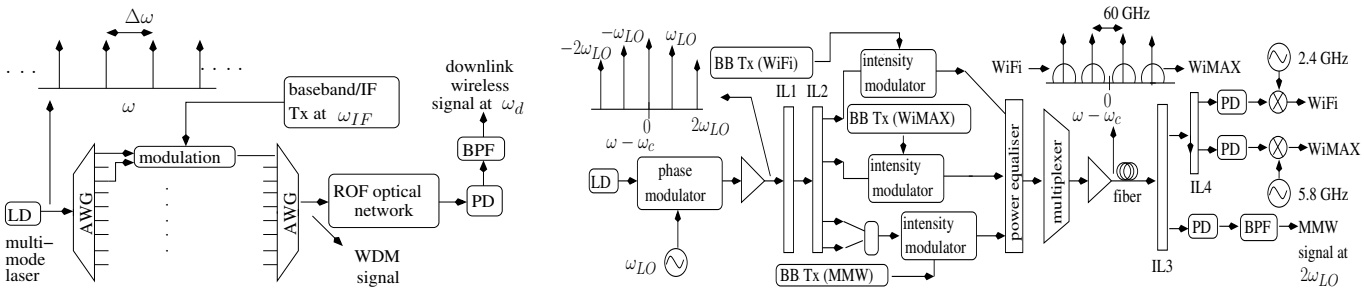

(a) WDM using a multimode optical source

(b) Employing phase modulation harmonics to generate WDM signal

Fig. 75. Techniques to reduce the number of lasers (LD- Laser Diode; WDM- Wavelength Division Multiplexing; PD- Photo-diode; BPF- Band Pass Filter; IL- Interleaver; MMW- Millimeter Wave; BB Tx- Baseband Transmitter)

71(a), is intensity modulated by a RF signal at $f_d = \frac{\omega_d}{2\pi}$ Hz. The modulated optical signal is then combined with the unmodulated output of the laser LD1 operating at λ_1 of Fig. 71(a). As shown in Fig. 74, this combined signal is transmitted from the BS to the RAP over the fiber, where the optical signal at λ_d is photo-detected by the EAM, while the optical signal at λ_1 is modulated by the EAM using the UL RF signal at $f_u = \frac{\omega_u}{2\pi}$ Hz [114]. The UL optical signal is transmitted from the RAP to the BS over the fiber and then it is photo-detected, filtered and detected.

Let us now consider the family of techniques proposed for reducing the number of lasers that are employed in the BS, unlike the above wavelength re-use techniques that aim to make the RAP laser-free.

C. *Reducing the number of lasers*

While wavelength-reuse eliminates the need to have a laser source in the RAP, the BS still has to have several laser sources for supporting multiple RAPs by using the WDM signal of Fig. 22(a). The need to have several laser sources in a network employing WDM can be totally or partially relaxed in the following ways:

*1) **Using a multi-mode optical source**:* A single-mode laser produces a tone at a single frequency, while a multi-mode laser produces tones at multiple optical frequencies [127]. As shown in Fig. 75(a) [125], the various $\Delta\omega$ spaced modes of a multi-mode laser are separated using a DEMUX. Then, pairs of modes having a separation of $N\Delta\omega$ are employed in optical modulation using a BB/IF signal at $f_{IF} = \frac{\omega_{IF}}{2\pi}$ Hz, where each pair of modes constitutes a channel and N is a positive integer. Subsequently, the modulated channels are multiplexed to generate the WDM signal of Fig. 75(a), which is transmitted through a ROF optical network to the RAP, where the heterodyne detection of the modes in each channel generates the DL RF signal at $\omega_d = (N\Delta\omega + \omega_{IF})$. It has been shown in [125] that this technique can be used for generating upto 360 such channels, which can be used for supporting duplex communication with 180 RAPs. By additionally employing the SCM of Fig. 20 it is possible to support upto 10080 RF channels associated with a bandwidth of 250 MHz belonging to the unlicensed 60 GHz band [126]. The availability of a large number of channels can be exploited in the design of a dynamically reconfigurable WDM network carrying 60 GHz ROF signals [12].

*2) **Employing modulation harmonics**:* The harmonics that are imposed by the modulation of an RF tone on the laser's output can be beneficially harnessed as independent optical carriers [3] [106]. These modulation harmonics can support multi-band transmission to a single RAP. Fig. 75(b) illustrates an architecture in which the upper harmonics that are generated during phase modulation can be used for supporting the transmission of WiFi, WiMAX and 60 GHz signals to the RAP [106]. At the BS, the optical carrier is phase-modulated using a $f_{RF} = 30$ GHz $= \frac{\omega_{RF}}{2\pi}$ electronic tone at a phase modulation depth, which would result in first-order harmonic at $(\omega_c \pm \omega_{RF})$ and in significant second-order sidebands at $(\omega_c \pm 2\omega_{RF})$, in addition to the presence of the optical carrier at ω_c, as shown in Fig. 75(b) [106]. The optical carrier is removed by the first interleaver (IL1), while the second interleaver (IL2) separates the four sidebands, where there are two sidebands of the first-order and two of the second-order. The pair of second-order sidebands at $(\omega_c + 2\omega_{RF})$ and $(\omega_c - 2\omega_{RF})$ are considered as independent optical carriers and are modulated with the BB WiFi and BB WiMAX signals, respectively. The pair of $2f_{RF} = 60$ GHz spaced first-order sidebands at $(\omega_c + \omega_{RF})$ and $(\omega_c - \omega_{RF})$ are then combined and modulated with the BB data of the desired 60 GHz signal. The four sidebands are then combined to generate the spectrum seen in Fig. 75(b) and this multiplexed signal is transmitted from the BS to the RAP over the fiber. In the RAP, the first interleaver IL3 of Fig. 75(b) separates the first-order sidebands from the second-order sidebands [106]. The two first-order sidebands are heterodyne photo-detected to generate a 60 GHz millimeter-wave signal, while the second interleaver IL4 of Fig. 75(b) is used for separating the two second-order sidebands, followed by their individual photo-detection and upconversion to generate the 2.4 GHz WiFi and the 5.8 GHz WiMAX signals [106].

On the other hand, instead of supporting multiband transmission to a single RAP, as in Fig. 75(b), it is possible to employ the modulation harmonics as independent optical carriers that support multiple RAPs [5], [3], which could support DAS-based wireless MIMO communication [5]. As shown in Fig. 76, it is possible to generate multiple optical carriers by modulating the output of a LD, operating at an optical output of $f_c = \frac{\omega_c}{2\pi}$ Hz, using a sinusoidal modulating signal at $f_{LO} = \frac{\omega_{LO}}{2\pi}$ Hz and a high modulation depth [5],

This article has been accepted for publication in a future issue of this journal, but has not been fully edited. Content may change prior to final publication. Citation information: DOI 10.1109/COMST.2015.2394911, IEEE Communications Surveys & Tutorials

TABLE VI

RADIO OVER FIBER (ROF) COST REDUCTION TECHNIQUES (PART 3)

Technique	Year	Authors	Contribution
Reducing the number of lasers	2005	Kuri *et al.* [125]	Employed the modes of a multi-mode super-continuum laser to support multiple users, as shown in Fig. 75(a).
	2006	Nakasyotani *et al.* [126]	A Wavelength Division Multiplexing (WDM) ROF network relying on a mulit-mode laser was shown to support over 10000 channels and a total data rate of 1.56 Tbps.
	2007	Olmos *et al.* [12]	A dynamic reconfigurable WDM ROF network relying on a multi-mode laser to support multiple channels was proposed.
	2009	Chowdhury *et al.* [106]	It employed the harmonics generated by optical modulation to support multi-band transmission of RF signals including WIFi, WiMax and a 60 GHz signal.
	2013	Thomas *et al.* [3]	It employed the harmonics generated by optical modulation to support multiple RAPs.

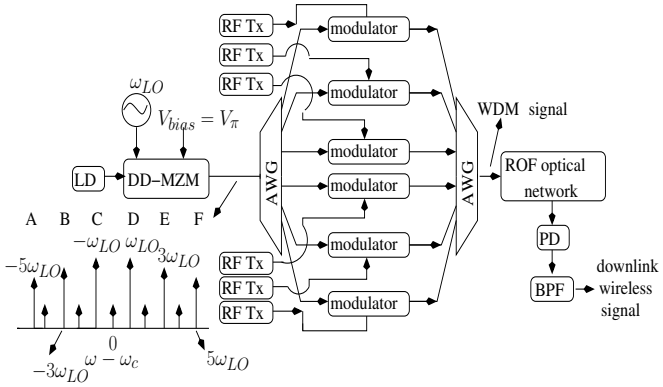

Fig. 76. Exploiting Mach-Zehnder Modulator non-linearity to generate a Wavelength Division Multiplexing (WDM) signal (LD- Laser Diode; PD- Photo-diode; BPF- Band Pass Filter; IL- Interleaver; MMW- Millimeter Wave; BB Tx- Baseband Transmitter)

[3]. This is achieved using the OCS architecture in Section III-A.3, which employs the dual-drive MZM of Fig. 8(b) that is biased at $V_{bias} = V_\pi$ and operating in the push-pull mode. As observed from the spectrum seen in Fig. 76, using a high modulation index results in the first harmonic at $(\omega_c \pm \omega_{LO})$, third harmonic at $(\omega_c \pm 3\omega_{LO})$ and fifth harmonic at $(\omega_c \pm 5\omega_{LO})$ having a significant magnitude. These can then be used as six independent optical carriers having an inter-carrier spacing of $2\omega_{LO}$ [5], [3], for supporting multiple RAPs, one of which is shown in Fig. 76.

TABLE VII

PARAMETER VALUES USED IN THE ROF ARCHITECTURE

Parameter	**Value**	**Parameter**	**Value**
RF DL f_{dwn1} & f_{dwn2}	2.47 GHz 5.8 GHz	PD receiver Noise Figure	6 dB
RF Modulation scheme	Binary Phase Shift Keying	PD receiver Trans-impedance	125 Ω
Fiber Dispersion	16 ps/km-nm	ADC Resolution	4 bits
laser frequency	1550 nm	PD responsivity	0.8 A/W
RF DL and UL Bit rate	32 MBPS 16 MBPS	RF UL f_{up1} & f_{up2}	2.416GHz 5.744GHz
RF channel width with guard band	60MHz (DL) 30MHz (UL)	Bandpass sampling rate f_s	64×10^6 sample/s
RRC filter roll-off	0.5	f_{LO} used in OCG	12.5 GHz
DL RF Diversity Scheme	Space Time Block Coding	length of fibre ring	25 km
UL RF Diversity Scheme	Maximal Ratio Combining	DD-MZM & Extinction Ratio	4 dB 35 dB

VII. DESIGN EXAMPLE

A hybrid architecture that uses the state-of-the-art DROF architecture of Fig. 56 with the conventional ROF of Fig. 3 can be designed, where the conventional ROF is referred to as Analogue ROF (AROF) in this section to distinguish it from DROF. In addition to the advantages of the DROF solution discussed in Section V-L, there is also the further advantage that multiple users may be optically Code Division Multiplexed (CDM) [3]. The MSs have different clock and carrier frequencies as well as different distances from the RAP. Hence, their UL signals arrive asynchronously at the RAPs. Additionally, imperfect power control as well as the inevitable multi-user interference result in the asynchronous wireless UL having a lower SNR than the synchronous DL [3]. Hence the more robust, but more costly DROF link of Fig. 56 can be employed for UL optical transmission, while the low-cost conventional AROF link of Fig. 3 can be employed for the DL, as shown in the architecture of Fig. 77(a) [3]. As a further benefit, wavelength re-use relying on the ORM technique of Fig. 68 may be invoked, because the UL Baseband (BB) signal of DROF may be transmitted by the same optical carrier as that used for transmitting the DL RF signal of AROF. This also increases the optical spectral efficiency. The lower optical transmit power requirement of the DROF mode also supports the re-use of the DL optical carrier power. Moreover, the ring topology of the architecture in Fig. 77(a) minimises the cost of fiber laying [3]. The technique of exploiting the modulation harmonics in an OCS signal, as discussed in Section VI-C.2, is also employed in the architecture of Fig. 77(a) [3] for supporting multiple RAPs. As discussed in Section I, wireless MIMO transmission, that relies on the use of DL transmit-antenna diversity and UL receive-antenna diversity, improves the wireless link performance of the ROF system in Fig. 77(a). The discussion of the architetcure seen in Fig. 77(a) is as follows:

a) Optical Carrier Generator (OCG): The spectrum of the non-linearly modulated OCS signal is as shown in Fig. 76. This technique is used for generating the optical carriers in the system of Fig. 77(a), where optical sidebands B to E of the spectrum in Fig. 76 support four RAPs.

b) BS Transmitter: The DL RF signals transmitted to each RAP at frequencies $f_{dwn1} = 2.47\ GHz$ and $f_{dwn2} = 5.8\ GHz$ are Sub-Carrier Multiplexed (SCM) and are then used for intensity modulating the optical sidebands B to E in

This article has been accepted for publication in a future issue of this journal, but has not been fully edited. Content may change prior to final publication. Citation information: DOI 10.1109/COMST.2015.2394911, IEEE Communications Surveys & Tutorials

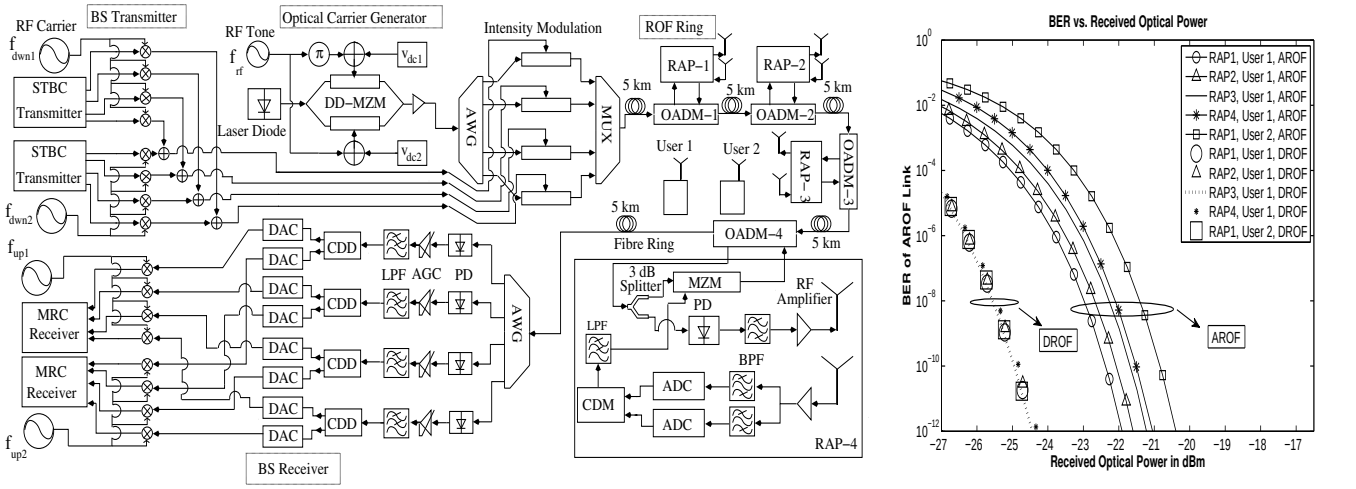

(a) Hybird Analog/Digitized ROF

(b) BER performance of the AROF and DROF links

Fig. 77. System architecture and performance results

the output of OCG. Each of these sidebands now transmits a ODSB DL optical signal to the 4 RAPs [3]. Transmit diversity is achieved in the generation of the RF signals with the aid of Space Time Block Coding (STBC) [15]. A single user per RF carrier is assumed.

c) ROF Ring: The DL ROF signals are transmitted through the fiber, where the 4 major sidebands in the OCG output are used for supporting 4 RAPs in the ring. Duplex optical transmission is used by each RAP at a single OCG output sideband via an OADM and ORM [3]. The block diagram of a RAP is shown in Fig. 77(a). The optical signal dropped at RAP-i is fed to a 3 dB splitter. One of the splitter outputs is photo-detected and amplified for recovering the DL RF signal, while the other output is modulated by the UL BB DROF signal. The BB data modulates the reused DL optical carrier and corrupts the two DL sidebands, which is not a problem since the DL signal has already been detected [3]. The users' wireless UL signals at f_{up1} Hz and f_{up2} Hz are received at all RAPs and then combined by a Maximal Ratio Combining (MRC) [128] at the BS [3]. In the UL optical transmitter of the RAP, the digitization of the received RF signals is performed using the concept of bandpass sampling. The pair of digitized RF signals are then Code Division Multiplexed [128] prior to optical modulation and transmission over the optical UL [3].

d) BS Receiver: The UL optical signal that is received at the RAP is fed into a 1×4 AWG, each of whose outputs are photo-detected and amplified using an Automatic Gain Control (AGC) amplifier. The amplified signals are Low Pass Filtered (LPF) to remove the corrupted DL RF signals and their intermodulation products. The filtered BB CDM DROF signals are code division de-multiplexed (CDD) to separate the two digitized UL RF signals received from each RAP, which are then fed into DACs for recovering the RF signals [3]. Since the UL wireless signals arriving from the two mobile users are received at all the RAPs, four copies of the two UL RF signals are obtained [3]. These are then down-converted and fed to MRC detection blocks [128]. The system of Fig. 77(a) was simulated using the parameter values of Table. VII. The performance results shown in Fig. 77(b) indicate a better performance for the DROF UL than for the AROF DL. It can also be seen that the DROF UL performance, unlike the AROF DL performance, of all the four RAPs is similar and hence DROF is capable of supporting longer fiber lengths than AROF. Fig.78 shows the performance of the overall DL and UL, including the wireless transmission, where an optical power of 15 dBm was employed. It can be seen that the overall system performance is dominated by the wireless performance, because near error-free transmission was achieved in the fiber link.

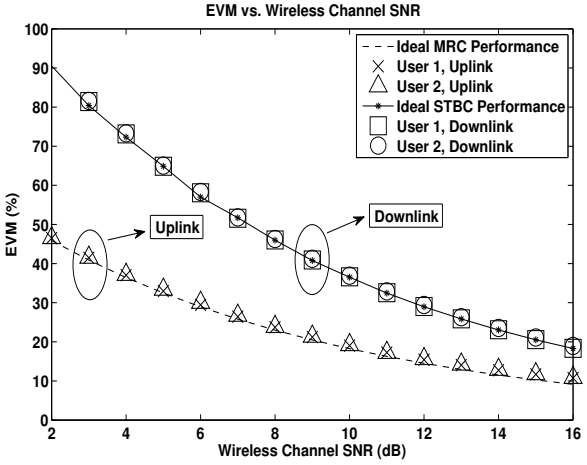

Fig. 78. Uplink performance using MRC & BPSK modulation and DL performance using STBC & BPSK modulation

VIII. Design Guidelines

The sensitivity of a ROF link is defined as the received optical power at which a BER of 10^{-9} is achieved [24]. On the other hand, the linearity of the ROF link, among others, may be expressed in terms of the suppression of the harmonics and intermodulation products in the photo-detected signal and also

This article has been accepted for publication in a future issue of this journal, but has not been fully edited. Content may change prior to final publication. Citation information: DOI 10.1109/COMST.2015.2394911, IEEE Communications Surveys & Tutorials

in terms of the BER degradation imposed by the fiber's non-linearity. Also, the user-support capacity of the ROF system may be defined as the number of RAPs or as the number of MSs that are supported by it. The first step in designing a ROF system is to set target values for the above performance metrics, based on the requirements of the wireless network, for which the ROF system forms the backhaul. Next, we go about designing a basic ROF link, based on the techniques listed in Fig. 5.

The simplest ROF link is one that employs direct modulation of the optical carrier's intensity discussed in Section II-A for generating the ODSB signal discussed in Section III-A.1, which is then detected by direct photo-detection, as highlighted in Section II-C, with multiplexing being implemented using the SCM technique discussed in Section IV-A. However, the designer would be constrained to use external modulation, if the RF carrier is beyond the modulation bandwidth of the laser. For a high RF carrier, like a millimeter-wave carrier, the chromatic dispersion-induced power penalty would require the designer to employ the OSSB or OCS modulations discussed in Sections III-A.2 and III-A.3, respectively. In such a scenario, the designer may use an optical filter after the external modulator or alternatively employ a dual-drive MZM. However, if the sensitivity, i.e. BER requirements are too stringent for an intensity-modulated direct-detected link, then the designer may employ the optical angle modulation technique discussed in Section III-B along with the coherent photo-detection of Section II-C. Coherent photo-detection requires an additional laser in the receiver, which may be avoided by using the optical discriminator of Section III-B. This, however, would be at the expense of a performance degradation. Additionally, the designer may opt for the more complex WDM, instead of the SCM, if a large number of RAPs (or mobile users) have to be supported.

Having designed a basic ROF link, the next priority of the designer should be to incorporate maximum possible cost saving techniques listed in Fig. 23, while ensuring that the performance targets are still met. In urban areas, where a signficant extent of fiber has already been laid for digital fiber-based services, the ROF network designer may employ the family of ROF techniques for integrating ROF communication with the existing FTTH networks, as discussed in Section VI-A. This must, however, ensure that the quality of service of the fiber-based digital services is not compromised. The designer may also employ the family of techniques designed for wavelength re-use, as discussed in Section VI-B. However, the allocation of a portion of the DL optical power for UL communication would degrade the DL performance and hence it must be ensured that the sensitivity targets are met. The wavelength re-use technique of OCRR may require high-selectivity optical filtering. This requirement is relaxed in the wavelength re-use technique of ORM, which however imposes the restrictive conditions discussed in Section VI-B.2. When employing a modulator-cum-photo-detector, conceiving the half-duplex regime of Fig. 72 is straightforward. By contrast, the full-duplex communication scenario of Fig. 73 or Fig. 74 either involves a DL versus UL performance trade-off or employs a pair of optical wavelengths, respectively. Finally, cost saving may be achieved by reducing the number of lasers, as discussed in Section VI-C.

When the basic ROF link does not meet one or more of the performance targets set by the wireless network, this may be alleviated by employing the performance improvement techniques listed in Fig. 23. The employment of a cost-saving technique might provide a signficant economic advantage to the designer, but also result in the performance targets not being met. In this scenario too, the designer may employ the cost-saving technique in conjunction with a performance improvement technique, provided the total system's cost remains low. If the target sensitivity of the ROF link is not met, then the designer may employ a technique from the family of techniques for increasing depth of optical modulation, for noise-reduction or for overcoming chromatic dispersion, which were discussed in Sections V-B to V-F and in Section V-K. Among these techniques, the ones employing carrier suppression, balanced photo-detection and dispersion-tolerant modulation schemes are easier to implement. On the other hand, if the target linearity of the ROF link is not met, then the designer may increase the linearity of optical modulation, as discussed in Sections V-E to V-I or aim for overcoming the fiber non-linearity, as discussed in Section V-J. Employing linearized optical modulators reduces the strength of the required RF signal along with the suppression of the non-linear products, thereby degrading the link's sensitivity. Both OIL and optical feed-forward linearization provides noise-reduction in addition to improving the linearity of optical modulation, while the technique of electronic pre- and post-compensation is the simplest to implement. Finally, if the target number of users cannot be supported by the ROF link, then the designer may opt for improving the optical spectral efficiency, as discussed in Section V-A.

Moreover, when it is not possible to meet the performance targets, the analog optical link can be replaced by the Digitized Radio Over Fiber architecture listed in Fig. 23. Alternatively, the sampled RF over fiber technique discussed in Section V-L may be employed. As discussed in Section V-L, this architecture employs the more robust digital optical link, but has a more complex RAP.

IX. Conclusions

In this paper, we introduced the concept of Radio Over Fiber (ROF) transmissions in Section I and then proceeded to discuss the various techniques and design trade-offs of the ROF link of Fig. 3 in Sections II, III and IV, including the optical transmitter, the optical fiber, the optical receiver and the optical network. These trade-offs were summarised in the stylized illustration of Fig. 5. We then continued our discourse in Section V by characterizing the main architectures that may be used for improving the ROF communications system's performance, which were categorized in Fig. 23. The wavelength-interleaved multiplexing technique discussed in Section V-A increases the optical spectral efficiency and hence the throughput of the

This article has been accepted for publication in a future issue of this journal, but has not been fully edited. Content may change prior to final publication. Citation information: DOI 10.1109/COMST.2015.2394911, IEEE Communications Surveys & Tutorials

ROF link, while the carrier suppression technique discussed in Section V-B improves the receiver sensitivity by increasing the depth of the optical modulation. On the other hand, the noise imposed by the optical link can be reduced by the techniques discussed in Sections V-C and V-D, namely by low-biasing the optical modulator and by employing balanced photo-detection. These techniques have been illustrated in Fig. 33 and Fig. 34, respectively. The techniques of Optical Injection Locking and optical feed-forward linearization discussed in Sections V-E and V-F, respectively, not only help in noise-reduction but also in increasing the linearity of the optical modulation. We then went on to discuss other techniques conceived for increasing the linearity of optical modulation, including the employment of linearized modulators, of optical filters as well as of electronic pre-distortion or post-compensation filters, which were portrayed in Fig. 39 to Fig. 45. We then discussed the multiple fiber transmission scheme of Fig. 46 designed for overcoming the non-linear effects of the optical fiber, followed by a discussion of the various schemes of Fig. 47 to Fig. 54 aimed at overcoming chromatic dispersion. These arrangements included the use of dispersion tolerant modulation schemes, fiber gratings, chirped optical signals, self-phase modulation and finally the use of optical phase conjugation. We then concluded our discussions by presenting the Digitized ROF architecture of Fig. 56, which aims for incorporating the benefits of digital optical communication in the conventional ROF link of Fig. 3, at the cost of a more complex Radio Access Point (RAP) design.

Naturally, we have to strike a cost versus performance trade-off in the various ROF techniques. Since the performance enhancment techniques of Section V increase the cost of the ROF link, in Section VI we additionally detail the main cost reduction techniques that may be used in the ROF link of Fig. 3. The integration of the ROF network with the Fiber To The Home (FTTH) network, as seen in Fig. 57 to Fig. 62, would reduce the installation costs. However, in such a scenario, the designer has to strike a trade-off between the performance of the baseband optical transmission of the FTTH network and the attainable performance of the ROF transmission. Cost reductions can also be achieved by making the RAP laser-free by re-using the DL optical signal for UL communication, as seen in the architectures of Fig. 63 to Fig. 74. These wavelength re-use techniques rely on Optical Carrier Recovery and Reuse (OCRR), Optical Re-modulation (ORM) or on the use of a modulator-cum-photo-detector, which were discussed in Sections VI-B.1, VI-B.2 and VI-B.3, respectively. The OCRR techniques of Fig. 63 to Fig. 66 rely on the separation of the DL optical carrier from the DL modulation sidebands, while the ORM techniques of Fig. 67 to Fig. 70 re-modulate the optical signal carrying the DL wireless signal with the uplink wireless signal as well. On the other hand, a modulator-cum-photo-detector detects the DL optical signal besides simultaneously performing UL optical modulation in the RAP. Finally, another technique of reducing the ROF system's cost in a multi-RAP and/or multi-user scenario is to decrease the number of lasers employed in the BS, which can be achieved by using multi-mode laser sources, as shown in Fig. 75(a) or by employing the modulation harmomics as shown in Fig. 75(b) and Fig. 76. We then present the design guidelines in Section VIII.

We conclude by stating that there are numerous open areas for futher research. Some of these areas include, although are not limited to, integrating various millimeter-wave techniques with a ROF backhaul [129] [130], the use of mode-division multiplexing in multimode optical fibers for ROF [131], employing phased array antennas in a ROF link [132] and the use of plastic optical fiber for indoor personal area networks [133]. Multimode optical fibers, especially plastic optical fibers, are less expensive than single mode fibers. Having a large core size simplifies their connections and they can be used with low-cost Light Emitting Diodes (LEDs) and Vertical-Cavity Surface Emitting Lasers (VCSELs). However, the multimode nature of their propagation inevitably limits their employable bandwidth and lengths. Significant research efforts are being invested in overcoming this drawback through efficient signal processing.

REFERENCES

[1] D. Wake, A. Nkansah, and N. Gomes, "Radio Over Fiber Link Design for Next Generation Wireless Systems," *IEEE/OSA Journal of Lightwave Technology*, vol. 28, pp. 2456 –2464, August 2010.

[2] X. Fernando, "Radio over fiber -an optical technique for wireless access," *IEEE communiations society presentation*, October 2009.

[3] V. Thomas, S. Ghafoor, M. El-Hajjar, and L. Hanzo, "A full-duplex diversity-assisted hybrid analogue/digitized radio over fibre for optical/wireless integration," *IEEE Communications Letters*, vol. 17, pp. 1–4, February 2013.

[4] V. A. Thomas, S. Ghafoor, M. El-Hajjar, and L. Hanzo, "Baseband radio over fiber aided millimeter-wave distributed antenna for optical/wireless integration," *IEEE Communications Letters*, vol. 17, pp. 1012–1015, May 2013.

[5] S. Ghafoor and L. Hanzo, "Sub-carrier-multiplexed duplex 64-qam radio-over-fiber transmission for distributed antennas," *IEEE Communications Letters*, vol. 15, pp. 1368–1371, December 2011.

[6] S. Ghafoor, V. A. Thomas, and L. Hanzo, "Duplex digitized transmission of 64-QAM signals over a single fiber using a single pulsed laser source," *IEEE Communications Letters*, vol. 16, pp. 1312–1315, August 2012.

[7] W. Stephens, T. Joseph, and B. Chen, "Analog microwave fiber optic communications links," in *IEEE MTT-S International Microwave Symposium Digest*, pp. 533 –534, June 1984.

[8] N. J. Gomes, P. P. Monteiro, and A. Gameiro, "Next generation wireless communications using radio over fiber," *John Wiley & Sons, Ltd, 2012*.

[9] X. N. Fernando, "Radio over fiber for wireless communications: From fundamentals to advanced topics," *John Wiley & Sons, Ltd, 2014*.

[10] J. Johny, "Radio over fiber- a new communication era: Future broadband wireless access," *Academic Publishing, 2012*.

[11] K. Kitayama, A. Stohr, T. Kuri, R. Heinzelmann, D. Jager, and Y. Takahashi, "An approach to single optical component antenna base stations for broad-band millimeter-wave fiber-radio access systems," *IEEE Transactions on Microwave Theory and Techniques*, vol. 48, pp. 2588–2595, December 2000.

[12] J.J. Vegas Olmos, T. Kuri and K. Kitayama, "Dynamic reconfigurable wdm 60-ghz millimeter-waveband radio-over-fiber access network: Architectural considerations and experiment," *IEEE/OSA Journal of Lightwave Technology*, vol. 25, pp. 3374–3380, November 2007.

[13] L. Hanzo, M. El-Hajjar, and O. Alamri, "Near-capacity wireless transceivers and cooperative communications in the mimo era: Evolution of standards, waveform design, and future perspectives," *Proceedings of the IEEE*, vol. 99, pp. 1343–1385, August 2011.

[14] L. Hanzo, O. Alamri, M. El-Hajjar, and N. Wu, "Near-Capacity Multi-Functional MIMO Systems: Sphere-Packing, Iterative Detection and Cooperation," *Wiley/IEEE Press, First Edition, 2009*.

This article has been accepted for publication in a future issue of this journal, but has not been fully edited. Content may change prior to final publication. Citation information: DOI 10.1109/COMST.2015.2394911, IEEE Communications Surveys & Tutorials

TABLE VIII

FREQUENTLY USED ABBREVIATIONS

ADC	Analog to Digital Convertor	ASE	Amplified Spontaneous Emission
AROF	Analog ROF	AM	Amplitude Modulation
AWG	Arrayed Waveguide Grating	BB	Baseband
BB Tx	Baseband Transmitter	BER	Bit Error Ratio
BPF	Band Pass Filter	BPSK	Binary Phase Shift Keying
BS	Base Station	CDM	Code Division Multiplexing
DAC	Digital to Analog Convertor	DAS	Distributed Antenna System
DBPSK	Differential BPSK	DC	Direct Current
DCF	Dispersion Compensation Fiber	DL	Downlink
DEMUX	Demultiplexer	DROF	Digitized ROF
DSP	Digital Signal Processing	DWDM	Dense WDM
EAM	Electron Absorbtion Modulator	EDFA	Erbium Doped Fiber Amplifiers
E-O	Electronic to Optical	FBG	Fiber Bragg Gratings
FTTH	Fiber To The Home	FWHM	Full Width at Half Maximum
FWM	Four Wave Mixing	GVD	Group Velocity Dispersion
IF	Intermediate Frequency	IL	Interleaver
IM	Intensity Modulation	IMP	Inter-Modulation Product
LD	Laser Diode	LSB	Lower Side Band
MATB	MATP Biasing	MATP	Maximum Transmission Point
MIMO	Multiple Input Multiple Output	MITP	Minimum Transmission Point
MITB	MITP Biasing	MS	Mobile Station
MZI	Mach-Zehnder Interferometer	MZM	Mach-Zehnder Modulator
NF	Noise Figure	OADM	Optical Add Drop Multiplexers
OC	Optical Circulator	OCR	Optical Carrier Recovery
ODSB	Optical Double Side Band	O-E	Optical to Electronic
OIPLL	Optical Injection Phase Locked Loop	OOK	On Off Keying
		OIL	Optical Injection Locking
OPC	Optical Phase Conjugator	OSSB	Optical Single Side Band
PC	Polarization Controller	PD	Photo-Diode
P-I	Power-Current	PM	Phase Modulation
QoS	Quality of Service	QP	Quadrature Point
QB	Quadrature Biasing	RAPs	Radio Access Points
RIN	Relative Intensity Noise	RF	Radio Frequency
RF Tx	RF Transmitter	ROF	Radio Over Fiber
SCM	Sub-Carrier Multiplexing	SBS	Stimulated Brillouin Scattering
SFDR	Spurious Free Dynamic Range	SOA	Semiconductor Optical Amplifier
SNR	Signal to Noise Ratio	SRS	Stimulated Raman Scattering
SMF	Single-Mode Fiber	TE	Transverse Electric
TM	Transverse Magnetic	UL	Uplink
USB	Upper Side Band	WDM	Wavelength Division Multiplexing
WiFi	Wireless Fidelity	WiMax	Worldwide Interoperability for Microwave Access
W-I WDM	Wavelength-Interleaved WDM	WR	Wavelength Reuse
XPM	Cross Phase Modulation	LED	Light Emitting Diode
VCSEL	Vertical Cavity Surface Emitting Laser		

[15] L. Hanzo, Y. Akhtman, L. Wang and M. Jiang, "MIMO-OFDM for LTE, WiFi and WiMax: Coherent versus Non-coherent and co-operative Turbo Tranceivers," *John Wiley and Sons, First Edition, 2011*.

[16] H. Al-Raweshidy and S. Komaki, "Radio over fiber technologies for mobile communication networks," *Artech House, First Edition, 2002*.

[17] J.-M. Kelif and M. Coupechoux, "Impact of topology and shadowing on the outage probability of cellular networks," in *IEEE International Conference on Communications (ICC)*, pp. 1–6, June 2009.

[18] T. Naveh, "Mobile backhaul: Fiber vs. microwave," *Ceragon White Paper*, vol. 1, pp. 1–11, October 2009.

[19] E. Dahlman, S. Parkvall, and J. Sköld, "4g: Lte/lte-advanced for mobile broadband," *Academic Press, 2011*.

[20] T. Kanesan, W. P. Ng, Z. Ghassemlooy, and C. Lu, "Experimental full duplex simultaneous transmission of lte over a dwdm directly modulated rof system," *IEEE/OSA Journal of Optical Communications and Networking*, vol. 6, pp. 8–17, Jan 2014.

[21] T. Rappaport, S. Sun, R. Mayzus, H. Zhao, Y. Azar, K. Wang, G. Wong, J. Schulz, M. Samimi, and F. Gutierrez, "Millimeter wave mobile communications for 5g cellular: It will work!," *IEEE Access*, vol. 1, pp. 335–349, May 2013.

[22] C. Cox III, E. Ackerman, R. Helkey, and G. Betts, "Direct-detection analog optical links," *IEEE Transactions on Microwave Theory and Techniques*, vol. 45, pp. 1375–1383, August 1997.

[23] C. Carlsson, A. Larsson, and A. Alping, "RF transmission over multi-mode fibers using VCSELs-comparing standard and high-bandwidth multimode fibers," *IEEE/OSA Journal of Lightwave Technology*, vol. 22, pp. 1694 – 1700, july 2004.

[24] G.P. Agrawal, "Fiber-Optic Communication Systems," *John Wiley and Sons, Third Edition, 2002*.

[25] J. Ma, J. Yu, C. Yu, X. Xin, J. Zeng, and L. Chen, "Fiber dispersion influence on transmission of the optical millimeter-waves generated using LN-MZM intensity modulation," *IEEE/OSA Journal of Lightwave Technology*, vol. 25, pp. 3244–3256, November 2007.

[26] R. Kalman, J. Fan, and L. Kazovsky, "Dynamic range of coherent analog fiber-optic links," *IEEE Journal ofLightwave Technology*, vol. 12, pp. 1263–1277, July 1994.

[27] G. Smith, D. Novak, and Z. Ahmed, "Overcoming chromatic-dispersion effects in fiber-wireless systems incorporating external modulators," *IEEE Transactions on Microwave Theory and Techniques*, vol. 45, pp. 1410 –1415, aug 1997.

[28] G. L. Li and P. K. Yu, "Optical intensity modulators for digital and analog applications," *IEEE/OSA Journal of Lightwave Technology*, vol. 21, pp. 2010–2030, September 2003.

[29] K. Ikeda, T. Kuri, and K. Kitayama, "Simultaneous three-band modulation and fiber-optic transmission of 2.5-Gb/s baseband, microwave, and 60-GHz-band signals on a single wavelength," *IEEE/OSA Journal of Lightwave Technology*, vol. 21, pp. 3194–3202, December 2003.

[30] H.J.R. Dutton, "Understanding Optical Communications," *IBM, First Edition, 1998*.

[31] X. Fernando, "Improved expression for intensity noise in multimedia over fiber networks," in *First International Conference on Industrial and Information Systems*, pp. 425–429, Aug 2006.

[32] X. Fernando and A. Anpalagan, "On the design of optical fiber based wireless access systems," in *IEEE International Conference onCommunications (ICC)*, vol. 6, pp. 3550–3555 Vol.6, June 2004.

[33] W. Roh, J.-Y. Seol, J. Park, B. Lee, J. Lee, Y. Kim, J. Cho, K. Cheun, and F. Aryanfar, "Millimeter-wave beamforming as an enabling technology for 5g cellular communications: theoretical feasibility and prototype results," *IEEE Communications Magazine*, vol. 52, pp. 106–113, February 2014.

[34] G. Smith and D. Novak, "Broad-band millimeter-wave (38 GHz) fiber-wireless transmission system using electrical and optical SSB modulation to overcome dispersion effects," *Photonics Technology Letters, IEEE*, vol. 10, pp. 141 –143, jan. 1998.

[35] J. Corral, J. Marti, and J. Fuster, "General expressions for IM/DD dispersive analog optical links with external modulation or optical up-conversion in a Mach-Zehnder electrooptical modulator," *IEEE Transactions on Microwave Theory and Techniques*, vol. 49, pp. 1968–1976, October 2001.

[36] J. Park, W. Sorin, and K. Lau, "Elimination of the fibre chromatic dispersion penalty on 1550 nm millimetre-wave optical transmission," *IEEE Electronics Letters*, vol. 33, pp. 512–513, March 1997.

[37] R. Kashyap, "Fiber bragg gratings," *Academic Press, First Edition, 1999*.

[38] J. Yu, Z. Jia, L. Xu, L. Chen, T. Wang, and G. K. Chang, "DWDM optical millimeter-wave generation for radio-over-fiber using an optical phase modulator and an optical interleaver," *IEEE Photonics Technology Letters*, vol. 18, pp. 1418–1420, July 2006.

[39] G. Smith, D. Novak, and Z. Ahmed, "Technique for optical SSB generation to overcome dispersion penalties in fibre-radio systems," *IEEE Electronics Letters*, vol. 33, pp. 74–75, January 1997.

[40] Z. Jia, J. Yu, and G. K. Chang, "A full-duplex radio-over-fiber system based on optical carrier suppression and reuse," *IEEE Photonics Technology Letters*, vol. 18, pp. 1726–1728, August 2006.

[41] M. Weiss, M. Huchard, A. Stohr, B. Charbonnier, S. Fedderwitz, and D. Jager, "60-GHz photonic millimeter-wave link for short to medium range wireless transmission up to 12.5 Gb/s," *IEEE/OSA Journal of Lightwave Technology*, vol. 26, pp. 2424–2429, August 2008.

[42] V. Urick, F. Bucholtz, P. Devgan, J. McKinney, and K. Williams, "Phase modulation with interferometric detection as an alternative to intensity modulation with direct detection for analog-photonic links," *IEEE Transactions on Microwave Theory and Techniques*, vol. 55, pp. 1978–1985, September 2007.

[43] M. LaGasse and S. Thaniyavaru, "Bias-free high-dynamic-range phase-modulated fiber-optic link," *IEEE Photonics Technology Letters*, vol. 9, pp. 681–683, May 1997.

[44] J. Wyrwas and M. Wu, "Dynamic range of frequency modulated direct-detection analog fiber optic links," *IEEE/OSA Journal of Lightwave Technology*, vol. 27, pp. 5552–5562, December 2009.

[45] H. Chi, X. Zou, and J. Yao, "Analytical models for phase-modulation-based microwave photonic systems with phase modulation to intensity modulation conversion using a dispersive device," *IEEE/OSA Journal of Lightwave Technology*, vol. 27, pp. 511–521, March 2009.

[46] R. Olshansky, "Microwave subcarrier multiplexing: new approach to wideband lightwave systems," *IEEE Circuits and Devices Magazine*, vol. 4, pp. 8–14, November 1988.

[47] H. Toda, T. Yamashita, T. Kuri, and K. Kitayama, "Demultiplexing using an arrayed-waveguide grating for frequency-interleaved DWDM millimeter-wave radio-on-fiber systems," *IEEE/OSA Journal of Lightwave Technology*, vol. 21, pp. 1735–1741, August 2003.

[48] C. Oh and W. Gu, "Fiber induced distortion in a subcarrier multiplexed lightwave system," *IEEE Journal on Selected Areas in Communications*, vol. 8, pp. 1296–1303, September 1990.

[49] R. Hui, B. Zhu, R. Huang, C. Allen, K. Demarest, and D. Richards, "Subcarrier multiplexing for high-speed optical transmission," *Journal of Lightwave Technology*, vol. 20, pp. 417–427, March 2002.

[50] R. Gross and R. Olshansky, "Multichannel coherent FSK experiments using subcarrier multiplexing techniques," *IEEE/OSA Journal of Lightwave Technology*, vol. 8, pp. 406–415, March 1990.

[51] R. Yuen and X. Fernando, "Analysis of sub-carrier multiplexed radio over fiber link for the simultaneous support of WLAN and WCDMA Systems," *Kluwer Wireless Personal Communication Journal*, vol. 33, pp. 1–20, April 2005.

[52] K. Iniewski, C. McCrosky and D. Minoli, "Network infrastructure and architecture: designing high-availability networks," *John Wiley and Sons, First Edition, 2008*.

[53] M. Smit and C. Van Dam, "PHASAR-based WDM-devices: principles, design and applications," *IEEE Journal of Selected Topics in Quantum Electronics*, vol. 2, no. 2, pp. 236–250, 1996.

[54] C. Lim, A. Nirmalathas, D. Novak, R. Tucker, and R. Waterhouse, "Technique for increasing optical spectral efficiency in millimetre-wave wdm fibre-radio," *IEEE Electronics Letters*, vol. 37, pp. 1043–1045, aug 2001.

[55] M. Bakaul, A. Nirmalathas, C. Lim, D. Novak, and R. Waterhouse, "Simultaneous multiplexing and demultiplexing of wavelength-interleaved channels in DWDM millimeter-wave fiber-radio networks," *IEE/OSA Journal of Lightwave Technology*, vol. 24, pp. 3341–3352, September 2006.

[56] M. Attygalle, C. Lim, G. Pendock, A. Nirmalathas, and G. Edvell, "Transmission improvement in fiber wireless links using fiber bragg gratings," *IEEE Photonics Technology Letters*, vol. 17, pp. 190–192, January 2005.

[57] H. K. Xijia Gu, Yifeng He and X. Fernando, "Transmission efficiency improvement in microwave fiber-optic link using sub-picometer optic bandpass filter," *Proceedings of the SPIE Conference Photonic North*, vol. 5971, pp. 597123–1–6, September 2005.

[58] M. Farwell, W. Chang, and D. Huber, "Increased linear dynamic range by low biasing the mach-zehnder modulator," *IEEE Photonics Technology Letters*, vol. 5, pp. 779–782, July 1993.

[59] E. Ackerman, G. Betts, W. Burns, J. Campbell, I. Cox, C.H., N. Duan, J. Prince, M. Regan, and H. Roussell, "Signal-to-noise performance of two analog photonic links using different noise reduction techniques," in *IEEE/MTT-S International Microwave Symposium*, pp. 51–54, June 2007.

[60] J. McKinney, M. Godinez, V. Urick, S. Thaniyavarn, W. Charczenko, and K. Williams, "Sub-10-dB noise figure in a multiple-GHz analog optical link," *IEEE Photonics Technology Letters*, vol. 19, pp. 465–467, April 2007.

[61] R.-P. Braun, G. Grosskopf, D. Rohde, and F. Schmidt, "Low-phase-noise millimeter-wave generation at 64 GHz and data transmission using optical sideband injection locking," *IEEE Photonics Technology Letters*, vol. 10, pp. 728–730, May 1998.

[62] L. Johansson and A. Seeds, "Generation and transmission of millimeter-wave data-modulated optical signals using an optical injection phase-lock loop," *IEEE/OSA Journal of Lightwave Technology*, vol. 21, pp. 511–520, February 2003.

[63] L. Chrostowski, X. Zhao, and C. Chang-Hasnain, "Microwave performance of optically injection-locked vcsels," *Microwave Theory and Techniques, IEEE Transactions on*, vol. 54, pp. 788 – 796, feb. 2006.

[64] A. Ng'oma, D. Fortusini, D. Parekh, W. Yang, M. Sauer, S. Benjamin, W. Hofmann, M. Amann, and C. Chang-Hasnain, "Performance of a multi-Gb/s 60 GHz radio over fiber system employing a directly modulated optically injection-locked VCSEL," *IEEE/OSA Journal of Lightwave Technology*, vol. 28, pp. 2436–2444, August 2010.

[65] T. Ismail, C.-P. Liu, J. Mitchell, and A. Seeds, "High-dynamic-range wireless-over-fiber link using feedforward linearization," *IEEE/OSA Journal of Lightwave Technology*, vol. 25, pp. 3274–3282, November 2007.

[66] C. Lim, M. Attygalle, A. Nirmalathas, D. Novak, and R. Waterhouse, "Analysis of optical carrier-to-sideband ratio for improving transmission performance in fiber-radio links," *IEEE Transactions on Microwave Theory and Techniques*, vol. 54, pp. 2181–2187, May 2006.

[67] M. Attygalle, C. Lim, and A. Nirmalathas, "Extending optical transmission distance in fiber wireless links using passive filtering in conjunction with optimized modulation," *IEEE/OSA Journal of Lightwave Technology*, vol. 24, pp. 1703–1709, April 2006.

[68] A. Karim and J. Devenport, "Noise figure reduction in externally modulated analog fiber-optic links," *IEEE Photonics Technology Letters*, vol. 19, pp. 312–314, March 2007.

[69] R. Welstand, C. Sun, S. Pappert, Y. Liu, J. Chen, J. Zhu, A. Kellner, and P. Yu, "Enhanced linear dynamic range property of franz-keldysh effect waveguide modulator," *IEEE Photonics Technology Letters*, vol. 7, pp. 751–753, July 1995.

[70] C. Sun, S. Pappert, R. Welstand, J. Zhu, P. Yu, Y. Liu, and J. Chen, "High spurious free dynamic range fibre link using a semiconductor electroabsorption modulator," *IEEE Electronics Letters*, vol. 31, pp. 902–903, May 1995.

[71] J. Li, S. Fu, K. Xu, J. Q. Zhou, P. Shum, J. Wu, and J. Lin, "Photonic-assisted microwave frequency measurement with higher resolution and tunable range," *OSA Optics Letter*, vol. 34, pp. 743–745, March 2009.

[72] X. J. Meng, T. Chau, and M. Wu, "Improved intrinsic dynamic distortions in directly modulated semiconductor lasers by optical injection locking," *IEEE Transactions on Microwave Theory and Techniques*, vol. 47, pp. 1172–1176, July 1999.

[73] H. K. Sung, E. Lau, and M. Wu, "Optical single sideband modulation using strong optical injection-locked semiconductor lasers," *IEEE Photonics Technology Letters*, vol. 19, pp. 1005–1007, July 2007.

[74] L. Goldberg, H. Taylor, J. Weller, and D. Bloom, "Microwave signal generation with injection-locked laser diodes," *IEEE Electronics Letters*, vol. 19, pp. 491–493, June 1983.

[75] L. Johansson and A. Seeds, "36-GHz 140-Mb/s radio-over-fiber transmission using an optical injection phase-lock loop source," *IEEE Photonics Technology Letters*, vol. 13, pp. 893–895, August 2001.

[76] S. Korotky and R. De Ridder, "Dual parallel modulation schemes for low-distortion analog optical transmission," *IEEE Journal on Selected Areas in Communications*, vol. 8, pp. 1377–1381, September 1990.

[77] H. Skeie and R. V. Johnson, "Linearization of electro-optic modulators by a cascade coupling of phase-modulating electrodes," vol. 1583, pp. 153–164, December 1991.

[78] E. Ackerman, "Broad-band linearization of a mach-zehnder electrooptic

modulator," *IEEE Transactions on Microwave Theory and Techniques*, vol. 47, pp. 2271–2279, December 1999.

[79] B. Masella, B. Hraimel, and X. Zhang, "Enhanced spurious-free dynamic range using mixed polarization in optical single sideband mach-zehnder modulator," *IEEE/OSA Journal of Lightwave Technology*, vol. 27, pp. 3034–3041, August 2009.

[80] C. Lim, A. Nirmalathas, K.-L. Lee, D. Novak, and R. Waterhouse, "Intermodulation distortion improvement for fiber ndash;radio applications incorporating ossb+c modulation in an optical integrated-access environment," *IEEE/OSA Journal of Lightwave Technology*, vol. 25, pp. 1602–1612, June 2007.

[81] X. G. H. Kosek, Yifeng He and X. Fernando, "All-optical demultiplexing of WLAN and Cellular CDMA radio signals," *IEEE/OSA Journal of Lightwave Technology*, vol. 25, pp. 1401–1409, June 2007.

[82] X. Fernando and A. Sesay, "Adaptive asymmetric linearization of radio over fiber links for wireless access," *IEEE Transactions on Vehicular Technology*, vol. 51, pp. 1576–1586, November 2002.

[83] L. Roselli, V. Borgioni, F. Zepparelli, F. Ambrosi, M. Comez, P. Faccin, and A. Casini, "Analog laser predistortion for multiservice radio-over-fiber systems," *IEEE/OSA Journal of Lightwave Technology*, vol. 21, pp. 1211–1223, May 2003.

[84] L. Johnson and H. Roussell, "Linearization of an interferometric modulator at microwave frequencies by polarization mixing," *IEEE Photonics Technology Letters*, vol. 2, pp. 810–811, November 1990.

[85] B. Haas and T. Murphy, "A simple, linearized, phase-modulated analog optical transmission system," *IEEE Photonics Technology Letters*, vol. 19, pp. 729–731, May 2007.

[86] Y. Chiu, B. Jalali, S. Garner, and W. Steier, "Broad-band electronic linearizer for externally modulated analog fiber-optic links," *IEEE Photonics Technology Letters*, vol. 11, pp. 48–50, January 1999.

[87] F. Yang, M. Marhic, and L. Kazovsky, "Nonlinear crosstalk and two countermeasures in SCM-WDM optical communication systems," *IEEE/OSA Journal of Lightwave Technology*, vol. 18, pp. 512–520, April 2000.

[88] J. Marti, J. Fuster, and R. Laming, "Experimental reduction of chromatic dispersion effects in lightwave microwave/millimetre-wave transmissions using tapered linearly chirped fibre gratings," *IEEE Electronics Letters*, vol. 33, pp. 1170–1171, June 1997.

[89] F. Ramos, J. Marti, V. Polo, and J. Fuster, "On the use of fiber-induced self-phase modulation to reduce chromatic dispersion effects inmicrowave/millimeter-wave optical systems," *IEEE Photonics Technology Letters*, vol. 10, pp. 1473–1475, October 1998.

[90] H. Sotobayashi and K. Kitayama, "Cancellation of the signal fading for 60 GHz subcarrier multiplexed optical DSB signal transmission in nondispersion shifted fiber using midway optical phase conjugation," *IEEE/OSA Journal of Lightwave Technology*, vol. 17, pp. 2488–2497, December 1999.

[91] J. Yu, Z. Jia, L. Yi, Y. Su, G. K. Chang, and T. Wang, "Optical millimeter-wave generation or up-conversion using external modulators," *IEEE Photonics Technology Letters*, vol. 18, pp. 265–267, January 2006.

[92] A. Nirmalathas, P. Gamage, C. Lim, D. Novak, R. Waterhouse, and Y. Yang, "Digitized rf transmission over fiber," *IEEE Microwave Magazine*, vol. 10, pp. 75–81, June 2009.

[93] Y. Yang, C. Lim, and A. Nirmalathas, "Investigation on transport schemes for efficient high-frequency broadband ofdm transmission in fibre-wireless links," *Lightwave Technology, Journal of*, vol. 32, no. 2, pp. 267–274, 2014.

[94] U. Gliese, S. Norskov and T. N. Nielsen, "Chromatic dispersion in fiber-optic microwave and millimeter-wave links," *IEEE Transactions on Microwave Theory and Techniques*, vol. 44, pp. 1716–1724, October 1996.

[95] H. Kim and A. Gnauck, "Chirp characteristics of dual-drive. mach-zehnder modulator with a finite dc extinction ratio," *IEEE Photonics Technology Letters*, vol. 14, pp. 298–300, March 2002.

[96] L. Chen, Y. Shao, X. Lei, H. Wen, and S. Wen, "A novel radio-over-fiber system with wavelength reuse for upstream data connection," *IEEE Photonics Technology Letters*, vol. 19, pp. 387–389, March 2007.

[97] P. Winzer and R. Essiambre, "Advanced optical modulation formats," *Proceedings of the IEEE*, vol. 94, pp. 952–985, May 2006.

[98] D. Blumenthal, J. Laskar, R. Gaudino, S. Han, M. Shell, and M. Vaughn, "Fiber-optic links supporting baseband data and subcarrier-multiplexed control channels and the impact of MMIC photonic/microwave interfaces," *IEEE Transactions on Microwave Theory and Techniques*, vol. 45, pp. 1443–1452, August 1997.

[99] T. Kamisaka, T. Kuri, and K. Kitayama, "Simultaneous modulation and fiber-optic transmission of 10-Gb/s baseband and 60-GHz-band radio signals on a single wavelength," *IEEE Transactions on Microwave Theory and Techniques*, vol. 49, pp. 2013–2017, October 2001.

[100] Z. Jia, J. Yu, A. Chowdhury, G. Ellinas, and G. K. Chang, "Simultaneous generation of independent wired and wireless services using a single modulator in millimeter-wave-band radio-over-fiber systems," *IEEE Photonics Technology Letters*, vol. 19, pp. 1691–1693, October 2007.

[101] Z. Jia, J. Yu, G. Ellinas, and G. K. Chang, "Key enabling technologies for optical x2013;wireless networks: Optical millimeter-wave generation, wavelength reuse, and architecture," *IEEE/OSA Journal of Lightwave Technology*, vol. 25, pp. 3452–3471, November 2007.

[102] C.-T. Lin, J. Chen, P.-C. Peng, C.-F. Peng, W.-R. Peng, B.-S. Chiou, and S. Chi, "Hybrid optical access network integrating fiber-to-the-home and radio-over-fiber systems," *IEEE Photonics Technology Letters*, vol. 19, pp. 610–612, April 2007.

[103] R. Llorente, T. Alves, M. Morant, M. Beltran, J. Perez, A. Cartaxo, and J. Marti, "Ultra-wideband radio signals distribution in FTTH networks," *IEEE Photonics Technology Letters*, vol. 20, pp. 945–947, June 2008.

[104] M. Huchard, M. Weiss, A. Pizzinat, S. Meyer, P. Guignard, and B. Charbonnier, "Ultra-broadband wireless home network based on 60-GHz WPAN cells interconnected via RoF," *IEEE/OSA Journal of Lightwave Technology*, vol. 26, pp. 2364–2372, August 2008.

[105] M. Bakaul, A. Nirmalathas, C. Lim, D. Novak, and R. Waterhouse, "Hybrid multiplexing of multiband optical access technologies towards an integrated DWDM network," *IEEE Photonics Technology Letters*, vol. 18, pp. 2311–2313, November 2006.

[106] A. Chowdhury, H.-C. Chien, Y.-T. Hsueh, and G. K. Chang, "Advanced system technologies and field demonstration for in-building optical-wireless network with integrated broadband services," *IEEE/OSA Journal of Lightwave Technology*, vol. 27, pp. 1920–1927, June 2009.

[107] C. Lim, A. Nirmalathas, D. Novak, R. Waterhouse, and G. Yoffe, "Millimeter-wave broad-band fiber-wireless system incorporating baseband data transmission over fiber and remote lo delivery," *IEEE/OSA Journal of Lightwave Technology*, vol. 18, pp. 1355–1363, October 2000.

[108] J. Wu, J. S. Wu, and H. W. Tsao, "A fiber distribution system for microcellular radio," *IEEE Photonics Technology Letters*, vol. 6, pp. 1150–1152, September 1994.

[109] J. S. Wu, J. Wu, and H. W. Tsao, "A radio-over-fiber network for microcellular system application," *IEEE Transactions on Vehicular Technology*, vol. 47, pp. 84–94, February 1998.

[110] R. Welstand, S. Pappert, C. Sun, J. Zhu, Y. Liu, and P. Yu, "Dual-function electroabsorption waveguide modulator/detector for optoelectronic transceiver applications," *IEEE Photonics Technology Letters*, vol. 8, pp. 1540–1542, November 1996.

[111] L. Westbrook and D. Moodie, "Simultaneous bi-directional analogue fibre-optic transmission using an electroabsorption modulator," *IEEE Electronics Letters*, vol. 32, pp. 1806–1807, September 1996.

[112] L. Noel, D. Wake, D. Moodie, D. Marcenac, L. Westbrook, and D. Nesset, "Novel techniques for high-capacity 60-GHz fiber-radio transmission systems," *IEEE Transactions on Microwave Theory and Techniques*, vol. 45, pp. 1416–1423, August 1997.

[113] D. Wake, D. Johansson, and D. Moodie, "Passive picocell: a new concept in wireless network infrastructure," *IEEE Electronics Letters*, vol. 33, pp. 404–406, February 1997.

[114] A. Stohr, K. Kitayama, and D. Jager, "Full-duplex fiber-optic RF subcarrier transmission using a dual-function modulator/photodetector," *IEEE Transactions on Microwave Theory and Techniques*, vol. 47, pp. 1338–1341, July 1999.

[115] A. Nirmalathas, D. Novak, C. Lim, and R. Waterhouse, "Wavelength reuse in the WDM optical interface of a millimeter-wave fiber-wireless antenna base station," *IEEE Transactions on Microwave Theory and Techniques*, vol. 49, pp. 2006–2012, October 2001.

[116] T. Kuri, K. Kitayama, and Y. Takahashi, "A single light-source configuration for full-duplex 60-GHz-band radio-on-fiber system," *IEEE Transactions on Microwave Theory and Techniques*, vol. 51, pp. 431–439, February 2003.

[117] M. Bakaul, A. Nirmalathas, and C. Lim, "Multifunctional WDM optical interface for Millimeter-wave fiber-radio antenna base station,"

IEEE/OSA Journal of Lightwave Technology, vol. 23, pp. 1210–1218, March 2005.

[118] A. Kaszubowska, L. Hu, and L. Barry, "Remote downconversion with wavelength reuse for the radio/fiber uplink connection," *IEEE Photonics Technology Letters*, vol. 18, pp. 562–564, February 2006.

[119] L. Chen, H. Wen, and S. Wen, "A radio-over-fiber system with a novel scheme for millimeter-wave generation and wavelength reuse for up-link connection," *IEEE Photonics Technology Letters*, vol. 18, pp. 2056–2058, October 2006.

[120] J. Yu, Z. Jia, T. Wang, and G. Chang, "A novel radio-over-fiber configuration using optical phase modulator to generate an optical mm-wave and centralized lightwave for uplink connection," *IEEE Photonics Technology Letters*, vol. 19, pp. 140–142, February 2007.

[121] Y. Y. Won, H. C. Kwon, and S. K. Han, "1.25-Gb/s wavelength-division multiplexed single-wavelength colorless radio-on-fiber systems using reflective semiconductor optical amplifier," *IEEE/OSA Journal of Lightwave Technology*, vol. 25, pp. 3472–3478, November 2007.

[122] M. F. Huang, J. Yu, Z. Jia, and G. K. Chang, "Simultaneous generation of centralized lightwaves and double/single sideband optical millimeter-wave requiring only low-frequency local oscillator signals for radio-over-fiber systems," *IEEE/OSA Journal of Lightwave Technology*, vol. 26, pp. 2653–2662, August 2008.

[123] X. Yu, T. Gibbon, and I. Monroy, "Bidirectional radio-over-fiber system with phase-modulation downlink and RF oscillator-free uplink using a reflective SOA," *IEEE Photonics Technology Letters*, vol. 20, pp. 2180–2182, December 2008.

[124] H. C. Ji, H. Kim, and Y. C. Chung, "Full-duplex radio-over-fiber system using phase-modulated downlink and intensity-modulated uplink," *IEEE Photonics Technology Letters*, vol. 21, pp. 9–11, January 2009.

[125] T. Kuri, T. Nakasyotani, H. Toda, and K.-I. Kitayama, "Characterizations of supercontinuum light source for WDM millimeter-wave-band radio-on-fiber systems," *IEEE Photonics Technology Letters*, vol. 17, pp. 1274–1276, June 2005.

[126] T. Nakasyotani, H. Toda, T. Kuri, and K. Kitayama, "Wavelength-division-multiplexed millimeter-waveband radio-on-fiber system using a supercontinuum light source," *Journal of Lightwave Technology*, vol. 24, pp. 404–410, January 2006.

[127] P. Delfyett, S. Gee, M.-T. Choi, H. Izadpanah, W. Lee, S. Ozharar, F. Quinlan, and T. Yilmaz, "Optical frequency combs from semiconductor lasers and applications in ultrawideband signal processing and communications," *IEEE/OSA Journal of Lightwave Technology*, vol. 24, pp. 2701–2719, July 2006.

[128] L. Hanzo, L.L. Yang, E.L. Kuan,and K. Yen, "Single and Multicarrier DS-CDMA: Multi User Detection, Space-Time Spreading, Synchronization, Standards and Networking," *1st edition, John Wiley and Sons, 2003*.

[129] H.-T. Huang, C.-T. Lin, Y.-T. Chiang, C.-C. Wei, and C.-H. Ho, "Simple 2x2 mimo 60-ghz optical/wireless system with extending fiber transmission distance," *Journal of Lightwave Technology*, Early Access 2014.

[130] S. Mikroulis, O. Omomukuyo, M. Thakur, and J. Mitchell, "Investigation of a smf-mmf link for a remote heterodyne 60-ghz ofdm rof based gigabit wireless access topology," *Journal of Lightwave Technology*, Early Access 2014.

[131] G. Gordon, M. Crisp, R. Penty, T. Wilkinson, and I. White, "Feasibility demonstration of a mode-division multiplexed mimo-enabled radio-over-fiber distributed antenna system," *Journal of Lightwave Technology*, Early Access 2014.

[132] K. Lau, G. Lutes, and R. Tjoelker, "Ultra-stable rf-over-fiber transport in nasa antennas, phased arrays and radars (invited)," *Journal of Lightwave Technology*, Early Access 2014.

[133] A. Koonen and E. Tangdiongga, "Photonic home area networks," *Journal of Lightwave Technology*, vol. 32, pp. 591–604, Feb 2014.

Varghese Antony Thomas is a PhD student in the wireless communications research group in the University of Southampton. He received his BE (Honours) degree in Electrical and Electronics Engineering from Birla Institute of Technology and Science, Pilani (Goa Campus) in 2010. He then received an MSc in Wireless Communications from the University of Southampton, UK in 2011. He is the recipient of the several academic awards including the Commonwealth Scholarship of the Government of UK and Mayflower Scholarship of University of Southampton. His research interests are mainly in optical communications, optical-wireless integration, backhaul for MIMO and radio over fiber systems.

Mohammed El-Hajjar is a lecturer in the Electronics and Computer Science in the University of Southampton. He received his BEng degree in Electrical Engineering from the American University of Beirut, Lebanon in 2004. He then received an MSc in Radio Frequency Communication Systems and PhD in Wireless Communications both from the University of Southampton, UK in 2005 and 2008, respectively. Following the PhD, he joined Imagination Technologies as a design engineer, where he worked on designing and developing Imagination's multi-standard communications platform, which resulted in three patents. In January 2012, he joined the Electronics and Computer Science in the University of Southampton as a lecturer in the Southampton Wireless research group. He is the recipient of several academic awards including the Dorothy Hodgkin postgraduate award and IEEE ICC2010 Best paper award. He has published a Wiley-IEEE book and in excess of 50 journal and international conference papers. His research interests are mainly in the development of intelligent communications systems including energy-efficient transceiver design, cross-layer optimisation for large-scale networks, MIMO, millimetre wave communications and Radio over fiber systems.

Lajos Hanzo (http://www-mobile.ecs.soton.ac.uk) FREng, FIEEE, FIET, Fellow of EURASIP, DSc received his degree in electronics in 1976 and his doctorate in 1983. In 2009 he was awarded the honorary doctorate "Doctor Honaris Causa" by the Technical University of Budapest. During his 38-year career in telecommunications he has held various research and academic posts in Hungary, Germany and the UK. Since 1986 he has been with the School of Electronics and Computer Science, University of Southampton, UK, where he holds the chair in telecommunications. He has successfully supervised about 100 PhD students, co-authored 20 John Wiley/IEEE Press books on mobile radio communications totalling in excess of 10 000 pages, published 1460 research entries at IEEE Xplore, acted both as TPC and General Chair of IEEE conferences, presented keynote lectures and has been awarded a number of distinctions. Currently he is directing an academic research team, working on a range of research projects in the field of wireless multimedia communications sponsored by industry, the Engineering and Physical Sciences Research Council (EPSRC) UK, the European IST Programme and the Mobile Virtual Centre of Excellence (VCE), UK. He is an enthusiastic supporter of industrial and academic liaison and he offers a range of industrial courses. He is also a Governor of the IEEE VTS. During 2009 - 2012 he was the Editor-in-Chief of the IEEE Press and a Chaired Professor also at Tsinghua University, Beijing. For further information on research in progress and associated publications please refer to http://www-mobile.ecs.soton.ac.uk